ROLE OF SURFACE ROUGHNESS FOR COLLOIDAL INTERACTIONS IN AQUEOUS MEDIA

A Thesis
Presented to
The Academic Faculty

by

Joanna Wilhelmina Tsao

In Partial Fulfillment
of the Requirements for the Degree
Doctor of Philosophy in the
School of Chemical & Biomolecular Engineering

Georgia Institute of Technology

December 2016

ROLE OF SURFACE ROUGHNESS FOR COLLOIDAL INTERACTIONS IN AQUEOUS MEDIA

Approved by:

Dr. Sven H. Behrens, Advisor
School of Chemical & Biomolecular Engineering
Georgia Institute of Technology

Dr. Victor Breedveld
School of Chemical & Biomolecular Engineering
Georgia Institute of Technology

Dr. Julie Champion
School of Chemical & Biomolecular Engineering
Georgia Institute of Technology

Dr. Carson Meredith
School of Chemical & Biomolecular Engineering
Georgia Institute of Technology

Dr. Sotira Yiacoumi
School of Civil and Environmental Engineering
Georgia Institute of Technology

Date Approved: September 12, 2016

for my family

ACKNOWLEDGEMENTS

There are so many people who have contributed to the completion of this thesis. Specifically, I would like to thank my advisor, Dr. Sven Behrens, for being a great mentor, patient teacher, for trusting that I would get eventually get the experiments to work, and for his continued support throughout my time at Georgia Tech.

I would like to thank my committee members: Dr. Victor Breedveld, Dr. Julie Champion, Dr. Carson Meredith, and Dr. Sotira Yiacoumi, for their helpful comments and suggestions throughout my PhD.

I've had the good fortune to work with a great group of people, and am grateful to past group members: Dr. Hongzhi Wang, Dr. Joohyung Lee, Dr. Abiola Shitta, and Dr. Yi Zhang, and all the present group members: Tony Du, Songcheng Wang, and Maritza Mujica, for being great coworkers.

To the friends I've made here: I could not have asked for a better group of misfits to spend the last four years with. I wouldn't have made it without you and am so honored to have you all in my life. I'd also like to acknowledge the person, or people, who took a chance so many years ago and tried roasting seeds from the *coffea arabica* plant, soaking them in hot water, and then decided that drinking the unknown liquid was a good idea.

And finally, I'd like to thank my family, and especially my parents, for their continued love and encouragement through everything.

tl;dr Thanks, everyone.

TABLE OF CONTENTS

ACKNOWLEDGEMENTS iii

LIST OF TABLES viii

LIST OF FIGURES ix

LIST OF SYMBOLS AND ABBREVIATIONS xiv

SUMMARY xviii

CHAPTER 1 1

1.1 Measurement of colloidal forces 1

1.2 DLVO interactions 3

1.3 Depletion interactions 5

1.4 Objectives 6

1.5 References 7

CHAPTER 2 10

2.1 Background 10

2.1.1 Gravitational attraction 10

2.1.2 The Derjaguin approximation 11

2.1.3 Electrostatic repulsion 11

2.1.3.1 Roughness effects on electrostatic repulsion 13

2.1.4 van der Waals attraction 14

2.1.4.1 Roughness effects on van der Waals attraction 16

2.1.5 Experimental variations of surface roughness 17

2.1.6 Total internal reflection microscopy 18

2.1.7 Optical trapping 19

2.2 Materials and Methods 20

2.2.1 E-S100 coated amine-functionalized polystyrene particle fabrication 20

2.2.1.1 Eudragit S100 particle fabrication 21

2.2.1.2 Fabrication of rough particles and subsequent tuning of surface roughness 22

2.2.1.3 Particle characterization: surface topography 23

2.2.1.4 Particle characterization: surface chemistry 26

2.2.2 Experimental set-up: Total internal reflection microscopy 28

2.2.2.1 TIRM cell preparation and measurement conditions 31

2.2.3 Calculation of DLVO parameters 33

2.3 Results 36

2.3.1 Determination of system parameters 37

2.3.1.1 Gravitational force and the calculation of probe particle size 37

2.3.1.2 The Debye length 39

2.3.1.2.1 Surface potentials 40

2.3.2 Calculation of DLVO parameters 42

2.3.2.1 Electrostatic interactions: discrepancy between theory and experiment 45

2.3.2.2 van der Waals interactions: discrepancy between theory and experiment .. 47

2.3.2.3 van der Waals interaction: empirical correction for surface roughness..... 49

2.3.2.4 Electrostatic interaction: normalization of surface roughness 53

2.4 Concluding remarks 57

2.5 References 60

CHAPTER 3 64

3.1 Background 64

3.1.1 Asakura-Oosawa (AO) depletion interaction potential..... 64

3.1.1.1 The oscillatory interaction 66

3.1.2 The Derjaguin approximation 68

3.1.3 Roughness effects on the depletion interaction 68

3.1.4 Total internal reflection microscopy: considerations for a depletant system 69

3.2 Methods..... 69

3.2.1 Aqueous solutions for TIRM measurements 70

3.2.2 TIRM measurements..... 72

3.2.3 Calculation of DLVO parameters 72

3.3 Results..... 74

3.3.1 Calculation of DLVO parameters: depletant free system 75

3.3.1.1 Calculation of DLVO parameters: depletant system 76

3.3.2 Roughness effects on the depletion interaction 77

3.3.2.1 Calculation of depletion interaction parameters 80

3.3.3 The oscillatory interaction 85

3.3.4 Particle variability 88

3.4 Concluding Remarks 89

3.5 References 91

CHAPTER 4 95

LIST OF TABLES

Table 1.1 Comparison of distance and force resolution of SFA, AFM, and TIRM[18] 3

Table 2.1 Debye screening length for NaCl solutions used to measure roughness effects on the depletion interaction..... 12

Table 2.2 Rms roughness of macroscopic surfaces coated with E-S100 particles 24

Table 2.3 Calculated gravitational force and radius of particles treated with varying concentrations of acetone..... 39

Table 2.4 Calculated Debye length and surface potentials of the glass slide and a smooth AFP-ES100 particle in low electrolyte solutions at pH 6..... 42

Table 2.5 Calculated surface potentials of the glass slide and AFP-ES100 particle in low electrolyte solutions 45

Table 2.6 Fitted surface potentials of the glass slide and AFP-ES100 particle in low electrolyte solutions 48

Table 2.7 Calculated parameters A^* and W for the van der Waals attraction 52

Table 2.8 Calculated $\Psi_{particle}$ (mV) for probe particles as a function of ion concentration 56

Table 3.1. Debye screening length for solutions used to measure roughness effects on the depletion interaction. All solutions were 0.5 mM sodium phosphate buffer. 72

Table 3.2 Calculated gravitational force and diameter of particles treated with varying concentrations of acetone..... 74

Table 3.3 Fitted Debye length, surface potentials for the colloidal particle and glass slide in the depletant-free system (pH 6.85, 0.5 mM sodium phosphate buffer) 75

Table 3.4 Fitted coupling constant A^* and characteristic decay length, W for the van der Waals interaction between the colloidal probe particle and glass slide in the depletant-free system (pH 6.85, 0.5 mM sodium phosphate buffer) 76

Table 3.5 Fitted surface potentials for the colloidal particle and glass slide in solutions with various E-S100 depletant concentrations..... 77

Table 3.6 Minimum potential energy for the colloidal particles in each of the depletant systems (pH 6.85, 0.5 mM sodium phosphate buffer)..... 79

LIST OF FIGURES

Figure 1.1. Common methods used to measure colloidal interactions: (A) SFA, (B) AFM, and (C) TIRM 3

Figure 2.1. Schematic of local surface-to-surface separation distances between two surfaces with roughness characterized by the Rms roughness, σi, around an average separation distance h. 13

Figure 2.2. Colloidal interactions between a 6.24 μm polystyrene particle and a glass slide coated with a 1 μm polystyrene film across a solution containing 1.1 mM SDS. The solid curves are predictions which consider the retarded van der Waals attraction (indicated with an arrow) and electrostatic repulsion.[12] The theoretical DLVO interactions systematically over-predict the van der Waals attraction compared to experimental data. 15

Figure 2.3. Schematic of an evanescent wave at a glass/water interface that occurs when the angle of incidence at the glass/water interface is larger than the critical angle, θc.... 19

Figure 2.4. Scheme for generating particles with varying degrees of surface roughness 21

Figure 2.5. Amine-functionalized polystyrene particles (a) prior to E-S100 particle deposition and E-S100 coated amine-functionalized particles exposed to solutions containing (b) 10%, (c) 30%, (d) 40%, (e) 50%, and (f) 70% acetone. Scale bars represent 500 nm. 23

Figure 2.6. Rough particles treated with (A) 10% and (C) 30% acetone solutions have similar surface topography as substrates treated with (B) 10% and (D) 30% acetone solutions, respectively. However, particles treated with (E) 50% acetone look more similar to substrates treated with (F) 35% acetone. Both particles treated with (G) 70% acetone and substrates treated with (H) 60% acetone solutions looks smooth. Scale bars correspond to 500 nm. 25

Figure 2.7. Schematic of the counter-ions surrounding a charged surface and the location of the shear plane. The zeta potential, ζ, is the electric potential, Ψ, measured at the shear plane and is an approximation of the surface potential. 26

Figure 2.8. Zeta potential measurements of particles exposed to 10, 30, 50, and 70% acetone solutions. Lines are meant to guide the eye. 27

Figure 2.9. Isoelectric points of E-S100 particle dispersion and dispersions of AFP-ES100 particles exposed to 10, 30, 50, and 70% acetone solutions. Error bars represent the root–mean square error of the cubic spline fit. 28

Figure 2.10. Schematic of TIRM set-up. The He:Ne laser (λ = 632.8 nm) is used to generate the evanescent wave. The He:Ne laser is positioned so it is normal to the

air/prism interface, ensuring the incidence angle at the glass/water interface (θi) is 70°. The intensity of light scattered by a particle impinging on the evanescent wave is measured using a photomultiplier tube (PMT) and visualized using a CCD camera. An Nd:YAG laser (λ = 532 nm) is used to generate the two-dimensional optical trap. Not drawn to scale. 29

Figure 2.11. 2.2 μm polystyrene particles in water illuminated with an evanescent wave (red). Particles that are closer to the bottom of the TIRM cell scatter more of the evanescent wave, resulting in the appearance of a brighter red light. 30

Figure 2.12. Schematic of the TIRM cell. (a) The measurement cell consists of a 1 mm rubber spacer sandwiched between two glass slides. The bottom slide is optically coupled to the dovetail prism using immersion oil. Two additional rubber spaces are used to sandwich the measurement cell into the (b) TIRM sample cell..... 32

Figure 2.13. (A) Scattering intensity data for a 6 μm polystyrene particle in low salt solution is converted into (B) a histogram of the scattering intensities. (C) Using **Equation 2.18**, the probability distribution of the scattering intensities is determined, and (D) are converted to a relative potential energy curve using **Equation 2.19**. 35

Figure 2.14. DLVO interactions for particles with varying degrees of surface roughness. The measurement was taken in a 1:1 electrolyte solution at pH 6. (A) The particle elevation decreases with increasing salt concentration, indicating a suppression of the electrostatic double layer repulsion for a particle treated with 50% acetone. (B) In a 3 mM salt concentration the particle-plate separation distances increases and the van der Waals attactive interaction becomes progressively weaker with increasing particle surface roughness. 37

Figure 2.15. Potential energy profile for a particle in 0.1 mM electrolyte solution. (a) The gravitational fit results in a 48.4 fN gravitational energy. (b) Once the gravitational energy has been removed, the DLVO interaction energy remains. 38

Figure 2.16. The electrostatic repulsive interaction for a (smooth) AFP-ES100 particle treated with 70% acetone in 0.1 mM (purple symbols) and 0.25 mM (blue symbols) 1:1 electrolyte solution at pH 6. The fitted Debye length is shown in black and the theoretical Debye length is shown in red..... 40

Figure 2.17. Zeta potential measurements for AFP-ES100 particles in a NaCl solution at pH 6 as a function of salt concentration (A) for particles with varying degrees of surface roughness and (B) the average zeta potentials of all the particles at a given salt concentration..... 41

Figure 2.18. DLVO fits for particle-plate interactions for a smooth particle in a 1:1 electrolyte at pH 6. The fits describe the interaction energy but result in physically impossible surface potentials, particularly in higher ionic strength solutions..... 44

Figure 2.19. The electrostatic repulsion exerted on a AFP-ES100 particle treated with 50% acetone in 0.1 mM (purple symbols) and 0.25 mM (blue symbols) 1:1 electrolyte solution at pH 6. The fitted Debye length is shown in black and the theoretical Debye length is shown in red. An SEM image of the particle is also shown (scale bar corresponds to 500 nm)..... 45

Figure 2.20. Experimental and fitted DLVO interactions for (A) a smooth particle-plate interaction. The particle was treated with 70% acetone. The fits work well for low ionic strength solutions but fail to describe particle-plate interactions in 1 mM electrolyte solution. (B) The fitted parameters completely fail to describe the DLVO interactions for a rough particle treated with 10% acetone. All measurements were taken in a 1:1 electrolyte solution at pH 6..... 47

Figure 2.21. Assuming surface roughness results in an offset in both the electrostatic and van der Waals attraction results in adequate fits of the (A) smooth particles but (B) fails to describe the van der Waals attraction at higher salt concentrations (orange triangles) if the particle surface has any degree of surface roughness (surfaces treated with 50% acetone). Measurements were taken in a 1:1 electrolyte at pH 6..... 48

Figure 2.22. Particle-plate interaction energy curves in a 1:1 electrolyte at pH 6 near the onset of the van der Waals attraction. The red line is used to guide the eye. Rather than provide a rigorous model, the data shows the growing importance of the van der Waals attraction as particle-plate separations decrease and qualitatively indicates the van der Waals attraction at a given separation distance is insensitive to salt concentration. 49

Figure 2.23. The calculated Debye length as a function of salt concentration and particle roughness. κ^{-1} increases systematically with increasing surface roughness and decreases with increasing salt concentration. For smooth particles the fitted apparent Debye length agrees very well with the theoretical expectation for a solution of the given electrolyte composition, but for very rough particles (treated with 10% (□) and 30% (◇) acetone), the apparent Debye length is at least 150% of the expected value. 51

Figure 2.24. Assuming an exponentially decaying van der Waals interaction, an offset in the electrostatic interaction due to surface roughness, and a roughness-dependent Debye length result in good fits for (A) smooth particles, and particles treated with (B) 50%, (C) 30% and (D) 10% acetone. 52

Figure 2.25. The calculated (A) Debye length and (B) mean Rms roughness. The Debye length appears to be only dependent on solution conditions and the mean Rms roughness decreases systematically with surface smoothing..... 54

Figure 2.26 Assuming an exponentially decaying van der Waals interaction and normalizing the interacting surfaces when calculating the electrostatic interaction resulted in in good fits for (A) smooth particles (treated with 70% acetone), and particles treated with (B) 50%, (C) 30% and (D) 10% acetone. 56

Figure 3.1. Schematic of a large particle with radius R and plate in a dilute depletant solution, where the depletant radius is α. The overlap volume is indicated in red..... 65

Figure 3.2. Measured potential curves (symbols) of a polystyrene sphere as a function of its distance *z* from a flat surface in poly(ethylene oxide) (PEO) concentrations of (A) $n = 0$, (B) $n = 7.6\mu m - 3$, (C) $n = 10.2\ \mu m - 3$, (D) $n = 12.7\ \mu m - 3$, and (E) $n = 25.5\ \mu m - 3$. The solid lines are predicted interaction energy, Φ_{total}, where $\Phi_{total} = \Phi_{grav} + \Phi_{edl} + \Phi_{dep}$.[6] 67

Figure 3.3. In a 0.5 mM sodium phosphate buffer at pH 6.85, the presence of surface roughness increases the particle-plate separation distance and weakens the van der Waals attraction. The smoothest particle (○) is the closet to the glass plate and has the deepest attractive well. While the roughest particle (◇), whose surface roughness is characterized by discrete spherical asperities samples similar particle elevations as the particle characterized by sinusoidal asperities (Δ), the attractive well (due to van der Waals interaction) is deeper for the smoother of the two particles..... 75

Figure 3.4. The fitted Rms roughness for particles treated with 30% (◇), 50% (△), and 70% (○) acetone in a 0.5 mM sodium phosphate buffer system without any depletants, 0.3% v/v E-S100, and 0.57% v/v E-S100. The Rms roughness for rough particles was larger than that for the smooth particle. 77

Figure 3.5. Depletant-mediated interaction for a smooth particle (70% acetone) in 0.5 mM phosphate buffer when the depletant concentration is 0% v/v (black symbols), 0.3% v/v (green symbols), and 0.57% v/v (red symbols). The depth of the attractive well increases noticeably as the depletant concentration increases. 78

Figure 3.6. Depletant-mediated interaction for a particle treated (A) with 30% acetone, and (B) with 50% acetone when the depletant concentration is 0% v/v (black symbols), 0.3% v/v (green symbols), and 0.57% v/v (red symbols). Both measurements were taken in 0.5 mM phosphate buffer solution. 79

Figure 3.7. Depletant-mediated interactions and fitted interaction energy curves for a particle treated (A) 30% acetone, (B) 50% acetone, and (C) 70% acetone when the depletant concentration in 0% v/v (black symbols), 0.3% v/v (green symbols), and 0.57% v/v (red symbols). All measurements were taken in 0.5 mM phosphate buffer solution. 81

Figure 3.8. Relaxing the constraints for the apparent depletant size resulted in better fitted interaction energy curves to experimental data for a particle treated 70% acetone when the depletant concentration in 0% v/v (black symbols), 0.3% v/v (green symbols), and 0.57% v/v (red symbols). All measurements were taken in 0.5 mM phosphate buffer solution..... 82

Figure 3.9. The apparent depletant size, α^*, decreases with increasing E-S100 concentration and at a given depletant concentration, increases as surface roughness increases. 84

Figure 3.10. In general, the osmotic pressure increases with E-S100 concentration but is much larger than expected and has a maximum at 0.3% v/v E-S100 for the particle treated with 50% acetone (Δ)..... 85

Figure 3.11. Depletant-mediated interactions for particles treated with 30% (◇), 50% (△), and 70% (○) acetone in 0.57% v/v E-S100. A small oscillation is visible for rough particles but is not as clear for the smooth particle..... 86

Figure 3.12. The depletant-mediated interaction energy curve for particles treated with 30% (◇), 50% (△), and 70% (○) acetone measured in 0.57% v/v E-S100 solution in 0.5 mM sodium phosphate buffer. The curves have all been normalized by the relative separation distance, h-h_m and indicate a collapse of the oscillation..... 87

Figure 3.13. Depletant-mediated interaction curves for two particles treated with 70% acetone. For (A) one particular particle, depletants increased the particle-plate attraction but did not influence the electrostatic repulsion, whereas for (B) another particle, the addition of depletants appeared to simultaneously suppress the electrostatic repulsion and increase the particle-plate interaction energy. 88

LIST OF SYMBOLS AND ABBREVIATIONS

A	Hamaker constant
$A(h)$	Hamaker function
A^*	van der Waals attraction prefactor
B	electrostatic coupling constant
c_i	concentration of species i
D	electrostatic repulsion offset
e	elementary charge
$F(h)$	interaction force at distance, h
g	gravitational acceleration
h	particle elevation/particle-plate separation distance
h_m	particle elevation corresponding to minimum potential energy
I_m	most sampled intensity
$I(h)$	scattering intensity at distance h from glass/water interface
I_0	scattering intensity at glass/water interface
k	Boltzmann constant
L	van der Waals attraction offset
m	particle mass
n	number density
N_A	Avagadro's constant
n_i	refractive index of material i
$N(I)$	number of observations of scattering intensity, I
$N(I_m)$	number of observations of for most sampled intensity bin
$p(h)$	probability of finding a particle at elevation h

$P(I)$	probability of observing intensity I
$P(I)\mathrm{d}I$	scattering intensity interval
Q	normalization constant
R	particle radius
R_{eff}	effective radius
R_i	radius of curvature for surface i
s	depletant radius multiplier
T	temperature (K)
U_{flat}	interaction energy per unit area between two infinite parallel plates
$V_{overlap}$	overlap volume
W	van der Waals decay length
z_i	charge of species i
α	depletant radius
α^*	apparent depletant radius
$\Delta\Pi$	osmotic pressure
ε_r	dielectric constant of solution
ε_0	vacuum permittivity
ζ-potential	zeta potential
θ_c	critical angle
θ_i	angle of incidence
κ^{-1}	Debye length
$(\kappa^*)^{-1}$	apparent Debye length
λ	wavelength of light
λ_c	electric oscillation factor

ξ^{-1}	evanescent wave decay length
ρ_f	fluid density
ρ_s	particle density
σ_m	mean Rms roughness
σ_i	standard deviation
σ_1	Rms roughness of surface 1
σ_2	Rms roughness of surface 2
Φ_{dep}	depletion interaction energy
Φ_{edl}	electrostatic double layer potential energy
Φ_{grav}	gravitational energy
Φ_{total}	total potential energy
Φ_{vdw}	van der Waals potential energy
$\Phi(h)$	interaction energy
Ψ_i	surface potential of substrate i

AFM	atomic force microscopy
AFP-ES100	coated amine-functionalized polystyrene
AO potential	Asakura-Oosawa potential
DLVO theory	Derjaguin-Laudau-Verwey-Overbeek theory
E-S100	Eudragit S-100
IEP	isoelectric point
He:Ne	helium-neon
NaH_2PO_4	monobasic sodium phosphate
Na_2HPO_4	dibasic sodium phosphate
Nd:YAG	neodymium-doped yttrium aluminium garnet

PMT	photomultiplier tube
Rms	root mean square
SDS	sodium dodecyl sulfate
SEM	scanning electron microscopy
SFA	surface force apparatus
TIRM	total internal reflection microscopy

SUMMARY

The stability of colloidal dispersions is important for many industrial applications. The effects of surface roughness on colloidal stability are well documented but are less well understood. Theoretical descriptions of roughness effects often do not match experimental results, in part because experimental methods used to vary surface topography simultaneously change the surface chemistry**.** The present study sought to experimentally isolate surface roughness effects on colloidal interactions, specifically by examining how surface roughness modulates the electrostatic interaction, van der Waals interaction and depletion interaction.

Roughness effects on these interactions were determined by measuring particle-plate interactions using colloidal probe particles with varied surface topography but similar surface chemistry. Rough particles were generated via the adsorption of chemically homogenous, negatively charged nanoparticles onto positively functionalized microparticles. Surface topography was tuned using a solvent-based method that partially dissolved and molecularly re-deposited polymers onto the core particle, progressively smoothing particles initially covered with spherical asperities to generate chemically uniform particle coatings characterized either still by spherical roughness features, or by roughly sinusoidal surface undulations, or by smooth surfaces. The effectiveness of the technique was determined through characterization of surface topography and of the isoelectric point of the modified particles, which is sensitive to changes in surface chemistry.

Total internal reflection microscopy (TIRM), a sensitive force measurement technique, was used to experimentally quantify the interactions of a colloidal probe particle with surface roughness and a flat glass substrate. The experiments provide the first set of benchmark studies that isolate the effect of surface topography on different interactions between colloidal bodies.

Measurements of the electrostatic and van der Waals interaction were taken using probe particles with varying degrees of surface roughness in a monovalent electrolyte. Qualitatively, the data indicated a weakening of the van der Waals attraction with increasing surface roughness.

Effects of roughness were quantified through its influence on the parameters used to characterize the electrostatic repulsion and van der Waals attraction. The van der Waals attraction was described as an exponentially decaying interaction using a purely empirical equation. The characteristic decay length and the prefactor to the exponential, which can be interpreted as a form of the Hamaker constant, varied systematically with surface roughness and supported the qualitative observation that the van der Waals attraction was suppressed with increasing surface roughness. Best fits to the electrostatic repulsion were obtained assuming a normal distribution of surface-to-surface separation distances with a standard deviation dependent on the Rms roughness of the two interacting surfaces, which indicates that surface roughness also influences the electrostatic repulsion in addition to the van der Waals attraction. The model provides excellent fits to the data and indicates that increasing surface roughness enhances the electrostatic repulsion. Regardless of salt concentration, the fitted Rms roughness correlates with the prepared surface roughness of the probe particles. However, the model

yields improbably low surface potentials and unrealistically large fitted surface roughness that decreases monotonically with increasing salt concentration.

While there are some uncertainties in the observed effects of roughness that will be due to particle-to-particle variability, we have experimentally demonstrated the robustness of several DLVO phenomena. This study showed that regardless of surface roughness, increasing the ionic strength of solution screened the electrostatic repulsion between interacting surfaces. This study was the first of its kind to qualitatively show the suppression of the van der Waals attraction as particle surface roughness is increased, a phenomena that is expected but has never been demonstrated using particles with variable surface topography but similar surface chemistry.

Roughness effects on the depletion interaction were determined by measuring depletant-mediated interactions for three particles with varying degrees of surface roughness. Qualitatively, increasing surface roughness was shown to suppress the depletion interaction, a phenomenon that has been predicted theoretically and has been shown for particles with varying surface chemistry and topography, but never for particles that differed only in surface topography.

Effects of surface roughness were quantified using the van der Waals attraction, electrostatic repulsion, and depletion potential. The DLVO parameters were determined using the models that best fit experimental data in the depletant-free system. The van der Waals parameters (the characteristic decay length and the prefactor to the exponential) were the same order of magnitude and followed similar roughness-dependent trends as parameters for the monoelectrolyte (1:1) system. The electrostatic repulsion was fit assuming a normal distribution of surface-to-surface separation distances. The fitted Rms

roughness was smaller for heavily smoothed particles than for particles designed to be rough.

The experimental data for depletion interaction were used to fit model expressions recommended for the case of highly charged nanoparticle depletants. While such fits worked well for rough probe particles, they under-predicted the attractive interaction and over-predicted the range of interaction for the smoothest probe particles, which also sample the smallest separations from the substrate. These discrepancies were tentatively credited to a partial loss of depletant charge in the gap region between particle and substrate via charge regulation.

Only one particle for each degree of surface smoothing was used to determine the depletion interaction fit parameters. The trends and fit parameters obtained here may not be sufficiently representative. Ultimately, more data are needed to allow for reliable quantitative conclusions regarding roughness effects on the depletion interaction.

This work was the first to experimentally combined roughness control with depletant-mediated interactions using depletants with the same surface chemistry and characteristic length scale as the particle roughness features. Although particle-to-particle variability needs to be taken into account when quantifying the extent that surface roughness influences the depletion interaction, results showed rather robustly that regardless of surface roughness, the addition of depletants results in an additional attractive force on the colloidal interaction. Furthermore, increasing the surface roughness reduced the strength of the depletion interaction, as expected theoretically, but has never measured when only surface roughness was varied.

This present experimental work demonstrates the influence of surface topography on the DLVO and depletion interactions. The data collected here will hopefully contribute a useful benchmark for future, improved models of colloidal interactions modulated by surface roughness.

CHAPTER 1

INTRODUCTION

Colloidal interactions are ubiquitous in nature and in many industries; particle aggregation and deposition in aqueous media play an important role in many processes, *e.g.*, membrane fouling in water filtration, dispersion destabilization, and the formation of river deltas.[1-4] Controlling particle stability in heterogeneous suspensions of differently-sized particles has been used for flocculation-based separation techniques and the self-assembly of colloidal macrostructures and colloidal crystals.[5-7] The topography of interacting surfaces and particles can greatly influence the observed colloidal stability. For example, the surface topography of interacting membranes and particles can greatly affect the rate of particle deposition and entrapment.[8, 9] However, no study has systematically isolated roughness effects on colloidal interactions.

1.1 Measurement of colloidal forces

There are several well-established techniques to measure colloidal forces: the surface force apparatus (SFA), atomic force microscopy (AFM), and total internal reflection microscopy (TIRM).[10-16]

The surface force apparatus directly measures the force between two surfaces immersed in vapor or a liquid medium. The technique relies on using force-measuring springs to bring two crossed cylinders, covered with molecularly smooth mica, close together (**Figure 1.1A**) while monitoring the surface separation interferometrically. The technique is able to resolve vertical separation distances as small as 0.1 nm, and has been

used to measure van der Waals forces, capillary forces, and adhesion forces, among others. The ability to observe Ångström separation distances also makes it possible to observe very short-range forces, such as solvent and structural forces. However, SFA is limited by the stiffness of the springs used to bring the crossed cylinders in close contact and is only able to resolve forces in the nanoNewton (10^{-8} N) range.[17, 18]

Force measurements by atomic force microscopy are similar to SFA measurements, but rather than measuring forces between two crossed cylinders, interaction forces are measured between a fine tip or particle attached to the end of a cantilever and a surface (**Figure 1.1B**).[11] Like SFA, measurements can be taken in vapor or a liquid medium, and many of the same forces can be resolved. Compared to the forces between two macroscopic surfaces measured in SFA, the forces probed by AFM are much smaller (in the picoNewton range).[11, 18] Even smaller inter-particle forces determine the stability of colloidal dispersions, but such weak interactions cannot be resolved by AFM, whose sensitivity is limited by the spring constant of the cantilever.

Total internal reflection microscopy can be described as "AFM without a cantilever". In TIRM, a particle is suspended freely in a liquid medium (of lower density than the particle) above a glass plate. The particle will settle toward the glass plate due to gravity, but will remain suspended above the plate due to repulsive colloidal forces (**Figure 1.1C**).[12] Unlike SFA or AFM, techniques that directly measure interaction forces, TIRM uses particle elevations to calculate interaction energies. TIRM is not as sensitive to separation distances as AFM or SFA and is unable to accurately probe strong, attractive forces. However, because the technique is not limited by a spring constant, it is

possible to probe femtoNewton forces (10^{-14} N) with TIRM.[18] A comparison of all three techniques is shown in **Table 1.1**.

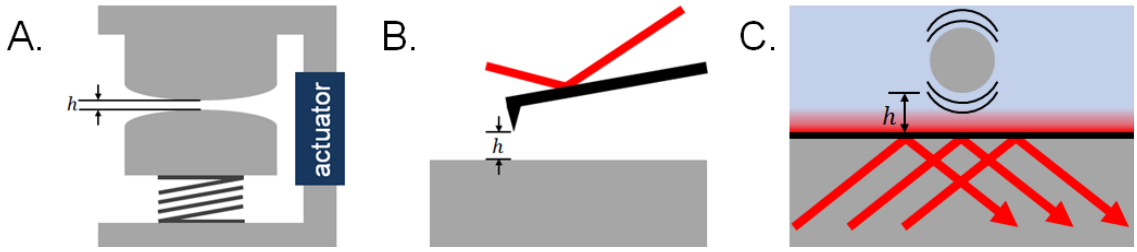

Figure 1.1. Common methods used to measure colloidal interactions: (A) SFA, (B) AFM, and (C) TIRM

Table 1.1 Comparison of distance and force resolution of SFA, AFM, and TIRM[18]

Technique	Vertical distance resolution (nm)	Force resolution (N)
SFA	0.1	10^{-8}
AFM	0.1	10^{-11}
TIRM	1	10^{-14}

Surface roughness on the nanometer scale influence interaction energies by fractions of kT (10^{-21} J) and influence both long and short range colloidal interactions.[19, 20] Consequently, it is more important to consider force resolution than distance resolution when measuring roughness effects. In this study, TIRM was used to probe the influence of nanoscale roughness on colloidal interactions.

1.2 DLVO interactions

The Derjaguin-Landau-Verwey-Overbeek (DLVO) theory is used to describe the aggregation of electrically charged colloidal particles in liquid media.[21, 22] Colloidal stability can only be maintained in a particle dispersion, when the ubiquitous van der Waals attraction is offset by repulsive particle interactions that result in an energy barrier between the particles that is too large to be overcome, on the timescale of interest, by thermal activation. In the case of charge-stabilized dispersions, the necessary repulsion

arises primarily from the electrostatic interaction between the charged particle surfaces, mediated by free ions in the surrounding solution. Classical DLVO theory describes the balance of van der Waals interaction and electrostatics, described at the mean-field level, without considering any non-idealities or additional types of interaction. It is by far the most widely used model of colloidal interactions and has been able to explain many qualitative features of colloidal stability, but often fails to predict interaction forces or aggregation rates quantitatively.[1]

The inherent roughness of almost all solid surfaces is among the most commonly cited factors used to explain the discrepancies between theoretical predictions of DLVO-type interactions and experimental observations.[23] Surface roughness has been accounted for via modification of the geometry[9, 19, 24, 25] as well as the physical properties of the interacting surfaces,[20, 26-28] but it is still difficult to quantitatively predict experimental observations.

Experimental isolation of roughness effects has also been traditionally difficult. Surface roughness is often experimentally varied using additive methods, *e.g.* coating colloidal particles with polymer dendrimers or nanoscale particles.[28, 29] Additive methods that vary surface roughness simultaneously change surface topography and surface chemistry, making it difficult to separate one cause from the other. Subtractive methods such as selective etching have also been used and are equally prone to changing surface chemistry.[30] The adsorption of dendrimers to vary surface roughness can also introduce non-DLVO interactions, such as hydrophobic attraction or steric repulsion.[29]

1.3 Depletion interactions

Depletion interaction occurs when two large interacting surfaces, *e.g.* the surfaces of large colloidal particles or of a large particle and a substrate, face each other in in the presence of macromolecules or small particles, called depletants. The osmotic pressure exerted by the small particles produces a net attractive force between the two large surfaces when the gap between them becomes too narrow to accommodate the depletants. This entropically driven force has been exploited to induce particle flocculation and colloidal self-assembly, among other phenomena. [5-7, 15] At high depletant concentration, the spatial ordering ("liquid structure") of depletants in gaps accommodating only a few depletant layers gives rise to oscillatory forces between the confining surfaces.[31, 32] These oscillatory forces may be thought of as a depletant-scale analogue of the so-called "structural forces" observed between atomically smooth surfaces with SFA and credited to the ordering of solvent molecules in gaps small enough to fit in only a few discrete solvent layers.[33] The oscillatory structural forces are known to be suppressed when the confining surfaces are rough, because the rough surfaces do not promote the ordering of solvent molecules in discrete layers.[18] By extension one might expect that the ordering of depletants can be suppressed by surface roughness on the length scale of the depletants, but to our knowledge this has not yet been shown.

Roughness effects on depletion interactions are also of particular interest because variations in surface topography have been used to control depletant-driven self-assembly.[6, 7] Surface roughness is known to decrease the depletion attraction.[7, 34] The extent to which surface roughness influences the depletion interaction, however, is less clear. Many methods used to generate particles with varying degrees of surface

roughness, such as dumbbell structures with rough and smooth poles, or platelets with roughened sides, vary the surface chemistry in addition to surface topography. Removing surface chemistry-based interactions between depletants and the probe particle has rarely been studied: the depletants used to drive the attractive force are often chemically different from the colloidal particles and are often smaller than the length scale of roughness features on the colloidal particle.[14, 35, 36] To our knowledge, no study has yet isolated the role of surface roughness for the depletion interaction when the depletants have the same surface chemistry and characteristic length scale as the roughness features.

1.4 Objectives

This study examines the extent of surface roughness effects on both DLVO and depletion interactions in aqueous media. Colloidal particle surfaces and depletant particles were prepared with a chemically homogeneous polymer, and surface topography was tuned using a smoothing method previously developed in our group that combines particle erosion by polymer dissolution with molecular re-deposition and plasticization/film formation. The success of the smoothing procedure was verified using several characterization techniques. Colloidal interactions were measured using total internal reflection microscopy (TIRM) and roughness effects were quantified using DLVO parameters and the depletion interaction potential.

1.5 References

1. D. F. Evans and H. Wennerström, *The Colloidal Domain: Where Physics, Chemistry, Biology, and Technology Meet, 2nd Edition*, Wiley-VCH, New York, NY, 1999.

2. S. Bhattacharjee and M. Elimelech, Surface element integration: a novel technique for evaluation of DLVO interaction between a particle and a flat plate. *J. Colloid Interface Sci.*, 1997, **193**, 273-285.

3. D. P. Jaisi, S. Ji, H. Dong, R. E. Blake, D. D. Eberl and J. Kim, Role of microbial Fe (III) reduction and solution chemistry in aggregation and settling of suspended particles in the Mississippi River delta plain, Louisiana, USA. *Clays Clay Miner.*, 2008, **56**, 416-428.

4. C. Shen, B. Li, C. Wang, Y. Huang and Y. Jin, Surface roughness effect on deposition of nano-and micro-sized colloids in saturated columns at different solution ionic strengths. *Vadose Zone Journal*, 2011, **10**, 1071-1081.

5. S. Ji and J. Y. Walz, Depletion forces and flocculation with surfactants, polymers and particles — Synergistic effects. *Curr. Opin. Colloid Interface Sci.*, 2015, **20**, 39-45.

6. K. Zhao and T. G. Mason, Directing colloidal self-assembly through roughness-controlled depletion attractions. *Phys. Rev. Lett.*, 2007, **99**, 268301.

7. S. Badaire, C. Cottin-Bizonne and A. D. Stroock, Experimental investigation of selective colloidal interactions controlled by shape, surface roughness, and steric layers. *Langmuir*, 2008, **24**, 11451-11463.

8. G. K. Darbha, T. Schäfer, F. Heberling, A. Lüttge and C. Fischer, Retention of latex colloids on calcite as a function of surface roughness and topography. *Langmuir*, 2010, **26**, 4743-4752.

9. E. M. V. Hoek, S. Bhattacharjee and M. Elimelech, Effect of Membrane Surface Roughness on Colloid−Membrane DLVO Interactions. *Langmuir*, 2003, **19**, 4836-4847.

10. J. Israelachvili, Y. Min, M. Akbulut, A. Alig, G. Carver, W. Greene, K. Kristiansen, E. Meyer, N. Pesika, K. Rosenberg and H. Zeng, Recent advances in the surface forces apparatus (SFA) technique. *Rep. Prog. Phys.*, 2010, **73**, 036601.

11. G. Binnig, C. F. Quate and C. Gerber, Atomic force microscope. *Phys. Rev. Lett.*, 1986, **56**, 930.

12. D. C. Prieve and N. A. Frej, Total internal reflection microscopy: a quantitative tool for the measurement of colloidal forces. *Langmuir*, 1990, **6**, 396-403.

13. M. Piech and J. Y. Walz, Depletion interactions produced by nonadsorbing charged and uncharged spheroids. *J. Colloid Interface Sci.*, 2000, **232**, 86-101.

14. D. Rudhardt, C. Bechinger and P. Leiderer, Direct measurement of depletion potentials in mixtures of colloids and nonionic polymers. *Phys Rev Lett*, 1998, **81**, 1330.

15. T. D. Edwards and M. A. Bevan, Depletion-Mediated Potentials and Phase Behavior for Micelles, Macromolecules, Nanoparticles, and Hydrogel Particles. *Langmuir*, 2012, **28**, 13816-13823.

16. S. Biggs, R. R. Dagastine and D. C. Prieve, Oscillatory packing and depletion of polyelectrolyte molecules at an oxide-water interface. *J. Phys. Chem. B*, 2002, **106**, 11557-11564.

17. J. N. Israelachvili and G. E. Adams, Measurement of forces between two mica surfaces in aqueous electrolyte solutions in the range 0–100 nm. *J. Chem. Soc., Faraday Trans. 1*, 1978, **74**, 975-1001.

18. J. N. Israelachvili, *Intermolecular and surface forces: revised third edition*, Academic press, 2011.

19. J. Y. Walz, L. Suresh and M. Piech, The effect of nanoscale roughness on long range interaction forces. *J. Nanopart. Res.*, 1999, **1**, 99-113.

20. M. A. Bevan and D. C. Prieve, Direct measurement of retarded van der Waals attraction. *Langmuir*, 1999, **15**, 7925-7936.

21. B. Derjaguin and L. Landau, Theory of the stability of strongly charged lyophobic sols and of the adhesion of strongly charged particles in solutions of electrolytes. *Acta Phys. Chim.*, 1941, **14**, 633-662.

22. E. Verwey and J. T. G. Overbeek, *Theory of Stability of Lyophobic Solids*, Elsevier, Amsterdam, 1948.

23. X. Huang, S. Bhattacharjee and E. M. Hoek, Is Surface Roughness a “Scapegoat” or a Primary Factor When Defining Particle− Substrate Interactions? *Langmuir*, 2009, **26**, 2528-2537.

24. D. F. Parsons, R. B. Walsh and V. S. Craig, Surface forces: Surface roughness in theory and experiment. *J. Chem. Phys.*, 2014, **140**, 164701.

25. L. Suresh and J. Y. Walz, Direct measurement of the effect of surface roughness on the colloidal forces between a particle and flat plate. *J. Colloid Interface Sci.*, 1997, **196**, 177-190.

26. J. L. Bitter, G. A. Duncan, D. J. Beltran-Villegas, D. H. Fairbrother and M. A. Bevan, Anomalous Silica Colloid Stability and Gel Layer Mediated Interactions. *Langmuir*, 2013, **29**, 8835-8844.

27. R. R. Dagastine, M. Bevan, L. R. White and D. C. Prieve, Calculation of van der Waals forces with diffuse coatings: Applications to roughness and adsorbed polymers. *J. Adhesion*, 2004, **80**, 365-394.

28. S. Rentsch, R. Pericet-Camara, G. Papastavrou and M. Borkovec, Probing the validity of the Derjaguin approximation for heterogeneous colloidal particles. *Phys. Chem. Chem. Phys.*, 2006, **8**, 2531-2538.

29. X. Gong, Z. Wang and T. Ngai, Direct measurements of particle–surface interactions in aqueous solutions with total internal reflection microscopy. *Chem. Commun.*, 2014, **50**, 6556-6570.

30. L. Li, V. Breedveld and D. W. Hess, Design and fabrication of superamphiphobic paper surfaces. *ACS Appl. Mater. Interfaces*, 2013, **5**, 5381-5386.

31. S. Ji and J. Y. Walz, Depletion Flocculation Induced by Synergistic Effects of Nanoparticles and Polymers. *J. Phys. Chem. B*, 2013, **117**, 16602-16609.

32. C. Bechinger, D. Rudhardt, P. Leiderer, R. Roth and S. Dietrich, Understanding depletion forces beyond entropy. *Phys. Rev. Lett.*, 1999, **83**, 3960.

33. J. N. Israelachvili and P. M. McGuiggan, Forces between surfaces in liquids. *Science*, 1988, **241**, 795-800.

34. E. Barry and Z. Dogic, Entropy driven self-assembly of nonamphiphilic colloidal membranes. *PNAS*, 2010, **107**, 10348-10353.

35. K. Zhao and T. G. Mason, Suppressing and enhancing depletion attractions between surfaces roughened by asperities. *Phys. Rev. Lett.*, 2008, **101**, 148301.

36. L. Helden, G. H. Koenderink, P. Leiderer and C. Bechinger, Depletion potentials induced by charged colloidal rods. *Langmuir*, 2004, **20**, 5662-5665.

CHAPTER 2

SURFACE ROUGHNESS EFFECTS ON DLVO INTERACTIONS

2.1 Background

Colloidal particles in an electrolyte solution in close proximity with other particles or surfaces interact with a particular energy that is dependent on their proximity to other surfaces. The total interaction energy felt by the particle, Φ_{total}, is the sum of three components: the gravitational attraction, Φ_{grav}, the electrostatic double layer repulsion. Φ_{edl}, and the van der Waals attraction, Φ_{vdw}:

$$\Phi_{total} = \Phi_{grav} + \Phi_{edl} + \Phi_{vdw} \quad 2.1$$

where $\Phi_{edl} + \Phi_{vdw}$ comprises the Derjaguin-Laudau-Verwey-Overbeek (DLVO) contribution.[1, 2] In this study, we will discuss interactions in the context of a spherical particle interacting with a glass plate.

2.1.1 Gravitational attraction

The gravitational contribution at a particle elevation h is given by:

$$\Phi_{grav}(h) = mgh = \frac{4}{3}\pi R^3(\rho_s - \rho_f)gh \quad 2.2$$

where is m the particle mass and g is 9.81 m/s^2. For practical purposes, the buoyancy-corrected particle mass is often described using the particle volume, $\frac{4}{3}\pi R^3$, and the difference between the particle density, ρ_s, and the solution density, ρ_f.[3]

2.1.2 The Derjaguin approximation

The simplest calculation of DLVO interactions is done for two infinitely large parallel plates. Colloidal interaction measurements done using curved surfaces (crossed-cylinder geometry in the surface force apparatus), or a sphere-plate geometry (atomic force microscopy, total internal reflection microscopy) require the interaction be calculated for the experimentally observed geometries. The Derjaguin approximation is used to relate the theoretical interaction energy per unit area between two infinite parallel plates, U(h), at a particular separation distance h to an interaction force, $F(h)$, for either a particle-plate or particle-particle geometry:

$$F_{curved}(h) = 2\pi R_{eff} U_{flat}(h) \quad 2.3$$

where the effective radius, $R_{eff} = (R_1 R_2)/(R_1 + R_2)$, and R_1 and R_2 are the radii of curvature for the interacting surfaces. In total internal reflection microscopy (TIRM), interactions are measured experimentally using a particle-plate geometry, $R_2 = \infty$, and R_{eff} is the radius of the probe particle, $R_{particle}$.[4, 5] The Derjaguin approximation is known to be reliable whenever the effective radius is large compared to the range of interaction. The electrostatic double layer force has an interaction range of several hundred nanometers and the van der Waals interaction has a range of 10-150 nm. These interaction ranges are small compared to the TIRM probe particle radii (>2.5 μm);

2.1.3 Electrostatic repulsion

For the electrolyte concentrations and separation distances measured using TIRM, the electrostatic repulsion energy between a flat plate and spherical particle across a monoelectrolyte solution can be described using the following expression:

$$\Phi_{edl}(h) = 16(4\pi\varepsilon_r\varepsilon_0)R\left(\frac{k_BT}{e}\right)^2 \tanh\left(\frac{e\Psi_1}{4kT}\right)\tanh\left(\frac{e\Psi_2}{4kT}\right)\exp(-\kappa h) \quad 2.4$$

where Ψ_i is the surface potential of surface i, κ^{-1} is the Debye length, $\varepsilon_r\varepsilon_0$ is the electric permittivity of the solvent, k is the Boltzmann constant, e is an elementary charge, and T is the temperature. For an electrolyte solution, the Debye length is given by:

$$\kappa^{-1} = \sqrt{\frac{\varepsilon_r\varepsilon_0 k_B T}{e^2 N_A \sum c_i {z_i}^2}} \quad 2.5$$

where e is the elementary charge, c_i is the concentration of the species i, z_i is the charge of species i, N_A is Avagadro's constant, ε_r is the dielectric constant, ε_0 is the vacuum permittivity, k is the Boltzmann constant, and T is the temperature. For a monoelectrolyte, *e.g.* NaCl, $\sum c_i {z_i}^2 = 2I$, where I is the ionic strength of the electrolyte. The Debye lengths for electrolyte solutions used in this study are shown in **Table 2.1**.

Table 2.1 Debye screening length for NaCl solutions used to measure roughness effects on the depletion interaction.

ionic strength (mM)	Debye length (nm^{-1})
0.1	30.3
0.25	19.2
1	9.6
3	5.6
5	4.3

Equation 2.4 is obtained by relating the interaction of curved surfaces to the interaction between flat surfaces via the Derjaguin approximation. For the interaction of the two flat surfaces with respective surface potential Ψ_i the derivation of **Equation 2.4** further assumes that the electrostatic potential in the gap between the surfaces can be approximated by superimposing solutions to the Poisson-Boltzmann equation for a single flat surface; this superposition approximation is known to work well for "weak"

interactions such as those between a substrate and a freely levitated TIRM probe particle. The electrostatic repulsion depends on the surface potentials, Ψ_i, and the Debye length, κ^{-1}. For simplicity, **Equation 2.6** is often written as:

$$\Phi_{edl}(h) = B\exp(-\kappa h) \qquad 2.6$$

where B is the electrostatic coupling constant and is used to describe the surface properties of the two interacting surfaces.

2.1.3.1 Roughness effects on electrostatic repulsion

The earliest corrections for surface roughness assumed the interacting surfaces were partially covered by hemispherical asperities, where the fractional coverage is used to "tune" the degree of surface roughness.[6, 7] More recently, the local surface-to-surface separation between two rough surfaces was considered to follow a normal distribution around an average separation distance, h, and a standard deviation characterized by the root mean square roughness of the surface, σ_i (**Figure 2.1**).[8, 9]

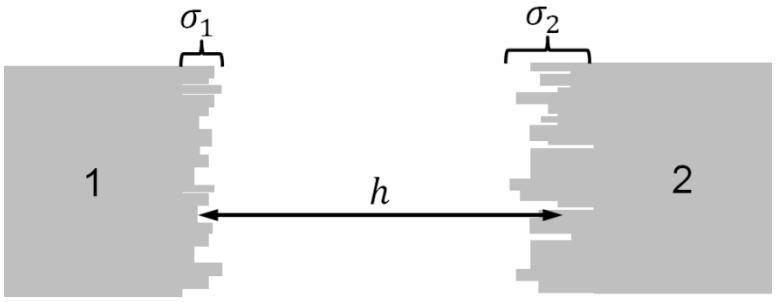

Figure 2.1. Schematic of local surface-to-surface separation distances between two surfaces with roughness characterized by the Rms roughness, σ_i, around an average separation distance *h*.

The electrostatic repulsion between two rough surfaces is then given by:

$$\Phi_{edl}(h) = \frac{B}{2}\operatorname{erfc}\left(\frac{h}{\sigma_m\sqrt{2}}\right) + \frac{B}{2}e^{-h/\kappa^{-1}}e^{{\sigma_m}^2/2(\kappa^{-1})^2}\left[1 + \operatorname{erf}\left(\frac{h - {\sigma_m}^2/\kappa^{-1}}{\sigma_m\sqrt{2}}\right)\right] \quad 2.7$$

where the mean surface roughness, σ_m, is described via the Rms roughness, σ_i, of the two interacting surfaces:

$$\sigma_m = \sqrt{{\sigma_1}^2 + {\sigma_2}^2} \quad 2.8$$

The dominant term of **Equation 2.7** indicates that surface roughness amplifies the electrostatic repulsion.

2.1.4 van der Waals attraction

The van der Waals attraction between a spherical particle and a flat plate is described by:

$$\Phi_{vdw}(h) = -\frac{A(h)R}{6h} \quad 2.9$$

where $A(h)$ is the Hamaker function, R is the particle radius, h is the particle-plate separation distance, and the Derjaguin approximation has again been used to account for the particle curvature.[10] The Hamaker function is dependent on the dielectric spectra of the interacting surfaces as well as solution properties and accounts for the distance-dependent retardation of the interaction.[11, 12] If we assume the van der Waals interaction is pairwise additive, the Hamaker function is often simplified to a single constant, the Hamaker constant, A.[13] When calculating the van der Waals attraction, pairwise additivity assumes that a molecule from one surface only interacts with a corresponding molecule on the second surface, and the total interaction is simply the sum of these paired interactions. The medium between the two surfaces is assumed to have negligible

influence on the interaction between the two surfaces.[14] While this assumption is apprproiate when two surfaces are interacting in air, but the contribution of the medium cannot be neglected when two surfaces are interacting in condensed media, *e.g.* and aqueous electrolyte.

Lifshitz theory provides a much more complete description of the van der Waals interaction. Pairwise additivity is no longer assumed; a single molecule from one surface interacts with every molecule of the second surface, and vice versa. The two surfaces, and the media in which they interact, are treated as continuous media defined by bulk properties, such as the dielectric constant or refractive index.[15] However, even the best available expressions for the Hamaker function from Lifshitz theory still over-estimate the van der Waals attraction when compared to experimental data (**Figure 2.2**).[3, 12]

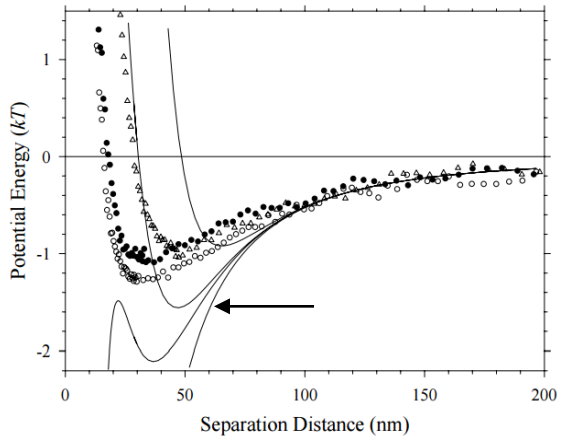

Figure 2.2. Colloidal interactions between a 6.24 μm polystyrene particle and a glass slide coated with a 1 μm polystyrene film across a solution containing 1.1 mM SDS. The solid curves are predictions which consider the retarded van der Waals attraction (indicated with an arrow) and electrostatic repulsion.[12] The theoretical DLVO interactions systematically over-predict the van der Waals attraction compared to experimental data.

Recently, a more pragmatic, semi-empirical approach has been used to describe the van der Waals attraction for colloidal bodies.[11, 16] The interaction is based on the

Lifshitz theory but assumes that the Hamaker function is dominated by the dielectric properties at a given wavelength, λ_c:

$$\Phi_{vdw}(h) = A\left\{\frac{2.45\lambda_c}{60\pi}\left(\frac{h-R}{h^2} - \frac{h+3R}{(h+2R)^2}\right)\right.$$
$$-\frac{2.17{\lambda_c}^2}{720\pi^2}\left(\frac{h-2R}{h^3} - \frac{h+4R}{(h+2R)^3}\right) \qquad 2.10$$
$$\left.+\frac{0.59{\lambda_c}^3}{5040\pi^3}\left(\frac{h-3R}{h^4} - \frac{h+5R}{(h+2R)^4}\right)\right\}$$

where λ_c, the characteristic wavelength of interaction, corresponds to the frequency in the dielectric spectrum that provides the dominant contribution to the van der Waals interaction according to Lifshitz theory. Based on previously tabulated values, the Hamaker constant, A, is assumed to be $3k_BT$ for **Equation 2.9** and **Equation 2.10**.[6, 11, 17] The characteristic wavelength of interaction for polystyrene-glass interactions across water is assumed to be 100 nm,[6, 7] but it can also be calculated via:

$$\lambda_c = 86.2 + 43.6\tanh\left[3.8\left(\log_{10}\frac{\kappa^{-1}}{nm} - 1.04\right)\right] \qquad 2.11$$

where κ^{-1} is the Debye length.[18]

2.1.4.1 Roughness effects on van der Waals attraction

The nanoscale roughness of smooth colloidal particles is usually cited as the cause for discrepancies between theoretical predictions of the van der Waals attraction and experimental data for colloidal particles interacting in aqueous electrolytes. When comparing experimental data to theoretical predictions, surface roughness is known to weaken the van der Waals attraction between interacting surfaces.[6, 7, 12, 16, 19]

The earliest corrections for surface roughness assumed the van der Waals attraction was a pairwise additive interaction whose range of interaction was affected by surface asperities modeled as hemispheres.[6, 7] The assumption of pairwise additivity is inappropriate for bodies interacting in a liquid medium. Later corrections attempted to use the complete Lifshitz theory to describe the interaction. The Lifshitz theory required knowledge of the complete dielectric spectra in order to calculate the van der Waals interaction. However, even the most complex descriptions failed to reconcile theoretical predictions with experimental results for the unmodified, smooth, colloidal particles.[12, 20, 21] Consequently, quantifying the extent that surface roughness influences the van der Waals attraction has rarely been considered.[22]

The best fits to experimental data for smooth colloidal particles have previously been obtained for the empirical equation:

$$\Phi_{vdw}(h) = -A^{*}\exp\left(\frac{-h}{W}\right) \qquad 2.12$$

where $A^{*} = 3k_{B}T$, and the decay length, W, is dependent on the two interacting surfaces.[12] The equation was based on the observation that for a smooth colloidal particle, the van der Waals interaction appeared independent of ion concentration.[12, 23] For polystyrene-glass interactions across water, W = 40 nm, while W = 50 nm for polystyrene-polystyrene interactions across water due to the increased roughness of polystyrene compared to glass.[12]

2.1.5 Experimental variations of surface roughness

Discussions regarding the effect of surface roughness are most commonly used to relate experimental results to theoretical predictions. Experimentally isolating roughness effects has been traditionally difficult, since most of the commonly used methods used to

change surface topography, *e.g.* etching or the adsorption of polymer particles onto smooth colloidal particles, also influence the surface chemisty.[24] The particles used in the comparison often have different surface chemistry in addition to varying surface topography.[21, 25, 26]

2.1.6 Total internal reflection microscopy

In this study, DLVO interactions were measured using total internal reflection microscopy (TIRM). Total internal reflection occurs when light travelling through a medium impinges on an interface with a medium of lower refractive index at an angle larger than the critical angle. The critical angle, θ_c, is described via:

$$\theta_c = \sin^{-1}\left(\frac{n_2}{n_1}\right) \qquad 2.13$$

Here, n_1 and n_2 are the refractive indices of the media on either side of the interface. In TIRM, the relevant interface is usually a glass/water boundary, where n_1 = 1.52, n_2 = 1.33, and the critical angle is 61°. When light undergoes total internal reflection, an evanescent wave is generated in the water phase.[27] The intensity of the evanescent wave, $I(h)$, decays exponentially with distance from the interface, h,:

$$I(h) = I_0 \exp(-\xi h) \qquad 2.14$$

where I_0 is intensity of the evanescent wave at the water/glass interface and ξ^{-1} is the decay length of the evanescent wave. A schematic of an evanescent wave is shown in **Figure 2.3**.

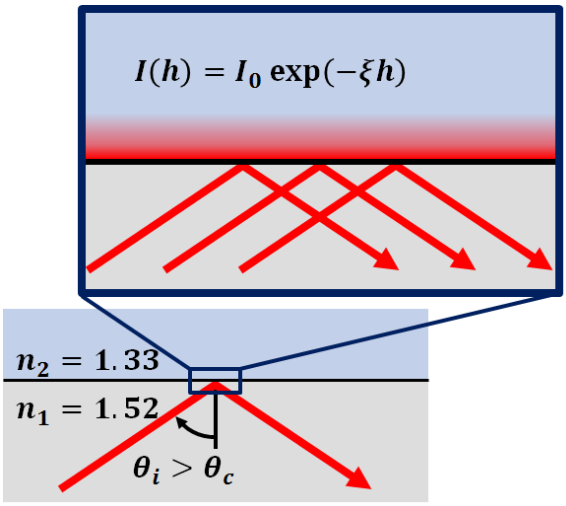

Figure 2.3. Schematic of an evanescent wave at a glass/water interface that occurs when the angle of incidence at the glass/water interface is larger than the critical angle, θ_c.

The decay length is dependent on the wavelength of light used to generate the evanescent wave, λ, the refractive indices of the two media, n_1 and n_2, and the angle in incidence, θ_i:

$$\xi^{-1} = \frac{1}{\left(\frac{4\pi}{\lambda}\sqrt{(n_1 \sin\theta_i)^2 - {n_2}^2}\right)} \qquad 2.15$$

When a particle with a refractive index different than the water settles near an interface where total internal reflection occurs, some of the evanescent wave is scattered by the particle.[27, 28] For particles smaller than 30 μm, the intensity of light scattered in any direction by the particle is exponentially dependent on the elevation of the particle from the glass/water interface, with the same characteristic decay length as the evanescent wave.[27, 29-31]

2.1.7 Optical trapping

Optical trapping uses the gradient force to drive a dielectric colloidal particle toward the electric field strength maximum in the focal point of a laser, and depends on the strength of the laser used to generate the trap and on the particle size.[32]

Optical trapping has been used to manipulate colloidal particles for a variety of purposes, such as measuring the force-extension relationship for DNA molecules and other biological phenomena, or observing lateral capillary forces at oil/water interfaces.[33-35] This study examined both long- and short-range interactions, the easiest way to observe both was to increase the salt concentration of solution. The optical trap was used to hold particles stationary while exchanging the surrounding solution.

2.2 Materials and Methods

Rough and smooth particles were fabricated using a previously described method to ensure that any changes in DLVO interactions were due to changes in surface topography only and not surface chemistry.[36, 37] Particle-plate interactions were measured using TIRM. All experiments were conducted using deionized water (Barnstead Easy Pure II System, 18.2 MΩ) in a monoelectrolyte solution.

2.2.1 E-S100 coated amine-functionalized polystyrene particle fabrication

The procedure used to fabricate rough particles is described in **Figure 2.4** and is a modification of a previously reported method.[36] Rough particles are prepared via the electrostatic adsorption of negatively charged polymer nanoparticles, prepared via nanoprecipitation, onto positively charged core particles. Rough particles are then immersed in solutions containing a volatile co-solvent that is a good solvent for the nanoparticle polymer. Solvent exposure dissolves the exposed polymer, smoothing the particle surface. The solvent extracts itself from solution over time, leading to the molecular re-deposition of dissolved polymer in a smooth film and filling in exposed areas of the underlying core particle. The degree of smoothing is dependent on the initial concentration of solvent in solution. After all the solvent in solution evaporated, any un-

adsorbed polymer material was removed from solution via rinsing of the particles and removing the supernatant.

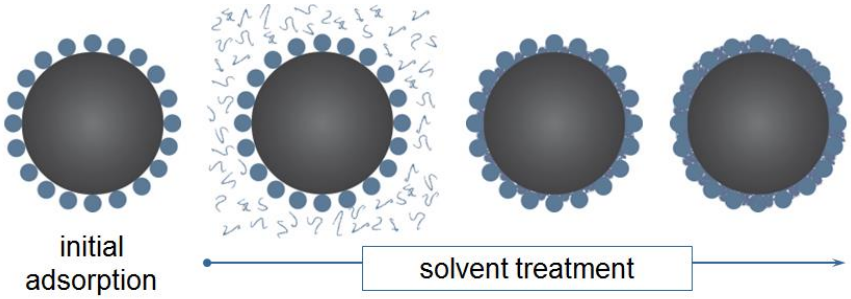

Figure 2.4. Scheme for generating particles with varying degrees of surface roughness

This method of changing particle surface topography ensured that the surface remained chemically homogeneous. Scanning electron microscopy (SEM) was used to characterize the surface topography and electrokinetic analysis (EKA) was used to characterize the surface topography.

2.2.1.1 Eudragit S100 particle fabrication

Chemically homogenous particles must be used to coat the core particles in order to ensure surface chemistry is unchanged during the solvent-based smoothing process. Eudragit S-100 (Evonik Industries AG), a copolymer of methyl methacrylate and methacrylic acid with its carboxyl groups distributed randomly throughout the polymer chain, was used to generate nanoparticles via nanoprecipitation. 0.5 g E-S100 powder was initially dissolved in 100 mL reagent alcohol. The alcohol solution was then rapidly poured into 200 mL deionized stirred at 300 rpm. Since E-S100 is insoluble in DI water, the polymer precipitated out of solution in particle form. The solution was stirred at 130^{o}C until all the alcohol had evaporated. The particle solution was then filtered through cellulose-based, medium porosity (particle retention = 5 – 10 μm) P5 Grade filter (Fisherbrand^{TM}) to remove any large aggregates that may have formed. Size and zeta

potential measurements were taken by dynamic and electrophoretic light scattering using Malvern Zetasizer Nanoseries ZS-90. The coefficient of variance (CV) was determined using a second order cumulant fit for the intensity autocorrelation function of the scattering signal. The 0.5% w/v solution yielded 60 nm particles with a CV of 30.8%.

2.2.1.2 Fabrication of rough particles and subsequent tuning of surface roughness

Core particles were 6 μm amine-functionalized polystyrene particles (Polyscience, Inc.). Coating of amine-functionalized polystyrene (AFP) particles was performed by mixing 0.08% w/v dispersion of AFP particles with a 0.03% w/v dispersion of E-S100 particles at pH 5.3. Enough 3 M NaCl was added to solution to reach a final concentration of 30 mM. The mixture was vortexed for 1 min and then left to rest for at least 6 hrs. The Eudragit-coated polystyrene (AFP-ES100) particles were then washed 4 times to remove non-adsorbed particles by allowing coated particles to sediment, then removing the supernatant and replacing it with fresh DI water at pH 5.6.

To accomplish the partial dissolution and plasticization of the E-S100 coating, AFP-ES100 particle dispersions were then mixed with aqueous acetone solution to reach a final concentration of 10, 30, 50, or 70 %v/v acetone. For the remainder of the study, the concentration of acetone used to smoothen the particle will be referred to as "% acetone treatment". Dispersions were left to rest in a closed container for 2 hours, and then the containers were opened to room temperature for 12 hours. Afterward, containers were transferred to the fume hood to allow the remaining acetone to evaporate. The process took a total of 48 hours. The particles were washed twice to remove non-adsorbed particles by allowing the coated particles to sediment, removing the supernatant, and replacing it with fresh DI water at pH 5.6. Using centrifugation to

remove excess particles was unsuccessful, as E-S100 particles sedimented in addition to the coated particles.

2.2.1.3 Particle characterization: surface topography

SEM images were taken using a Zeiss Ultra 60 SEM with an accelerating voltage of 5 kV. Small volumes of the particle dispersion were pipetted onto aluminum stubs covered with carbon tape and allowed to dry at room temperature. Prior to imaging, samples were coated with carbon using a Cressington 108A carbon coater. As shown in **Figure 2.5**, varying the acetone concentration in solution effectively tuned the surface roughness of the coated particles. Particles became progressively smoother as they were exposed to higher concentrations of acetone.

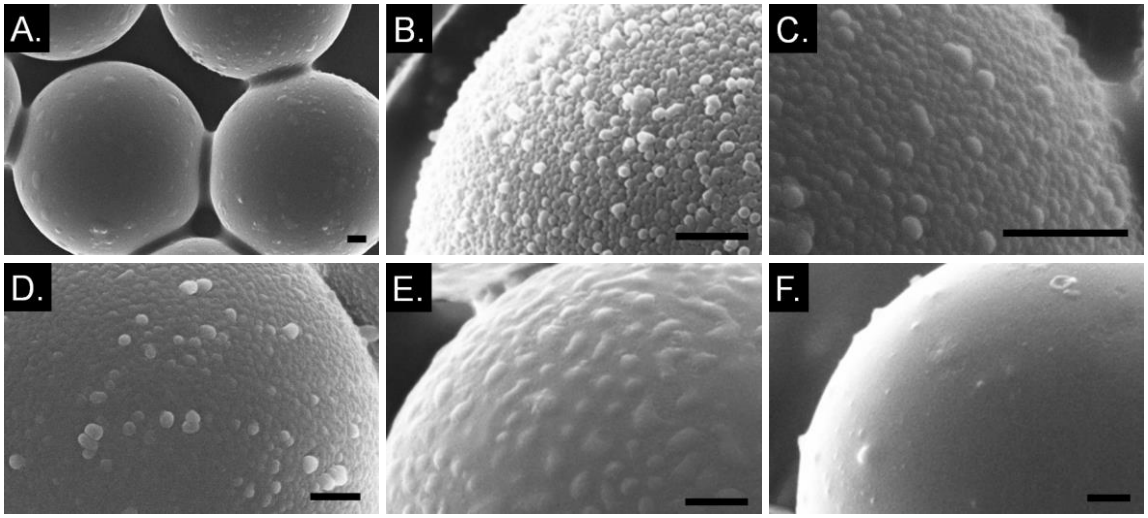

Figure 2.5. Amine-functionalized polystyrene particles (a) prior to E-S100 particle deposition and E-S100 coated amine-functionalized particles exposed to solutions containing (b) 10%, (c) 30%, (d) 40%, (e) 50%, and (f) 70% acetone. Scale bars represent 500 nm.

Qualitatively, the shape of the surface asperities changes with increasing acetone concentration. Rough particles are characterized by discrete spherical features, with "re-entrant spaces" or "overhangings". As particles were exposed to higher concentrations of

acetone, the interstitial spaces became filled with polymer and the surface of the particles appeared smoother.

Quantification of surface roughness was done using atomic force microscopy (AFM). Macroscopic substrates were used as a substitute for the roughened particles and were made using the same E-S100 particles and surface roughness was tuned using the same partial dissolution and plasticization technique. Measurements were carried out on a Veeco Dimension 3100 atomic force microscope using Mikromasch silicon NSC14Al probes. Roughness parameters were determined using Gwyddion freeware.[37] Surface roughness was characterized using the root mean square (Rms) roughness, which is more sensitive to deviations from the mean height than the average roughness.[21, 38] Rms measurements show that surface roughness decreases with increasing acetone treatment, shown in **Table 2.2**.

Table 2.2 Rms roughness of macroscopic surfaces coated with E-S100 particles

% acetone treatment	Rms roughness (nm)
0	16.5 ± 4.2
10	14.3 ± 2.9
20	13.4 ± 1.8
30	12.5 ± 1.7
40	9.8 ± 2.8
50	7.1 ± 2.1
60	4.7 ± 2.1
70	3.9 ± 1.7

The roughest substrates had an Rms roughness of 16.48 ± 4.18 nm, and the smoothest substrates had an Rms roughness of 3.87 ± 1.67 nm.[37] While the absolute value of the Rms roughness may not be identical between the microparticles and macroscopic surfaces, the same qualitative trends are expected based on the similarity suggested by SEM images. Rough particles have similar topography to macroscopic surfaces treated with the same concentration of acetone (**Figure 2.6A-D**) but smooth

particles were rougher than expected based on results from macroscopic surfaces (**Figure 2.6E-F**).

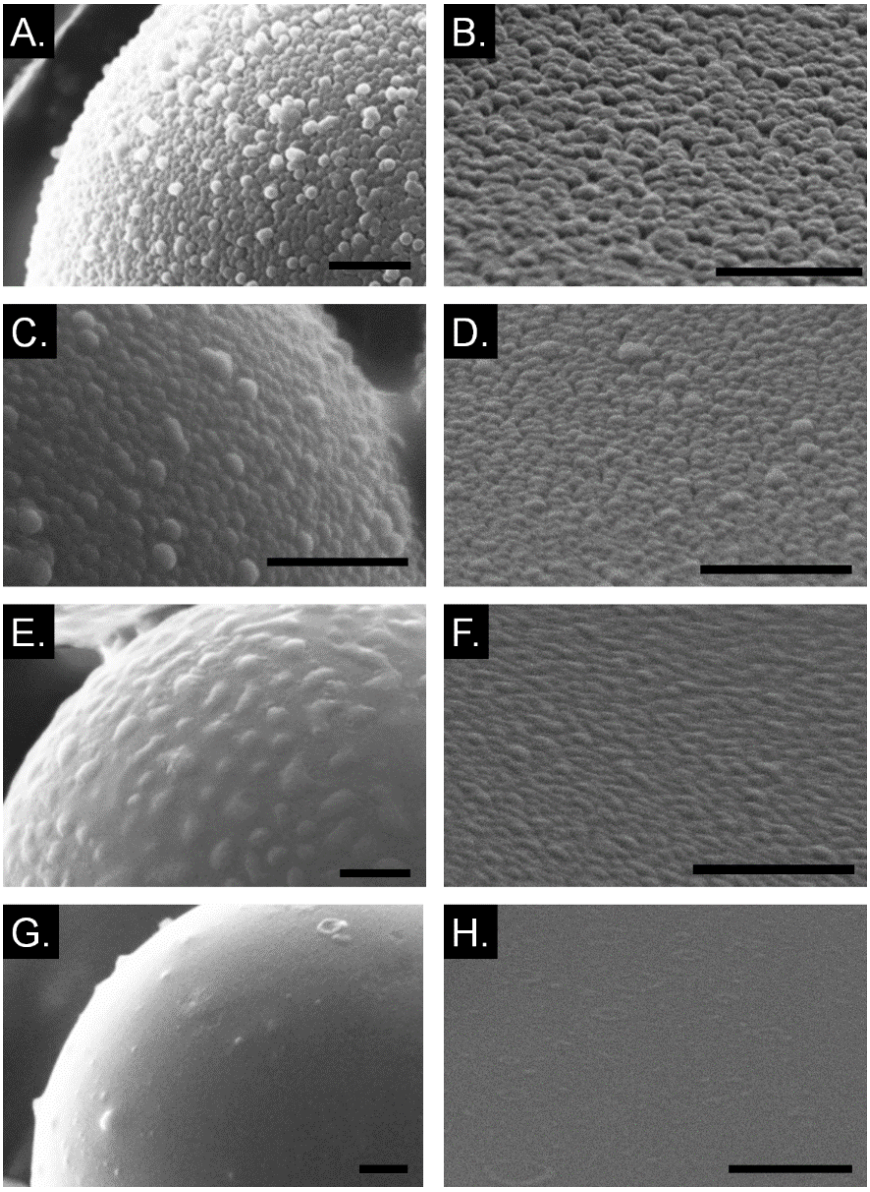

Figure 2.6. Rough particles treated with (A) 10% and (C) 30% acetone solutions have similar surface topography as substrates treated with (B) 10% and (D) 30% acetone solutions, respectively. However, particles treated with (E) 50% acetone look more similar to substrates treated with (F) 35% acetone. Both particles treated with (G) 70% acetone and substrates treated with (H) 60% acetone solutions looks smooth. Scale bars correspond to 500 nm.

2.2.1.4 Particle characterization: surface chemistry

The use of electrokinetic analysis to determine the surface chemistry of the AFP-ES100 particles is based on the principle that all surfaces acquire electric charge in water. The charged surface acquires a cloud of counter-ions to the surface, called the diffuse layer (**Figure 2.7**). The electrical potential at the hydrodynamic "shear plane" or "slip plane", is called the zeta potential (ζ-potential), and is often used as an approximation of the surface potential, Ψ.[39]

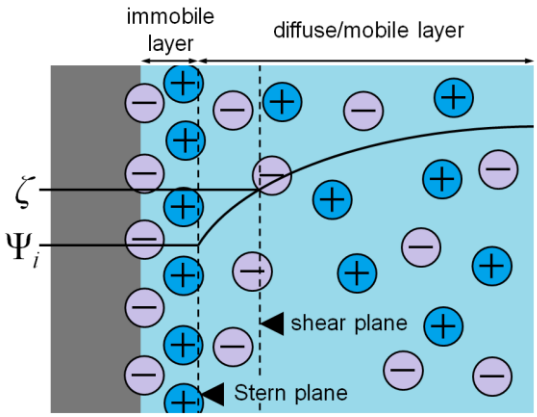

Figure 2.7. Schematic of the counter-ions surrounding a charged surface and the location of the shear plane. The zeta potential, ζ, is the electric potential, Ψ, measured at the shear plane and is an approximation of the surface potential.

While the zeta potential of a surface is dependent on environmental factors, *e.g.* the pH, ion concentration, type of electrolyte solution, as well as surface properties, *e.g.* surface roughness and surface chemistry, the pH at which a particular surface has no net charge, or the isoelectric point (IEP), is only dependent on the surface chemistry.[40] If the surface chemistry remained constant throughout the solvent-based smoothing process, the isoelectric point of AFP-ES100 particle dispersions should not be dependent on the concentration of acetone solution they were exposed to. Similarly, the isoelectric point of

AFP-ES100 dispersions should be similar to the isoelectric point of a dispersion of E-S100 particles.

The zeta potentials of the particle dispersions were measured using a Malvern Zetasizer (Malvern Nano ZS). Zeta potential measurements of particle dispersions were taken four times in 1 mM NaCl solution using 4 different pH values ranging from pH 4.5 and 7 (**Figure 2.8**).

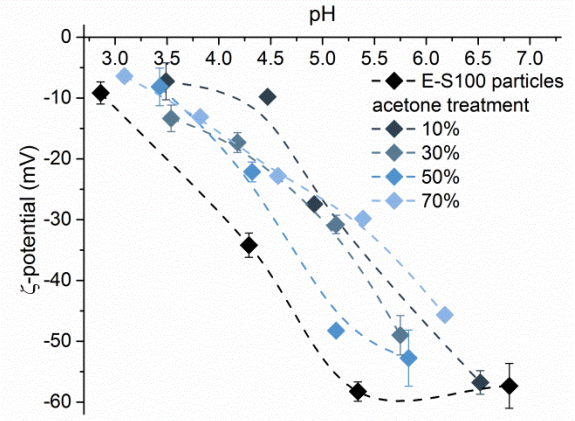

Figure 2.8. Zeta potential measurements of particles exposed to 10, 30, 50, and 70% acetone solutions. Lines are meant to guide the eye.

The IEP was calculated using a cubic spline fit using Matlab® (**Figure 2.9**). Statistical correlations for the dependence of the IEP on the % acetone solution were determined of Pearson's correlation coefficient. An *r*-value of -1 or 1 indicates a perfect negative or positive correlation, and an *r*-value of 0 indicates no correlation. In general, if $p < 0.05$, the correlation is considered significant.[41]

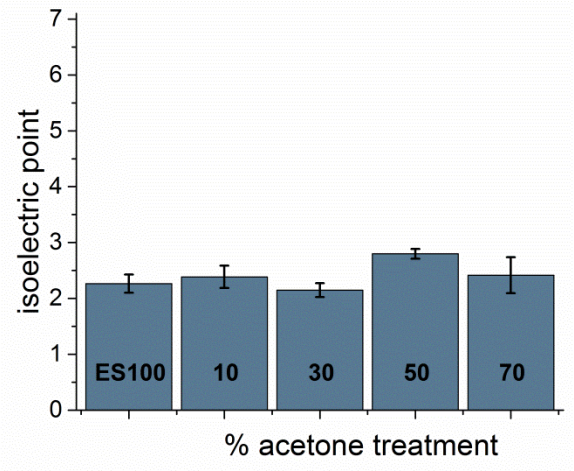

Figure 2.9. Isoelectric points of E-S100 particle dispersion and dispersions of AFP-ES100 particles exposed to 10, 30, 50, and 70% acetone solutions. Error bars represent the root–mean square error of the cubic spline fit.

Statistical analysis indicated no significant correlation between extent of surface smoothing and isoelectric point. The average isoelectric point for acetone-treated particles was 2.44 ± 0.27, with an *r*-value of 0.35and a *p*-value of 0.65. The isoelectric point of an E-S100 particle dispersion was 2.27 ± 0.03.

2.2.2 Experimental set-up: Total internal reflection microscopy

A schematic of the TIRM set-up is shown in **Figure 2.10**. An Olympus BX51WI microscope with a 60x objective was used to observe the particle and collect scattering intensity data. The evanescent wave was generated using a He:Ne laser (Coherent) operating at a wavelength of 632.8 nm and a power of 43.8 mW.

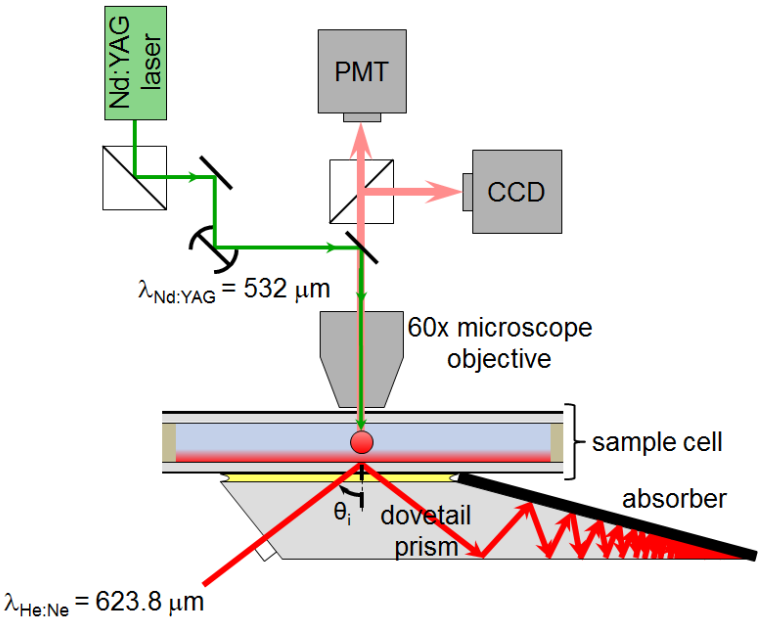

Figure 2.10. Schematic of TIRM set-up. The He:Ne laser (λ = 632.8 nm) is used to generate the evanescent wave. The He:Ne laser is positioned so it is normal to the air/prism interface, ensuring the incidence angle at the glass/water interface (θ_i) is 70°. The intensity of light scattered by a particle impinging on the evanescent wave is measured using a photomultiplier tube (PMT) and visualized using a CCD camera. An Nd:YAG laser (λ = 532 nm) is used to generate the two-dimensional optical trap. Not drawn to scale.

A BK-7 dovetail prism with an angle of 70° (n = 1.515) was optically coupled to a soda-lime glass slide (n = 1.522) with Nikon Type A immersion oil (n = 1.515). The laser was angled such that the beam was normal to the air/prism interface. This was done to ensure the incident beam was normal to the air/prism interface and would ensure the incidence angle at the glass/water interface would be 70°.[28, 42, 43] The back end of the prism was covered with electrical tape to absorb most of the light reflected back from the interface and minimize backscatter. Using **Equation 2.14**, the decay length is 100 nm. **Figure 2.11** shows particles illuminated by an evanescent wave.

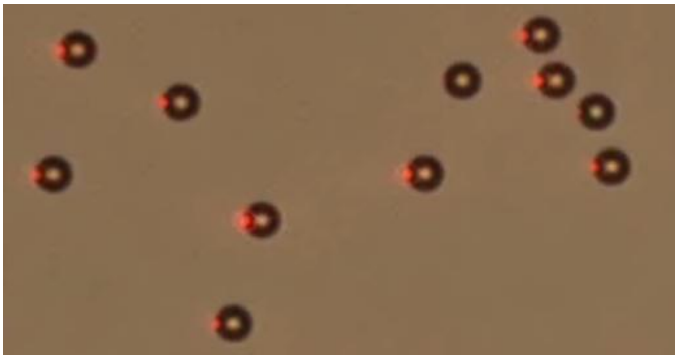

Figure 2.11. 2.2 μm polystyrene particles in water illuminated with an evanescent wave (red). Particles that are closer to the bottom of the TIRM cell scatter more of the evanescent wave, resulting in the appearance of a brighter red light.

A linear polarizer (Bernhard Halle Nachfolger, GmbH) was used to ensure that only p-polarized light was used to generate the evanescent wave.[43] If s-polarized light is used to generate the evanescent wave, the evanescent wave is reflected multiple times between the particle and the glass and the scattered intensity is no longer exponentially dependent on the distance from the glass/water interface.[44]

A 150 mW Nd:YAG laser (Compass^{TM}) with a wavelength of 532 nm was used to generate a two-dimensional optical trap.[18, 45] The trap was primarily used to ensure the particle would remain stationary during solvent exchange.

A Hamamatsu H7155-01 photomultiplier tube (PMT) connected to a digital correlator (ALV-5000/60XO Multiple Tau Digital Correlator) was used to measure the particle scattering intensity. Measurements were taken every 40 ms for at least 60 min for a total of at least 30,000 data points. Using a photomultiplier tube to measure scattering intensity, while more sensitive than video microscopy, only allows a single particle to be measured at a time. The sensitivity of TIRM and PMT also makes it difficult to avoid corrupting the scattering intensity signal with environmental factors, such as intensity fluctuations from the source laser and ambient light.

Fluctuations in source laser intensity, measured using a monitor diode, could potentially become a problem since the signal could vary over two orders of magnitude during a single measurement. All scattering intensity data were therefore normalized by the monitor diode reading to ensure changes in scattering intensity were the result of changes in particle elevation and not source intensity fluctuations.

In order to minimize background scatter, measurements were taken in a dark room to remove sources of ambient light. It was, however, impossible to remove all sources of ambient light and a normalization method was used post-measurement to remove background scatter. Background scatter signal, $I_{b,avg}$, was determined by measuring the intensity of light scattered when no particle was in the field of view. The simplest way to normalize the signal by the background is simply to subtract the average background signal, $I_{b,avg}$, from the scattering intensity of the particle, $I(h)$. This method is only valid when the ratio of the standard deviation for the background, σ_b, and standard deviation of the scattering intensity, σ_s, is less than 0.15.[46] The conditions used in this study meet the criteria.

2.2.2.1 TIRM cell preparation and measurement conditions

Prior to each measurement, the dovetail prism and TIRM cell were thoroughly cleaned. The dovetail prism was immersed in methyl ethyl ketone (VWR) for at least 30 min and cleaned with lens paper to remove any organic debris on the surface.

Due to the sensitivity of TIRM, the glass slides used to make the measurement cell, particularly the slide that is optically coupled to the dovetail prism, must not contain any debris that could contribute to background scatter or introduce debris into the cell solution. Glass slides were first cleaned with Alconox detergent, rinsed with tap and DI

water, then dried with an air gun. Immediately after drying, slides were placed in 2:1 piranha solution at 100°C (95-98% sulfuric acid, 30% hydrogen peroxide, VWR®) for at least 50 minutes. They were then rinsed with copious amounts of DI water and dried with an air gun. Slides were used to make the TIRM cell immediately after they were cleaned.

The measurement cell was made by separating two glass slides (Fisher Scientific) with a 1 mm thick rectangular rubber spacer to make a total cell volume of 1 mL (**Figure 2.12A**). Polyethylene tubing (Scientific Commodities Inc.) glued to 20 gauge needles (Weller) was used to flow solution through the measurement cell. The glass slides were sandwiched between two rubber spaces in a Teflon and metal case, making the sample cell (**Figure 2.12B**).

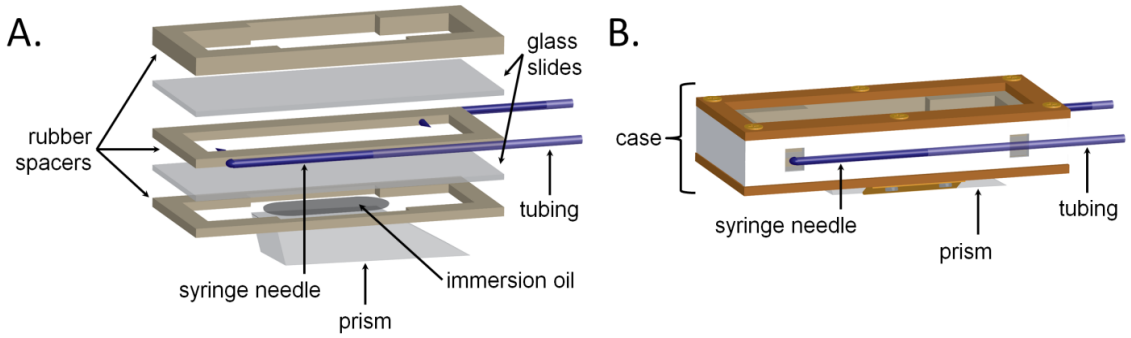

Figure 2.12. Schematic of the TIRM cell. (a) The measurement cell consists of a 1 mm rubber spacer sandwiched between two glass slides. The bottom slide is optically coupled to the dovetail prism using immersion oil. Two additional rubber spaces are used to sandwich the measurement cell into the (b) TIRM sample cell.

At the beginning of each experiment, a single particle was isolated from a dispersion using an optical trap. The unused particles were then flushed from the measurement cell and the particle elevation in 0.1, 0.25, 1, 3, and 5 mM 1:1 electrolyte solutions were measured in real time. A minimum of 6 mL (6x cell volume) was used to replace the previous solution to ensure complete solution exchange. At the end of each

measurement, the particle was then salted out, *i.e.* irreversibly attached to the bottom of the measurement cell, using 100 mM NaCl. [47]

The intensity of light scattered by the particle is a function of the particle elevation and the refractive index of the particle. The refractive index of E-S100 is 1.38, which is similar to water. In contrast to the refractive index of the core polystyrene particle (n = 1.45), the E-S100 particle coating will not contribute appreciably to the observed scattering intensity.

All 1:1 electrolyte solutions contained DI water at pH 6 and 0.05 mM sodium dodecyl sulfate (Sigma Aldrich). SDS has been previously used to impart negative charges on polystyrene particles and glass slides in TIRM.[12] The concentration of SDS used was well below the CMC to avoid any micelle formation in solution. Enough 100 mM NaCl was added to solution to reach the final concentrations used in TIRM measurements.[48]

2.2.3 Calculation of DLVO parameters

For colloidal particles in aqueous medium suspended above a glass plate, there will be a particular elevation where all the forces acting on the particle (gravitational, electrostatic, and van der Waals) are balanced. However, the particle does not remain stationary at the equilibrium elevation. Rather, it will sample elevations above and below the equilibrium via Brownian motion. The probability of finding the particle at any particular elevation, $p(h)$, is related to its potential energy, $\Phi(h)$, at that elevation by the Boltzmann equation:

$$p(h) = Q\exp\left[-\frac{\Phi(h)}{kT}\right] \qquad 2.16$$

where k is the Boltzmann constant, T is the temperature, and Q is a normalization constant such that $\int p(h)dh = 1$. The normalization constant, Q, can be eliminated by relating the potential energy of the particle to the smallest observed potential energy, $\Phi(h_m)$:

$$\frac{\Phi(h) - \Phi(h_m)}{k_B T} = \ln \frac{p(h_m)}{p(h)} \tag{2.17}$$

where h_m is the elevation corresponding to the minimum potential interaction energy. The probability of finding a particle at any given elevation interval, $p(h)\mathrm{d}h$, is related to the scattering intensity interval, $P(I)\mathrm{d}I$, via:

$$p(h) = -P(I)\frac{\mathrm{d}I}{\mathrm{d}h} = \xi P(I) I(h) \tag{2.18}$$

where ξ^{-1} is the decay length of the evanescent wave and $I(h)$ is the scattering intensity at height h. TIRM is used to measure the instantaneous particle elevation, h, of the particle; the particle elevations are then converted into a histogram. If the particle has had enough time to sample a statistically significant number of elevations (at least 10,000 data points), the probability of observing a particular intensity, $P(I)$, is proportional to the is the number of observations for a particular scattering intensity, $N(I)$.[31] In this study, the scattering intensity data of at least 2 30-min measurements were combined into a single histogram of at least 30,000 data points. **Equation 2.17** can be combined with **Equation 2.18**:

$$\frac{\Phi(h) - \Phi(h_m)}{k_B T} = \ln \frac{N(I_m) I_m}{N(I) I} \tag{2.19}$$

where $I_m = I(h_m)$ and $I = I(h)$. Here, I_m is the most sampled intensity and $N(I_m)$ is the number of observations for that intensity bin.

Using the Boltzmann equation, the number of observations for a particular intensity is related to the potential energy of a particle at a given elevation (**Figure 2.13**).

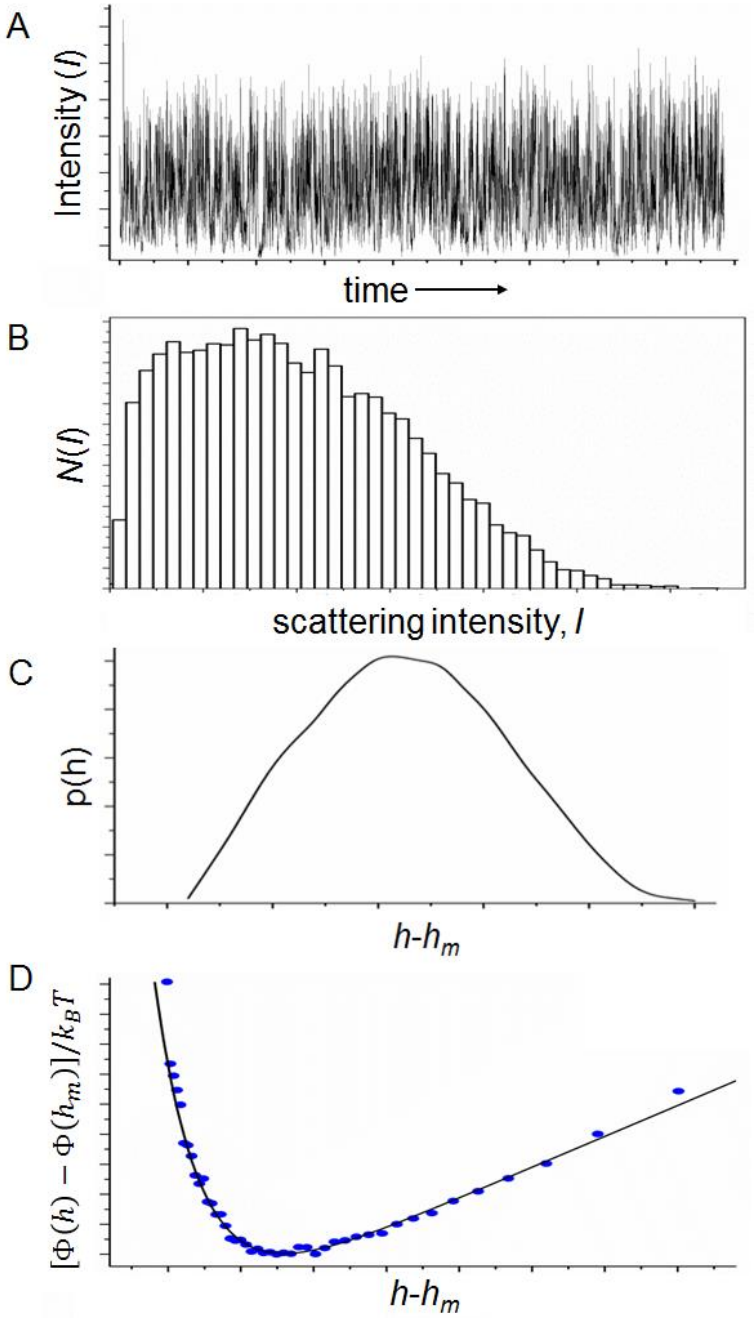

Figure 2.13. (A) Scattering intensity data for a 6 μm polystyrene particle in low salt solution is converted into (B) a histogram of the scattering intensities. (C) Using **Equation 2.18**, the probability distribution of the scattering intensities is determined, and (D) are converted to a relative potential energy curve using **Equation 2.19**.

Determination of I_0 for **Equation 2.14** is done experimentally by measuring the intensity of scattered light when the particle contacts the glass plate ($h = 0$). The gravitational, electrostatic, and van der Waals contributions to the total interaction energy were calculated using **Equations 2.2**, **2.5**, and **2.9**. All data analysis was done using Matlab R2015®.

2.3 Results

Experimental data of particle-plate interactions indicate a suppression of the electrostatic repulsion with increasing salt concentration and consequently enhanced screening of the electrostatic particle substrate interaction. At the highest electrolyte concentration (3 mM) the probe particle reaches small separation distances from the substrate and the onset of van der Waals attraction becomes clearly visible as a dip in the potential energy (**Figure 2.14A**). This dip corresponds to the secondary interaction energy minimum predicted by DLVO theory.[1, 2, 49] Results also indicate that increasing surface roughness weakens the van der Waals attraction (**Figure 2.14B**). The interaction energy dependence on salt concentration and surface roughness qualitatively match expected results.[12, 28] As will be discussed in more detail below, roughness is expected to both weaken the van der Waals attractive and amplify the electrostatic repulsion.

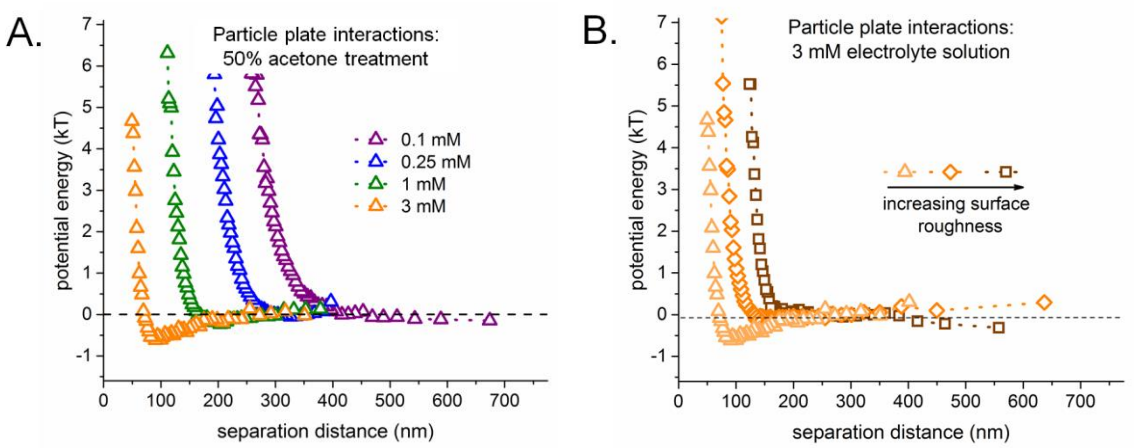

Figure 2.14. DLVO interactions for particles with varying degrees of surface roughness. The measurement was taken in a 1:1 electrolyte solution at pH 6. (A) The particle elevation decreases with increasing salt concentration, indicating a suppression of the electrostatic double layer repulsion for a particle treated with 50% acetone. (B) In a 3 mM salt concentration the particle-plate separation distances increases and the van der Waals attactive interaction becomes progressively weaker with increasing particle surface roughness.

2.3.1 Determination of system parameters

Quantitative model descriptions of the colloidal interactions at play rely on imperfect theories and tend to require the use of parameters (such as Hamaker constants, surface potentials, etc.) that cannot be determined independently with the desirable accuracy. In our analysis, the values for such parameters were obtained from fits to the experimental interaction energy profiles. As will be discussed below in more detail, in order to avoid the "meaningless fits" that typically result from the excessive use of free parameters, fit parameters were constrained, whenever possible, to intervals reflecting "reasonable" expectations, and the lowest complexity fits matching the experimental data were favored.

2.3.1.1 Gravitational force and the calculation of probe particle size

As shown in **Figure 2.15A**, when the particle elevation is very large (> 350 nm), the only force acting on the particle is due to gravity, and the potential energy can be

fitted to a straight line whose slope indicates the gravitational force and can be used, along with the uncertainty of the slope, to determine the particle size (along with a confidence interval). Fits of the gravitational energy were determined using data from (h – h_m + 50 nm) to (h – h_m + 250 nm), where h_m is the separation distance associated with the minimum interaction energy. The gravitational energy can be subtracted from the total potential energy curve (**Figure 2.15B**).

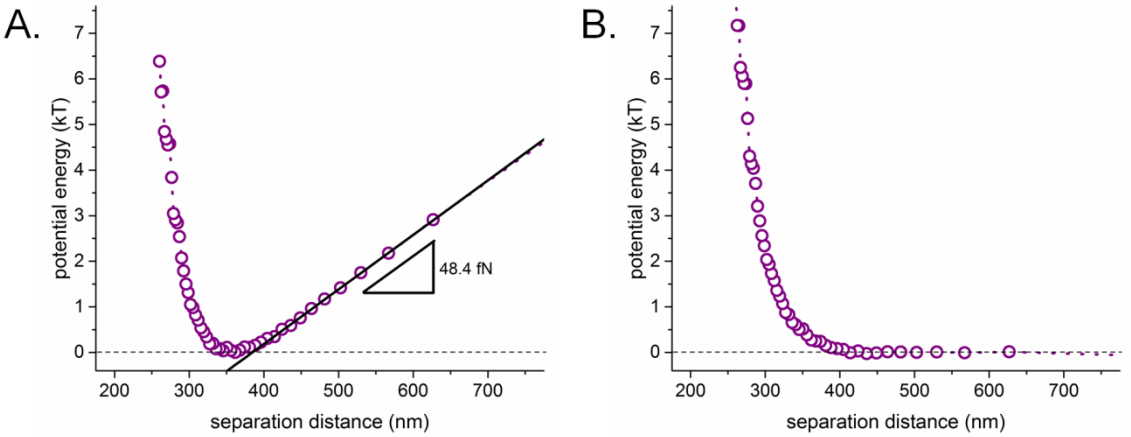

Figure 2.15. Potential energy profile for a particle in 0.1 mM electrolyte solution. (a) The gravitational fit results in a 48.4 fN gravitational energy. (b) Once the gravitational energy has been removed, the DLVO interaction energy remains.

Equation 2.2 was used to calculate the particle size and gravitational contribution to the potential energy profile:

$$\Phi_{grav}(h) = mgh = \frac{4}{3}\pi R^3(\rho_p - \rho_f)gh \qquad 2.2$$

Here, m is the particle mass, R is the particle radius, g is the gravitational acceleration, and ρ_p and ρ_f are the density of the particle and solvent, respectively.

The particle volume and radius were calculated assuming a particle density of 1050 kg/m^3 for the polystyrene particles and density of 1000 kg/m^3 for the aqueous solutions. The interaction energies for four particles were measured in this study. A comparison of the particle sizes used is shown in **Table 2.3**.

Table 2.3 Calculated gravitational force and radius of particles treated with varying concentrations of acetone

Particle roughness (% acetone treatment)	Gravitational force (fN)	Calculated particle diameter, D(μm) (with 95% confidence interval)
10 (roughest)	49.2 ± 0.1	5.8 (5.7, 5.9)
30	43.2 ± 0.1	5.5 (5.4, 5.6)
50	50.9 ± 0.2	5.8 (5.6, 6.0)
70 (smoothest)	48.4 ± 0.1	5.7 (5.7, 5.8)

All calculated particle sizes were consistent with microscopic observations and with the average particle size of 6 μm cited by the producer of the microparticles used as the core of our TIRM probe particles, and with reasonable expectations of 10% for the particle sample polydispersity.

With the optical trap, measurements at different electrolyte concentrations and separation distances could be carried out using the same probe particle with the size determined in the 'regime of purely gravitational force' as described above. By contrast, variations of the surface roughness did require working with different probe particles. All the measurements were taken using particles with similar size, however, which allows us to meaningfully compare roughness effects.

2.3.1.2 The Debye length

For suspended particles at low electrolyte concentration, the only significant force exerted on the particle besides gravity is the electrostatic repulsion. This interaction is dependent on the particle size, surface potential of the interacting surfaces, and the Debye length. The particle size has been determined using the gravitational interaction at large separations. The Debye length, in principle, can be calculated directly from a known electrolyte concentration (**Equation 2.15**). For a 0.1 mM and 0.25 mM 1:1 electrolyte solution, for example, the theoretical Debye length is 30.3 nm^{-1} and 19.24 nm^{-1}, respectively. As the inverse of the exponential decay rate of the electrostatic interaction

energy (**Equation 2.4**), the Debye length can also be obtained experimentally from the slope of the semi-logarithmically plotted experimental interaction energy. As shown in **Figure 2.16**, the Debye length from fits to experimental data agrees well with the theoretical value. The range of experimental data displayed in the Figure ($0.5kT < \Phi_{total} < 3.5kT$) is the range most appropriate for inclusion in the fit: energy values below this range suffer from a comparatively poor signal-to-noise ratio, whereas energies above this range indicate rarely observed separations and are thus less suitable for quantitative analysis because of comparatively poor sampling statistics.

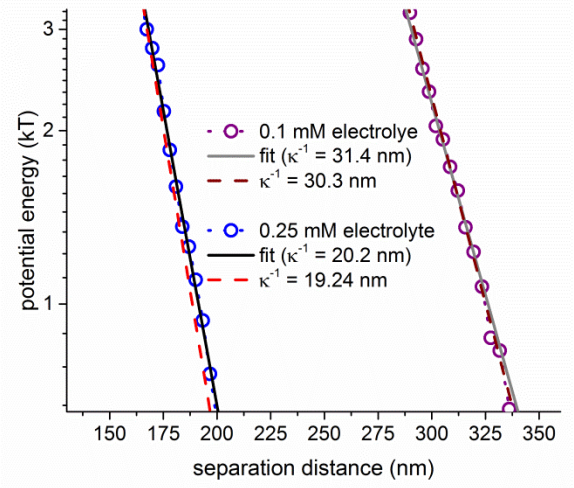

Figure 2.16. The electrostatic repulsive interaction for a (smooth) AFP-ES100 particle treated with 70% acetone in 0.1 mM (purple symbols) and 0.25 mM (blue symbols) 1:1 electrolyte solution at pH 6. The fitted Debye length is shown in black and the theoretical Debye length is shown in red.

2.3.1.2.1 Surface potentials

The electrostatic interaction is also dependent on the surface potential of the two interacting surface, $\Psi_{particle}$ and Ψ_{glass}. These two surface potentials determine the prefactor of the exponential electrostatic energy decay (**Equation 2.4**) and thus the intercept of the straight energy curves in semi-logarithmic representations such as **Figure 2.16**. Zeta potential measurements of particles treated with various concentrations of

acetone were measured electrophoretically (**Figure 2.17A**). While the absolute zeta potential for each particle and condition varied drastically, there was no systematic dependence of the zeta potential on surface roughness. As such, the average zeta potential for each salt concentration was then calculated and used as an approximation for $\Psi_{particle}$ (**Figure 2.17B**). From experimental zeta-potential measurements of silica[50] and AFP-ES100, $\Psi_{particle}/\Psi_{glass}$ = 1.6 ± 0.1.

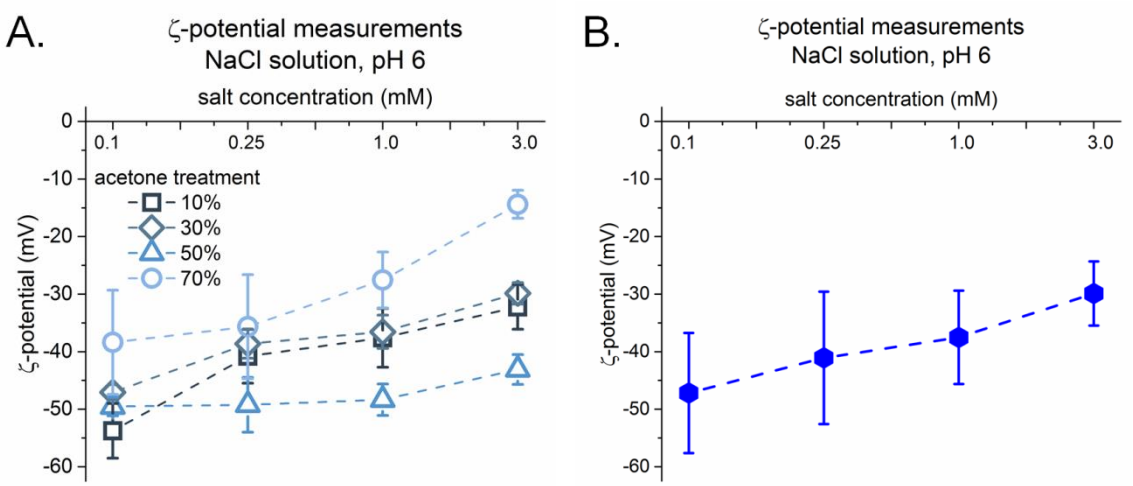

Figure 2.17. Zeta potential measurements for AFP-ES100 particles in a NaCl solution at pH 6 as a function of salt concentration (A) for particles with varying degrees of surface roughness and (B) the average zeta potentials of all the particles at a given salt concentration.

Empirically, colloidal stability of charge-stabilized dispersions requires that the particle surface potential has a magnitude of at least 25-30 mV. When fitting experimental data to the electrostatic double layer interaction, at low electrolyte concentrations, $-20\ mV < \Psi_{glass}, \Psi_{particle} < -100\ mV$ and $\Psi_{particle} = 1.6\Psi_{glass}$. The fitted surface potentials and Debye length are still within reasonable limits. The calculated parameters are shown in **Table 2.4**.

Table 2.4 Calculated Debye length and surface potentials of the glass slide and a smooth AFP-ES100 particle in low electrolyte solutions at pH 6

1:1 electrolyte concentration (mM)	Fitted Debye length κ^{-1} (nm)	Expected Debye length κ^{-1} (nm)	Fitted Ψ_{glass} (mV)	Fitted $\Psi_{particle}$ (mV)
0.1	31.4	30.3	-55.2	-88.3
0.25	20.2	19.2	-29.8	-47.7

As expected, the surface potential and Debye length both decrease with increasing ion concentration. Given the good agreement between the Debye length expected from the prepared electrolyte concentration and fits to the potential energy measurements at low electrolyte concentrations, we will treat the Debye length as a known parameter (allowing it to vary within 10% of its theoretical value) when calculating the electrostatic repulsion and van der Waals attraction energy.

2.3.2 Calculation of DLVO parameters

The electrostatic interaction was calculated using **Equation 2.4**:

$$\Phi_{edl}(h) = 64(\pi\varepsilon_r\varepsilon_0)R\left(\frac{k_BT}{e}\right)^2 \tanh\left(\frac{e\Psi_{glass}}{4k_BT}\right)\tanh\left(\frac{e\Psi_{particle}}{4k_BT}\right)\exp(-\kappa h) \qquad 2.4$$

where the parameters R and κ are constrained to values consistent with the particle size from gravity fits at low salt/large separation distance and the known electrolyte concentration (shown in red), whereas the surface potentials, Ψ_i, are allowed to vary freely (shown in blue). $\Psi_{particle}$ should decrease systematically as the salt concentration of solution increases.

Due perhaps to the inevitable nano- and micron-scale roughness of all surfaces, there has not yet been a study, to our knowledge, that reports quantitative agreement between experimentally observed van der Waals interactions between smooth surfaces and theoretical predictions.[6, 16, 51] The most recent corrections for the surface roughness of

smooth colloidal particles use a semi-empirical approach based on the Lifshitz theory.[18] We first used **Equation 2.9** to describe the van der Waals attraction:

$$\Phi_{vdw}(h) = A\left\{\frac{2.45\lambda_c}{60\pi}\left(\frac{h-R}{h^2}-\frac{h+3R}{(h+2R)^2}\right)\right.$$
$$-\frac{2.17{\lambda_c}^2}{720\pi^2}\left(\frac{h-2R}{h^3}-\frac{h+4R}{(h+2R)^3}\right) \qquad 2.9$$
$$\left.+\frac{0.59{\lambda_c}^3}{5040\pi^3}\left(\frac{h-3R}{h^4}-\frac{h+5R}{(h+2R)^4}\right)\right\}$$

where the characteristic wavelength of interaction, λ_c, is only dependent on the Debye length, which we have assumed is a known parameter:

$$\lambda_c = 86.2 + 43.6\tanh\left[3.8\left(\log_{10}\frac{\kappa^{-1}}{nm}-1.04\right)\right] \qquad 2.10$$

and particle radius, R, was allowed to vary within the 95% confidence limits (**Table 2.3**). The fitted parameters shown in red (A, λ_c, and R) were bounded by literature values for the Hamaker constant, the expected Debye length based on solution electrolyte concentration, and the particle size determined from the gravitational interaction, respectively. Based on parameter limits used in the literature, the Hamaker constant, A, was allowed to vary from $0.1kT$ to $3kT$.[16] The Hamaker constant would be used as a measure of roughness effects.

As shown in **Figure 2.18**, experimental data for a smooth particle interacting with the glass slide were well-described using **Equation 2.4** and **Equation 2.9**. However, the predicted surface potentials for the particle was larger than -1 V in 1 mM solution, which is physically unlikely to occur.

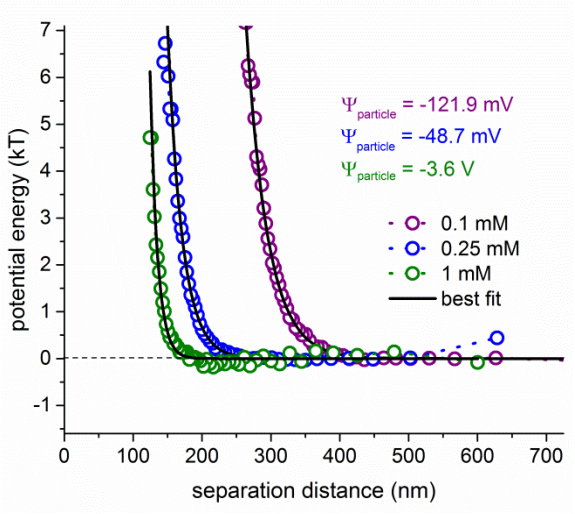

Figure 2.18. DLVO fits for particle-plate interactions for a smooth particle in a 1:1 electrolyte at pH 6. The fits describe the interaction energy but result in physically impossible surface potentials, particularly in higher ionic strength solutions.

It is possible that **Equation 2.4** is insufficient to describe the electrostatic repulsion for surfaces with any degree of surface roughness. When Ψ_{glass} and $\Psi_{particle}$ are constrained to physically feasible values, the influence of salt concentration on the surface potential of slightly rough particles becomes nonsensical. For a particle treated with 50% acetone, while the fitted Debye length is within 10% of the theoretical value for the weakest electrolyte solution, the Debye length fitted to the experimental slope of the electrostatic interaction in a 0.25 mM electrolyte solution is more than 10% larger than the expected Debye length (**Figure 2.19**). Furthermore, the fitted surface potentials of both the particle and glass slide appear to increase with increasing salt concentration (**Table 2.5**).

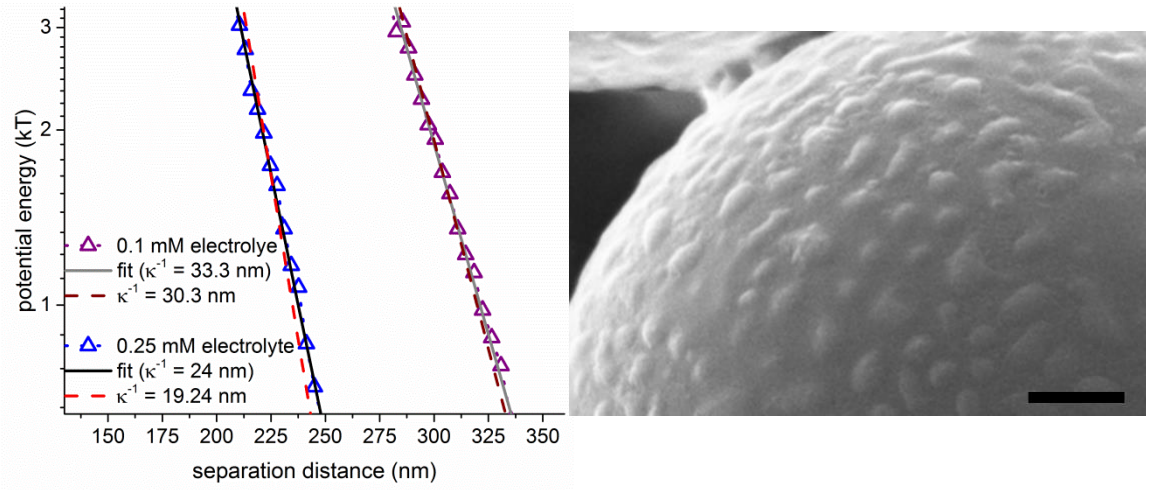

Figure 2.19. The electrostatic repulsion exerted on a AFP-ES100 particle treated with 50% acetone in 0.1 mM (purple symbols) and 0.25 mM (blue symbols) 1:1 electrolyte solution at pH 6. The fitted Debye length is shown in black and the theoretical Debye length is shown in red. An SEM image of the particle is also shown (scale bar corresponds to 500 nm).

Table 2.5 Calculated surface potentials of the glass slide and AFP-ES100 particle in low electrolyte solutions

1:1 electrolyte concentration (mM)	Debye length κ^{-1} (nm^{-1})	Fitted Ψ_{glass} (mV)	Fitted $\Psi_{particle}$ (mV)
0.1	33.2	-43.6	-69.7
0.25	24.0	-50.0	-80.1

The presence of a polymer coating has been known to influence the apparent surface charge, and resulting electrophoretic mobility, of colloidal particles in solution.[52] Since even the smoothest particles used in this have a polymer coating, it is unrealistic to assume that the electrostatic repulsion for even the smooth particles will be adequately described by **Equation 2.4.** A simple approach where surface roughness was assumed to change the apparent separation distance of the interacting surfaces was used to determine the electrostatic interaction.

2.3.2.1 Electrostatic interactions: discrepancy between theory and experiment

The electrostatic interaction was assumed to be off-set by a separation distance, D, that was allowed to vary freely:

$$\Phi_{edl}(h) = 64(\pi\varepsilon_r\varepsilon_0)R\left(\frac{k_BT}{e}\right)^2 * \tanh\left(\frac{e\Psi_{glass}}{4k_BT}\right)\tanh\left(\frac{e\Psi_{particle}}{4k_BT}\right)\exp\left[-\frac{(h-D)}{\kappa^{-1}}\right] \quad 2.20$$

The offset was used as a simple approximation accounting for the possibility that the charged groups of the polymer coating that contribute to the electrostatic repulsion protrude further into solution than the rest of the surface.[52, 53] The other parameters (shown in red) were constrained to physically feasible values using parameter bounds discussed in §2.3.1.

Assuming a constant offset in the electrostatic interactions was insufficient to describe the DLVO interactions even for a smooth particle (**Figure 2.20A**). While using **Equation 2.20** and **Equation 2.9** to describe experimental data worked well for low ionic strength solutions (0.1 mM and 0.25 mM electrolyte), the combination was unable to describe the DLVO interaction for a smooth particle in 1 mM electrolyte solution. The fits were even worse for rougher particles; the predicted DLVO interaction was 0 for particle-plate separation distances sampled in 0.25 mM and 1 mM electrolyte solutions (**Figure 2.20B**). This is somewhat expected because fits were not explicitly used to correct for surface roughness.

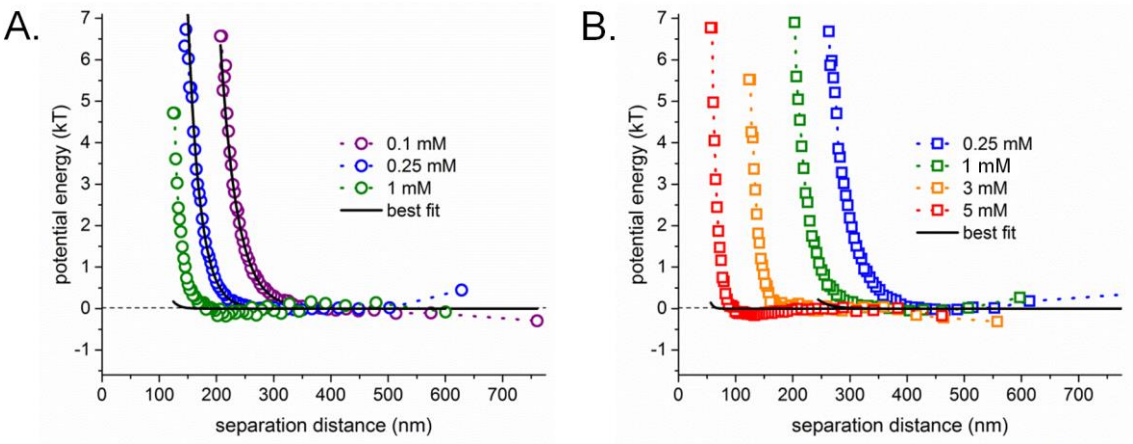

Figure 2.20. Experimental and fitted DLVO interactions for (A) a smooth particle-plate interaction. The particle was treated with 70% acetone. The fits work well for low ionic strength solutions but fail to describe particle-plate interactions in 1 mM electrolyte solution. (B) The fitted parameters completely fail to describe the DLVO interactions for a rough particle treated with 10% acetone. All measurements were taken in a 1:1 electrolyte solution at pH 6.

2.3.2.2 van der Waals interactions: discrepancy between theory and experiment

Since the outermost microparticle layer is composed of a polymer-coating with refractive index similar to the liquid medium it, and because of surface roughness, the outermost particle layer is expected not to contribute as much to the van der Waals interaction as a somewhat deeper layer within the particle material that still lies within the range of interaction with the substrate. To account for the fact that the dominant contribution comes from a material layer buried inside the particle, an additional distance offset L was introduced in the expression for the van der Waals interaction:

$$\Phi_{vdw}(h) = A\left\{\frac{2.45\lambda_c}{60\pi}\left(\frac{(h+L)-R}{(h+L)^2}-\frac{(h+L)+3R}{[(h+L)+2R]^2}\right)\right.$$
$$-\frac{2.17{\lambda_c}^2}{720\pi^2}\left(\frac{(h+L)-2R}{(h+L)^3}-\frac{h+4R}{[(h+L)+2R]^3}\right) \quad 2.21$$
$$\left.+\frac{0.59{\lambda_c}^3}{5040\pi^3}\left(\frac{h-3R}{(h+L)^4}-\frac{h+5R}{[(h+L)+2R]^4}\right)\right\}$$

where the fitted van der Waals offset, L, was unconstrained. The parameter bounds for A, λ_c, and R were the same as **Equation 2.9**. The electrostatic interaction was described with **Equation 2.20**. For the smoothest particle (**Figure 2.21A**), the particle never samples a low enough elevation for van der Waals to become a significantly influence the DLVO interaction. The addition of a van der Waals offset factor did allow better fits in all salt concentrations for the smooth particle, but was unable to fit data for rough particles where the strength of the van der Waals interaction is substantial (**Figure 2.21B**). The calculated surface potentials of the particles and glass slides varied non-systematically with salt concentration (**Table 2.6**).

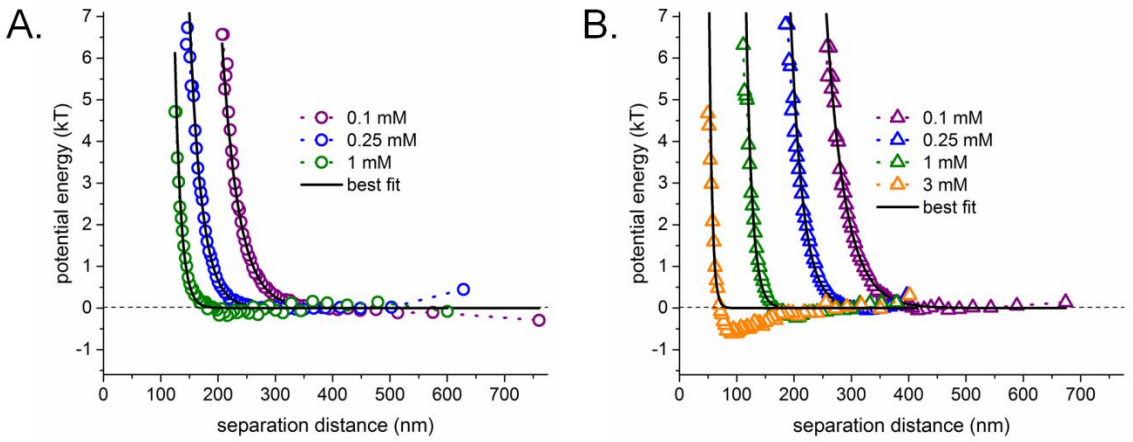

Figure 2.21. Assuming surface roughness results in an offset in both the electrostatic and van der Waals attraction results in adequate fits of the (A) smooth particles but (B) fails to describe the van der Waals attraction at higher salt concentrations (orange triangles) if the particle surface has any degree of surface roughness (surfaces treated with 50% acetone). Measurements were taken in a 1:1 electrolyte at pH 6.

Table 2.6 Fitted surface potentials of the glass slide and AFP-ES100 particle in low electrolyte solutions

[ion] (mM)	70% acetone treatment		50% acetone treatment	
	Ψ_{glass} (mV)	$\Psi_{particle}$ (mV)	Ψ_{glass} (mV)	$\Psi_{particle}$ (mV)
0.1	-39.0	-62.5	-26.8	-42.9
0.25	-24.7	-39.5	-41.8	-66.9
1	-43.4	-69.4	-40.2	-64.2
3	–	–	-31.3	-50.1

While there are other geometric corrections for surface roughness, *e.g.* modeling the surface as a series of hemispherical valleys and mountains on a flat substrate, the shape of the proposed surface roughness is not compatible with SEM images of AFP-ES100 particles.

2.3.2.3 van der Waals interaction: empirical correction for surface roughness

The equations used for the van der Waals attraction (**Equation 2.9**, **2.20**) uses the Debye length-dependent parameter, λ_c, to describe particle properties that influence the strength of the interaction:

$$\lambda_c = 86.2 + 43.6 \tanh\left[3.8\left(\log_{10}\frac{\kappa^{-1}}{nm} - 1.04\right)\right] \qquad 2.10$$

Experimental data, however, suggest a qualitative collapse of the van der Waals interaction onto a single curve independent of salt concentration. (**Figure 2.22**). The data also indicate the increasing importance of the van der Waals attraction as particle-plate separation distances decrease.

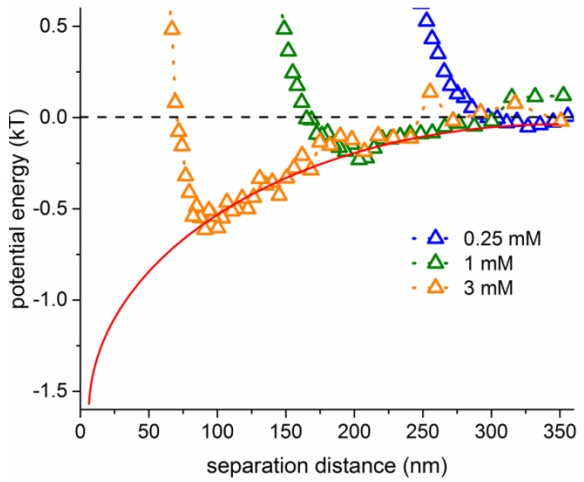

Figure 2.22. Particle-plate interaction energy curves in a 1:1 electrolyte at pH 6 near the onset of the van der Waals attraction. The red line is used to guide the eye. Rather than provide a rigorous model, the data shows the growing importance of the van der Waals attraction as particle-plate separations decrease and qualitatively indicates the van der Waals attraction at a given separation distance is insensitive to salt concentration.

The collapse of the van der Waals attraction onto a single curve for all different electrolyte concentrations is also reported in the literature.[12, 23] The van der Waals attraction for a polystyrene particle interacting with a glass plate can be described in a purely empirical fashion by:

$$\Phi_{vdw}(h) = -A^{*}\exp\left(\frac{-h}{W}\right) \qquad 2.22$$

where the van der Waals prefactor, A^{*}, was allowed to vary between $0.1kT$ and $3kT$, and the characteristic decay length, W, are unconstrained. The range of A was chosen based on previous fits to the van der Waals interaction.[16] For a smooth polystyrene particle interacting with a glass slide, $A^{*} = 3k_BT$ and W = 40 nm. The decay length, W, increases to 50 nm when the glass slide is coated with a polystyrene layer with the typical inherent surface roughness.[12] This suggests the decay length should increase as the van der Waals attraction becomes suppressed due to increased surface roughness; we might therefore expect to see an increase in W as particle roughness increases.

Repulsive interactions were better described when an offset, D, was applied to electrostatic repulsion (**Equation 2.20**), but did not fit the data well. In addition to the offset, the apparent Debye length was allowed to vary freely, rather than be constrained to the value matching the electrolyte concentration:

$$\Phi_{edl}(h) = 64(\pi\varepsilon_r\varepsilon_0)R\left(\frac{k_BT}{e}\right)^2 * \tanh\left(\frac{e\Psi_{glass}}{4k_BT}\right)\tanh\left(\frac{e\Psi_{particle}}{4k_BT}\right)\exp\left[-\frac{(h-D)}{(\kappa^{*})^{-1}}\right] \qquad 2.23$$

where κ^{*-1} is an apparent Debye length. Increasing the surface roughness of the particle resulted in an apparent change in the Debye length that increased systematically with surface roughness and decreased with increasing salt concentration (**Figure 2.22**). The

change in the apparent Debye length was only necessary for rough particles treated with 10% and 30% acetone, where the shape of the surface roughness is less sinusoidal and more spherical with many re-entrant spaces. Our results suggest that in the simplest case, the DLVO interactions observed for a rough particle in a given solution is equivalent to the particle-plate interactions for a smooth particle in a lower ionic strength solution.

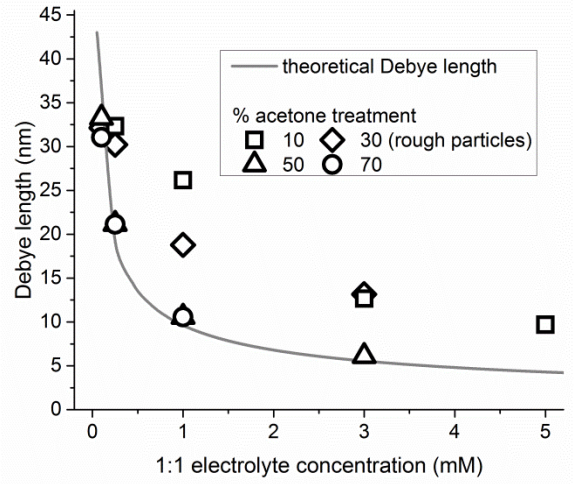

Figure 2.23. The calculated Debye length as a function of salt concentration and particle roughness. κ^{-1} increases systematically with increasing surface roughness and decreases with increasing salt concentration. For smooth particles the fitted apparent Debye length agrees very well with the theoretical expectation for a solution of the given electrolyte composition, but for very rough particles (treated with 10% (□) and 30% (◇) acetone), the apparent Debye length is at least 150% of the expected value.

Using **Equation 2.23** to describe the electrostatic repulsion and **Equation 2.22** to describe the van der Waals attraction resulted in good fits for all experimental particle-plate interactions (**Figure 2.24**).

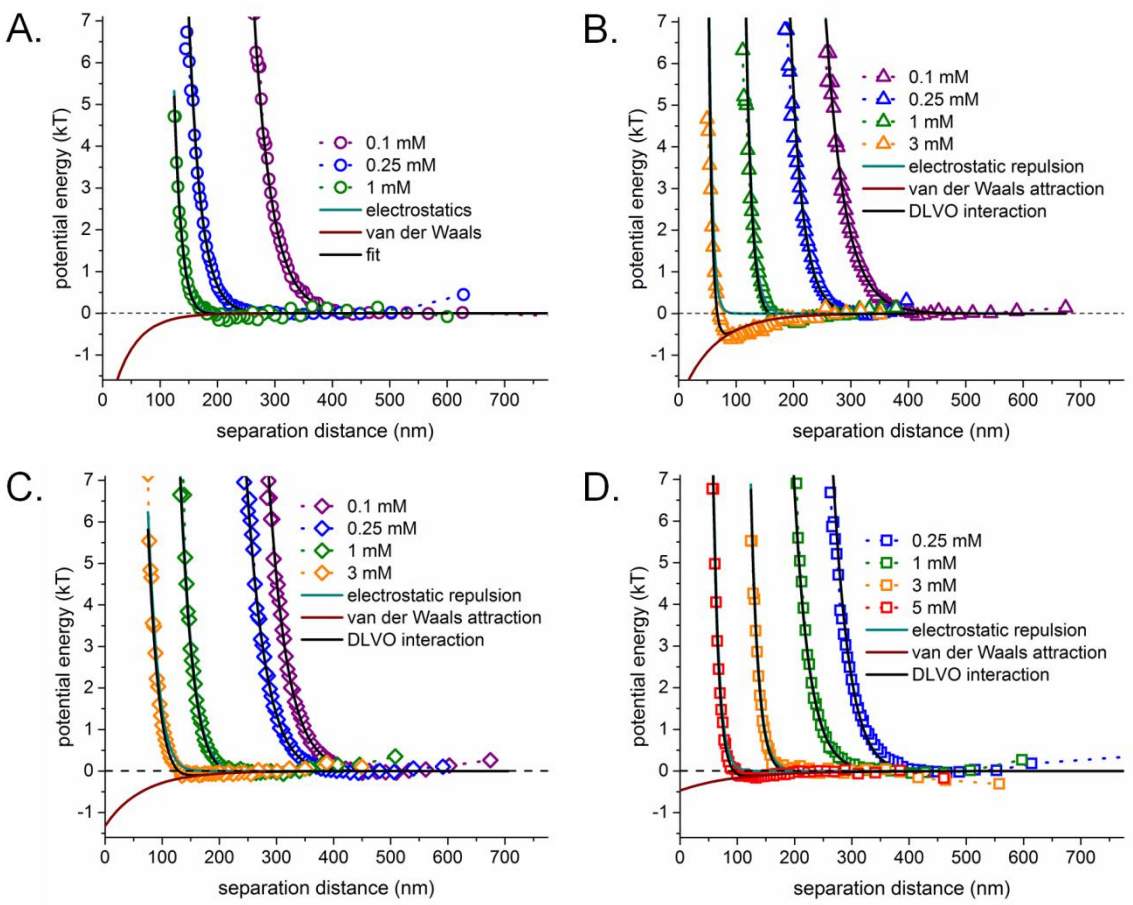

Figure 2.24. Assuming an exponentially decaying van der Waals interaction, an offset in the electrostatic interaction due to surface roughness, and a roughness-dependent Debye length result in good fits for (A) smooth particles, and particles treated with (B) 50%, (C) 30% and (D) 10% acetone.

The van der Waals prefactor, A^*, and the characteristic decay length, W, also vary systematically with surface roughness (**Table 2.7**). The van der Waals attraction is described using literature values for the smoothest particle (70% acetone treatment). Increasing particle surface roughness increases the characteristic decay length and decreases the prefactor, A^*.

Table 2.7 Calculated parameters A^* and W for the van der Waals attraction

% acetone treatment	A^* (k_BT)	W (nm)
10 (roughest)	0.5	95.2
30	1.3	65.2
50	2.1	60
70 (smoothest)	3	40

In order to obtain agreement between experimental data and predicted interactions, two incorrect assumptions were made: the Debye length was assumed to be dependent on surface roughness and the electrostatic interaction was offset from the measured interaction distance by a constant factor, *D*. An alternative description of the electrostatic repulsion assumes the roughness features of interacting surfaces are a series of peaks and valleys normally distributed around an average height.

2.3.2.4 Electrostatic interaction: normalization of surface roughness

If surface asperities are assumed to be normally distributed around an average height, the electrostatic interaction is given by:

$$\Phi_{edl}(h) = \frac{B}{2}\operatorname{erfc}\left(\frac{h}{\sigma_m\sqrt{2}}\right) + \frac{B}{2}e^{-h/\kappa^{-1}}e^{{\sigma_m}^2/2(\kappa^{-1})^2}\left[1+\operatorname{erf}\left(\frac{h-{\sigma_m}^2/\kappa^{-1}}{\sigma_m\sqrt{2}}\right)\right] \quad 2.6$$

where h is the measured particle-plate separation distance.[8] The dominant, exponential term of the equation indicates that the electrostatic repulsive interaction is amplified by surface roughness. The electrostatic coupling constant, B, is dependent on the particle radius and the particle and glass surface potentials, and σ_m, the average Rms roughness is defined as:

$$\sigma_m = \sqrt{{\sigma_{glass}}^2 + {\sigma_{particle}}^2} \quad 2.7$$

where σ_{glass} and $\sigma_{particle}$ are the Rms roughness of the glass slide and colloidal particle, respectively. The Rms roughness of glass was assumed to be negligible compared to the Rms roughness of the particle (σ_{glass} < 1 nm).[54] The electrostatic coupling constant, B, and Debye length, κ^{-1}, were again constrained by imposing that calculated surface

potentials were between -20 mV and -100 mV, and $\Psi_{particle} = 1.6\Psi_{glass}$. The apparent Rms roughness of the interacting surfaces, σ_m, was allowed to vary freely.

If the (local) surface-to-surface separation is assumed to be normally distributed around an average separation, *h*, it becomes possible to describe experimental DLVO interactions using **Equation 2.6** for the electrostatic repulsion and **Equation 2.22** for the van der Waals attraction. Parameters from Table 2.6 were used to calculate the van der Waals attraction. The calculated Debye length was only dependent on solution conditions (**Figure 2.25A**). Furthermore, the fitted Rms roughness of the particle surface correlated well with the degree of smoothing expected from the applied acetone treatment (**Figure 2.25B**).

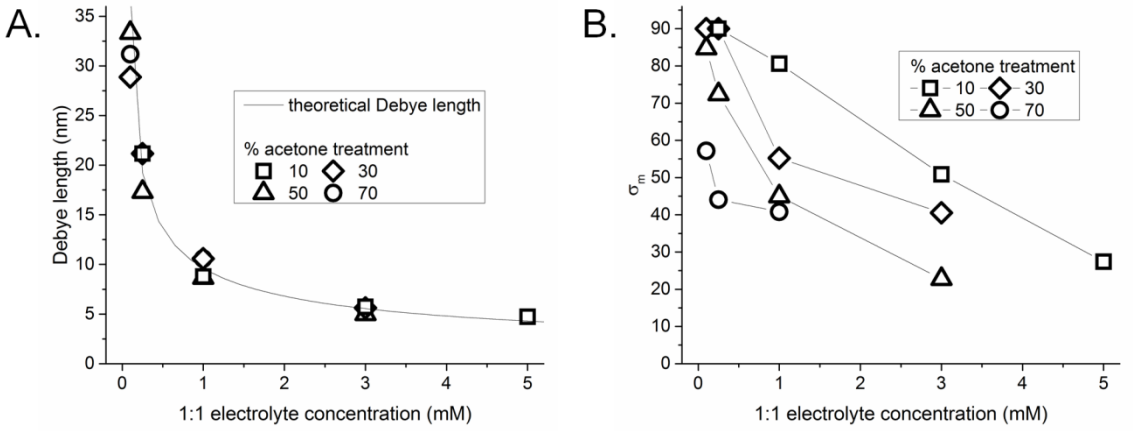

Figure 2.25. The calculated (A) Debye length and (B) mean Rms roughness. The Debye length appears to be only dependent on solution conditions and the mean Rms roughness decreases systematically with surface smoothing.

The apparent Rms roughness, σ_m, is seen to depend strongly on the Debye length of solution. When considering roughness effects on the electrostatic repulsion, local variations in separation distance are probed on a length scale of the Debye length. For the particles studied here, the roughness amplitude is tens of nanometers in length. When the Debye length increases, a larger portion of the roughness features can contribute to the

electrostatic repulsion, which may explain the observed decrease of apparent Rms roughness with decreasing Debye length (increasing electrolyte concentration). Nonetheless, the Rms roughness should appear independent of solution conditions, it the roughness was properly accounted for by the chosen distribution of surface elevations.

The fitted Rms roughness is also significantly larger than the Rms roughness measured by AFM. The difference between the fitted and measured Rms roughness could be due to several factors. AFM measurements are the convolution of the tip diameter and surface features, resulting in an Rms roughness that is smaller than the actual value. Additionally, AFM measurements were taken on glass slides coated with E-S100 particles; the inherent roughness of the glass is very small.[54] On the other hand, surface undulations on "smooth" 6 μm polystyrene particles can be as large as 40 nm.[12]

The combination adequately described the DLVO interactions for all particle systems, regardless of surface roughness (**Figure 2.26**). However, the calculated particle surface potentials for rough particles were -25.3 mV, regardless of the ionic strength of solution. If surface potentials were allowed to vary between -0.5 mV and -100 mV, which is very unrealistic, and $\Psi_{particle} = 1.6\Psi_{glass}$, then the fitted surface potentials are very small (< -10 mV) but generally decrease with increasing salt concentration as one would expect (**Table 2.8**).

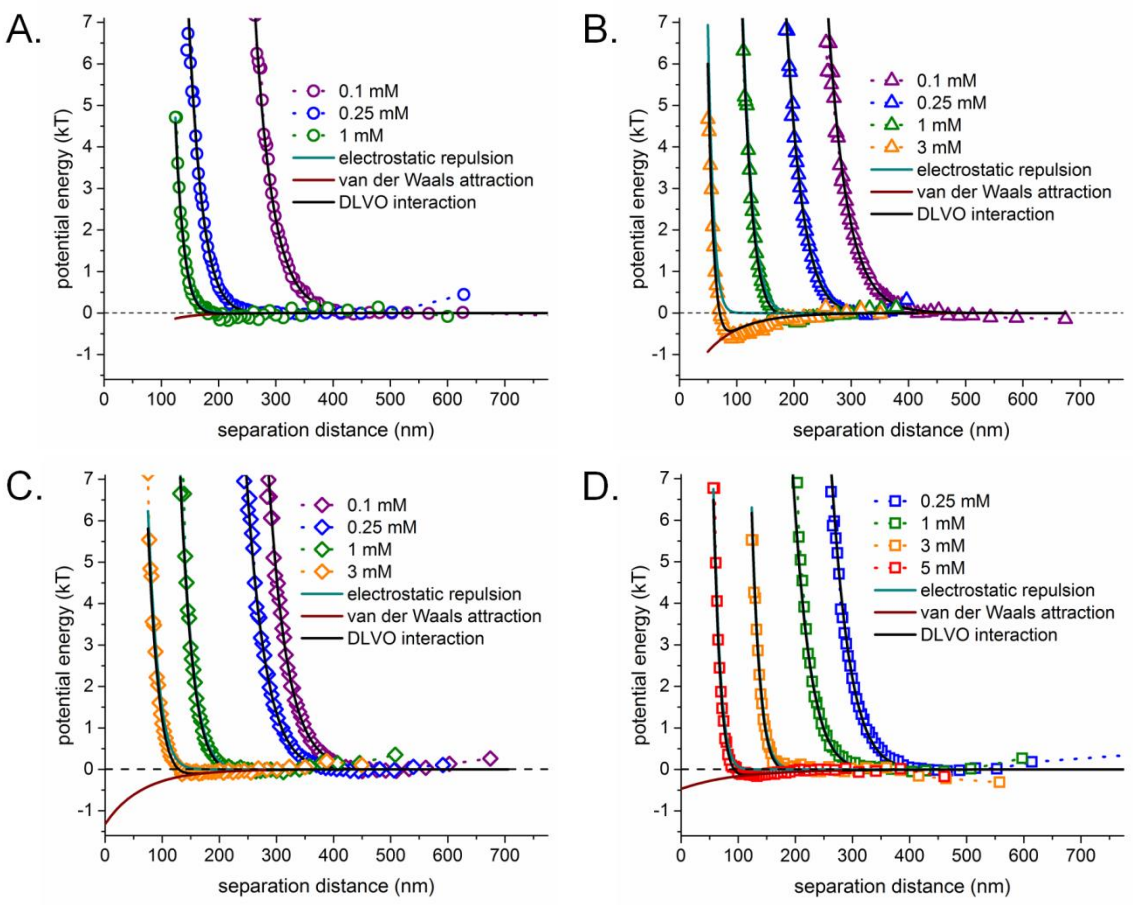

Figure 2.26 Assuming an exponentially decaying van der Waals interaction and normalizing the interacting surfaces when calculating the electrostatic interaction resulted in in good fits for (A) smooth particles (treated with 70% acetone), and particles treated with (B) 50%, (C) 30% and (D) 10% acetone.

Table 2.8 Calculated $\Psi_{particle}$ (mV) for probe particles as a function of ion concentration

[ion] (mM)	% acetone treatment			
	10 (roughest)	30	50	70 (smoothest)
0.1	--	-14.1	-4.0	-35.8
0.25	-9.7	-7.1	-3.8	-6.5
1	-5.0	-3.1	-3.8	-8.9
3	-3.4	-0.8	-1.9	--
5	-1.7	--	--	--

Particles with surface potentials smaller than 25-30 mV in magnitude are usually assumed to aggregate or sediment; since the particles remained suspended in solution during each measurement, it is more likely that the equations used to fit experimental

data were unable to adequately describe the effect of surface roughness on DLVO interactions.

One reason for the inconsistency in calculated surface potentials could be the distribution of surface roughness used to correct the interaction distance of the electrostatic repulsion. Assuming surface roughness is normally distributed means that interactions at negative separation distances and infinite separation distances still contribute, however minutely, to the overall electrostatic repulsion. Normal distribution of surface roughness does not adequately describe the surface roughness of the probe particles. From SEM images, the roughness features of the AFP-ES100 particles can be better described with the elevation distribution of a sinusoidal function than with a normal distribution. Using a normal distribution to weigh roughness features, *e.g.* in **Equation 2.6**, most heavily weighs the local separation distances around the *average* separation, whereas the probability distribution function of a sine function most heavily weighs the separation distances at highest and lowest surface elevation when calculating the electrostatic interaction.

2.4 Concluding remarks

The role of surface roughness for DLVO interactions was examined using colloidal probe particles with varying degrees of roughness. A solvent-based method that partially eroded and allowed for molecular re-deposition of dissolved polymer was used to vary surface topography of polymer-coated polystyrene particles. Surface characterization qualitatively and quantitatively confirmed the surface topography was successfully varied without simultaneously changing surface chemistry. Total internal reflection microscopy was used to measure particle-plate interactions.

Qualitatively, the results show that the van der Waals attraction is suppressed as surface roughness increases. The best fits of experimental data were done via an empirical expression for the van der Waals attraction and an electrostatic interaction with a normal distribution of surface-to-surface separations due to surface roughness. The partial success of modeling roughness features using a normal distribution also suggests that surface roughness amplifies the electrostatic double layer repulsion.

The van der Waals attraction was best described using a purely empirical expression for an exponentially decaying interaction. Both the characteristic decay length and the prefactor to the exponential, a coupling constant that may be interpreted as a form of Hamaker constant, were used as adjustable fit parameters to describe the van der Waals interaction and were found to vary systematically with surface roughness. Fits to experimental data showed the decay length to increase with increasing surface roughness in agreement with reported comparisons of particle interaction with smooth glass surfaces and rougher polymer surfaces. Moreover, the coupling constant A^* (prefactor to the exponential) systematically decreased with increasing surface roughness while remaining in the magnitude range expected for a Hamaker constant.

When calculating the electrostatic repulsion, local surface-to-surface separations were assumed to have a normal distribution with a standard deviation corresponding to an apparent Rms roughness. Regardless of electrolyte concentration, the fitted apparent Rms roughness increased systematically with increasing (prepared) surface roughness as one should expect. The adopted model provided excellent fits to the experimental data but yielded a larger-than-realistic apparent Rms roughness that decreases with increasing electrolyte concentration, as well as suspiciously low particle surface potentials. More

realistic assumptions about the distribution of the local separation distances between the rough particle and the substrate may provide a remedy for some of the shortcomings of the present model. Ultimately, it would be desirable to replace the empirical expression for the van der Waals interaction by a description based on first principles that holds up to experimental verification.

2.5 References

1. B. Derjaguin and L. Landau, Theory of the stability of strongly charged lyophobic sols and of the adhesion of strongly charged particles in solutions of electrolytes. *Acta Phys. Chim.*, 1941, **14**, 633-662.

2. E. Verwey and J. T. G. Overbeek, *Theory of Stability of Lyophobic Solids*, Elsevier, Amsterdam, 1948.

3. D. C. Prieve, Measurement of colloidal forces with TIRM. *Advances in Colloid and Interface Science*, 1999, **82**, 93-125.

4. B. V. Derjaguin, Untersuchungen über die Reibung und Adhäsion, IV. *Kolloid Z.*, 1934, **69**, 155-164.

5. D. F. Evans and H. Wennerström, *The Colloidal Domain: Where Physics, Chemistry, Biology, and Technology Meet, 2nd Edition*, Wiley-VCH, New York, NY, 1999.

6. L. Suresh and J. Y. Walz, Effect of surface roughness on the interaction energy between a colloidal sphere and a flat plate. *J. Colloid Interface Sci.*, 1996, **183**, 199-213.

7. L. Suresh and J. Y. Walz, Direct measurement of the effect of surface roughness on the colloidal forces between a particle and flat plate. *J. Colloid Interface Sci.*, 1997, **196**, 177-190.

8. D. F. Parsons, R. B. Walsh and V. S. Craig, Surface forces: Surface roughness in theory and experiment. *J. Chem. Phys.*, 2014, **140**, 164701.

9. H.-J. Butt, Capillary Forces: Influence of Roughness and Heterogeneity. *Langmuir*, 2008, **24**, 4715-4721.

10. G. Binnig, C. F. Quate and C. Gerber, Atomic force microscope. *Phys. Rev. Lett.*, 1986, **56**, 930.

11. J. Czarnecki, van der Waals attraction energy between sphere and half-space. *J. Colloid Interface Sci.*, 1979, **72**, 361-362.

12. M. A. Bevan and D. C. Prieve, Direct measurement of retarded van der Waals attraction. *Langmuir*, 1999, **15**, 7925-7936.

13. H.-J. Butt and M. Kappl, Normal capillary forces. *Adv. Colloid Interface Sci.*, 2009, **146**, 48-60.

14. J. N. Israelachvili, *Intermolecular and surface forces: revised third edition*, Academic press, 2011.

15. E. Lifshitz, The theory of molecular attractive forces between solids. 1956.

16. M. Nayeri, Z. Abbas and J. Bergenholtz, Measurements of screening length in salt solutions by total internal reflection microscopy: Influence of van der Waals forces and instrumental noise. *Colloids Surf., A*, 2013, **429**, 74-81.

17. V. A. Parsegian and G. H. Weiss, Spectroscopic parameters for computation of van der waals forces. *J. Colloid Interface Sci.*, 1981, **81**, 285-289.

18. M. Nayeri, *Colloidal interactions obtained from total internal reflection microscopy measurements and scattering data*, University of Gothenburg, Sweden, 2011.

19. M. A. Bevan and D. C. Prieve, Forces and Hydrodynamic Interactions between Polystyrene Surfaces with Adsorbed PEO−PPO−PEO. *Langmuir*, 2000, **16**, 9274-9281.

20. X. Huang, S. Bhattacharjee and E. M. Hoek, Is Surface Roughness a "Scapegoat" or a Primary Factor When Defining Particle− Substrate Interactions? *Langmuir*, 2009, **26**, 2528-2537.

21. E. M. V. Hoek, S. Bhattacharjee and M. Elimelech, Effect of Membrane Surface Roughness on Colloid−Membrane DLVO Interactions. *Langmuir*, 2003, **19**, 4836-4847.

22. V. Valmacco, M. Elzbieciak-Wodka, C. Besnard, P. Maroni, G. Trefalt and M. Borkovec, Dispersion forces acting between silica particles across water: influence of nanoscale roughness. *Nanoscale Horiz.*, 2016.

23. L. Helden, R. Eichhorn and C. Bechinger, Direct measurement of thermophoretic forces. *Soft Matter*, 2015, **11**, 2379-2386.

24. X. Gong, Z. Wang and T. Ngai, Direct measurements of particle–surface interactions in aqueous solutions with total internal reflection microscopy. *Chem. Commun.*, 2014, **50**, 6556-6570.

25. S. Rentsch, R. Pericet-Camara, G. Papastavrou and M. Borkovec, Probing the validity of the Derjaguin approximation for heterogeneous colloidal particles. *Phys. Chem. Chem. Phys.*, 2006, **8**, 2531-2538.

26. R. R. Dagastine, M. Bevan, L. R. White and D. C. Prieve, Calculation of van der Waals forces with diffuse coatings: Applications to roughness and adsorbed polymers. *J. Adhesion*, 2004, **80**, 365-394.

27. S. Lipson and H. Lipson, *Optical Physics*, Cambridge University Press, New York, 1981.

28. D. C. Prieve, Measurement of colloidal forces with TIRM. *Adv. Colloid Interface Sci.*, 1999, **82**, 93-125.

29. H. Chew, D.-S. Wang and M. Kerker, Elastic scattering of evanescent electromagnetic waves. *Appl. Opt.*, 1979, **18**, 2679-2687.

30. D. C. Prieve and J. Y. Walz, Scattering of an evanescent surface wave by a microscopic dielectric sphere. *Appl. Opt.*, 1993, **32**, 1629-1641.

31. D. C. Prieve and N. A. Frej, Total internal reflection microscopy: a quantitative tool for the measurement of colloidal forces. *Langmuir*, 1990, **6**, 396-403.

32. A. Ashkin, J. Dziedzic, J. Bjorkholm and S. Chu, Observation of a single-beam gradient force optical trap for dielectric particles. *Opt. Lett.*, 1986, **11**, 288-290.

33. K. Svoboda and S. M. Block, Biological applications of optical forces. *Annu Rev Biophys.*, 1994, **23**, 247-285.

34. B. J. Park and E. M. Furst, Attractive interactions between colloids at the oil–water interface. *Soft Matter*, 2011, **7**, 7676-7682.

35. M. D. Wang, H. Yin, R. Landick, J. Gelles and S. M. Block, Stretching DNA with optical tweezers. *Biophys. J.*, 1997, **72**, 1335.

36. A. San-Miguel and S. H. Behrens, Influence of nanoscale particle roughness on the stability of Pickering emulsions. *Langmuir*, 2012, **28**, 12038-12043.

37. J. W. Tsao, Master's Thesis, Georgia Institute of Technology, 2014.

38. E. Gadelmawla, M. Koura, T. Maksoud, I. Elewa and H. Soliman, Roughness parameters. *J. Mater. Process. Technol.*, 2002, **123**, 133-145.

39. R. J. Hunter, *Zeta potential in colloid science: principles and applications*, Academic press London, 1981.

40. C. Schnitzer and S. Ripperger, Influence of surfae roughness on streaming potential method. *Chem. Eng. Technol.*, 2008, **31**, 1696-1700.

41. D. A. Kenny, *Statistics for the social and behavioral sciences*, Little, Brown Boston, 1987.

42. J. L. Bitter, G. A. Duncan, D. J. Beltran-Villegas, D. H. Fairbrother and M. A. Bevan, Anomalous Silica Colloid Stability and Gel Layer Mediated Interactions. *Langmuir*, 2013, **29**, 8835-8844.

43. C. Hertlein, N. Riefler, E. Eremina, T. Wriedt, Y. Eremin, L. Helden and C. Bechinger, Experimental verification of an exact evanescent light scattering model for TIRM. *Langmuir*, 2008, **24**, 1-4.

44. L. Helden, E. Eremina, N. Riefler, C. Hertlein, C. Bechinger, Y. Eremin and T. Wriedt, Single-particle evanescent light scattering simulations for total internal reflection microscopy. *Appl. Opt.*, 2006, **45**, 7299-7308.

45. J. Y. Walz and D. C. Prieve, Prediction and measurement of the optical trapping forces on a microscopic dielectric sphere. *Langmuir*, 1992, **8**, 3073-3082.

46. P. C. Odiachi and D. C. Prieve, Removing the effects of additive noise from TIRM measurements. *J. Colloid Interface Sci.*, 2004, **270**, 113-122.

47. L. Diéguez, N. Darwish, M. Mir, E. Martínez, M. Moreno and J. Samitier, Effect of the refractive index of buffer solutions in evanescent optical biosensors. *Sensor Lett.*, 2009, **7**, 851-855.

48. D. Haughey and J. Earnshaw, Studies of colloidal interactions using total internal reflection microscopy. *Colloids Surf., A*, 1998, **136**, 217-230.

49. S. H. Behrens and M. Borkovec, Influence of the secondary interaction energy minimum on the early stages of colloidal aggregation. *J. Colloid Interface Sci.*, 2000, **225**, 460-465.

50. Y. Gu and D. Li, The ζ-potential of glass surface in contact with aqueous solutions. *J. Colloid Interface Sci.*, 2000, **226**, 328-339.

51. J. Y. Walz, L. Suresh and M. Piech, The effect of nanoscale roughness on long range interaction forces. *J. Nanopart. Res.*, 1999, **1**, 99-113.

52. R. J. Hill, D. Saville and W. Russel, Electrophoresis of spherical polymer-coated colloidal particles. *J. Colloid Interface Sci.*, 2003, **258**, 56-74.

53. L. A. Rosen and D. A. Saville, The dielectric response of polystyrene latexes: Effects of alterations in the structure of the particle surface. *J. Colloid Interface Sci.*, 1990, **140**, 82-92.

54. P. K. Gupta, D. Inniss, C. R. Kurkjian and Q. Zhong, Nanoscale roughness of oxide glass surfaces. *J. Non-Cryst. Solids*, 2000, **262**, 200-206.

CHAPTER 3

SURFACE ROUGHNESS EFFECTS ON DEPLETION INTERACTIONS

3.1 Background

The total interaction energy, Φ_{total}, felt by a colloidal particle suspended in a dilute solution of depletants interacting with a flat plate is the sum of the gravitational interaction, the DLVO interaction, and the depletion interaction:

$$\Phi_{total} = \Phi_{grav} + \Phi_{edl} + \Phi_{vdw} + \Phi_{dep} \quad 3.1$$

where Φ_{grav} is the gravitational energy, the DLVO interaction is comprised of the repulsive electric double layer interaction, Φ_{edl}, and the attractive van der Waals interaction, Φ_{vdw}, and Φ_{dep} is the depletion interaction.

3.1.1 Asakura-Oosawa (AO) depletion interaction potential

The earliest quantitative description of the depletion interaction was given by Asakura and Oosawa,[1] and later by Vrij,[2] who proposed the interaction energy between two surfaces suspended in a suspension of depletants was:

$$\Phi_{dep} = -V_{overlap}\Delta\Pi \quad 3.2$$

where $V_{overlap}$ is the overlap volume of the "depletion zones" around large particles or confining walls, from which the depletants are excluded because of their finite size; and the osmotic pressure, $\Delta\Pi$, is described by van't Hoff's law as the number concentration of depletants in solution, n, multipled by the Boltzmann constant, k, and temperature, T:

$$\Delta\Pi = nkT \quad 3.3$$

The excluded volume $V_{overlap}$ is dependent on the geometries of the two interacting surfaces and the size of the depletants. The overlap volume for a sphere interacting with a flat plate in a solution with depletants is given by:

$$V_{overlap} = \begin{cases} \frac{4}{3}\alpha^3 + 4\alpha^2 R - 4\alpha R h + R h^2 - \alpha h^2 & h < 2\alpha \\ 0 & h > 2\alpha \end{cases} \quad 3.4$$

where α is the depletant radius, R is the radius of the sphere, and h is the particle-plate separation distance (**Figure 3.1**).[1]

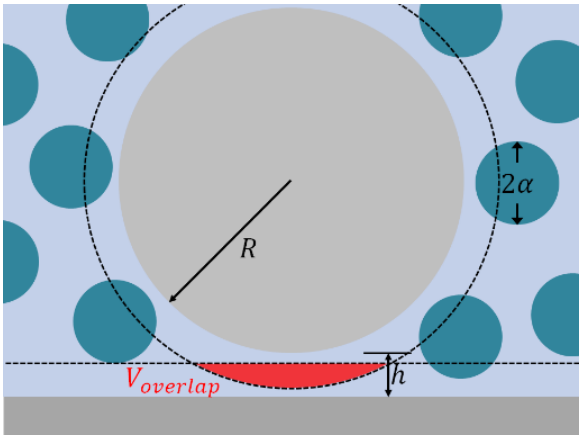

Figure 3.1. Schematic of a large particle with radius R and plate in a dilute depletant solution, where the depletant radius is α. The overlap volume is indicated in red.

Since the AO potential was first proposed, corrections have been proposed to better reconcile experimental results with theoretical predictions. For example, recent descriptions of the depletion interaction account for depletion interaction at surface separations where depletants are present in the gap, but at a local concentration different from the bulk depletant concentration.[3] In this case, ΔΠ is dependent on the ratio of depletants within and outside of the gap, along with depletant properties (*e.g.* radius, surface potential) and the Debye screening length and temperature of solution.

Another common correction to the AO potential affects deviations from hard sphere interaction of the depletant with the confining surfaces. In order to account for the

"softer" interactions of charged depletants it is customary to assume that the characteristic length of the depletion interaction is not governed by the actual size of the depletants, but by an effective depletant size, α^*:

$$\alpha^* = \alpha + s\kappa^{-1} \quad 3.5$$

where α is the actual depletant radius, s is a multiplier, and κ^{-1} is the Debye screening length. Non-ionic depletants are assumed to be independent of the Debye length (s = 0), but for nanobubble depletants s = 1 and for highly charged polymeric depletants, s = 4.7 have produced better agreement with experiments.[4-6]

3.1.1.1 The oscillatory interaction

Equation 3.4 describes the depletion interaction is a monotonically attractive interaction. In practice, this is only true at low depletant concentrations.[7, 8] At higher depletant concentrations, spatial ordering of depletants occurs in the particle-plate gap. The accumulation of depletants in a gap that can only accommodate a few depletant layers gives rise to the oscillatory forces.[9, 10] These oscillatory forces may be thought of as a depletant-scale analogue of the so-called "structural forces" observed between atomically smooth surfaces with SFA and attributed to the ordering of solvent molecules in gaps small enough to fit in only a few discrete solvent layers.[11-13] The oscillatory structural forces are known to be suppressed when the confining surfaces are rough, because the rough surfaces do not promote the ordering of solvent molecules in discrete layers.[14] By extension, the ordering of depletant particles in the particle-plate gap and the amplitude of the oscillations may also be suppressed by the surface roughness of the colloidal particle. To our knowledge, no one has studied the influence of surface roughness on the oscillatory depletion force.

A literature example of TIRM measurements in a depletant system is shown in **Figure 3.2**. Initially, there is no polymer in the system (**Figure 3.2A**). At higher concentrations, the depletants begin to order in the gap, resulting in a small oscillation, indicated with a red circle, in the interaction energy (**Figure 3.2B**). However, once the depletant concentration is too high, the particle becomes trapped in the secondary energy well (**Figure 3.2C-E**).[6]

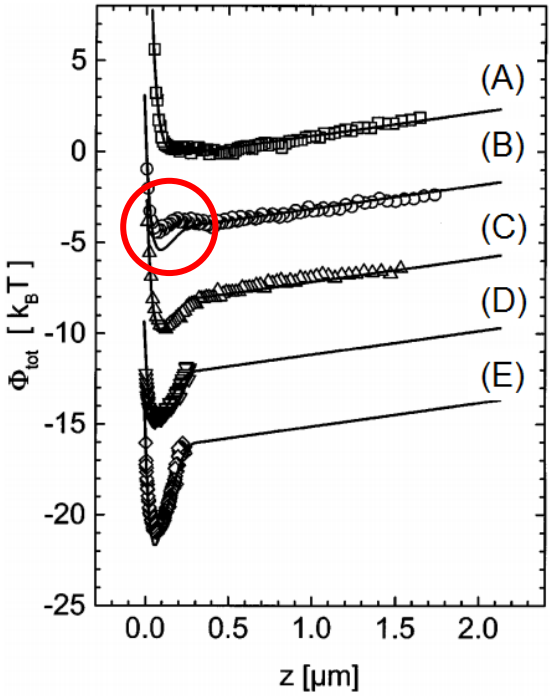

Figure 3.2. Measured potential curves (symbols) of a polystyrene sphere as a function of its distance *z* from a flat surface in poly(ethylene oxide) (PEO) concentrations of (A) $n = 0$, (B) $n = 7.6\mu m^{-3}$, (C) $n = 10.2\ \mu m^{-3}$, (D) $n = 12.7\ \mu m^{-3}$, and (E) $n = 25.5\ \mu m^{-3}$. The solid lines are predicted interaction energy, Φ_{total}, where $\Phi_{total} = \Phi_{grav} + \Phi_{edl} + \Phi_{dep}$.[6]

When an oscillation in the attractive interaction occurs, it has been shown to have a periodicity that is dependent on the characteristic length scale of the depletant; for highly charged particle or micelle depletants, the characteristic length is defined using **Equation 3.5**. The multiplier *s* is dependent on the type of depletant in solution, if the

system contains more than one type of depletant.[7, 8] For single depletant systems, the depth of the second attractive wells depend on depletant concentration and size.[7, 15]

3.1.2 The Derjaguin approximation

The Derjaguin approximation (§2.1.3) can be used to convert particle-plate depletion interactions (**Equation 3.4**) to describe other geometries, such as the interaction between two colloidal particles in a depletant system. The approximation is only valid when the radii of curvature for the interacting surfaces is much larger than the range of interaction. For depletion interactions, the range of interaction is dependent on the depletant size, and is usually smaller than 300 nm.[16] Since the interaction range is much smaller than the radii of curvature of the probe particle (> 2.5 μm), it is appropriate to use the Derjaguin approximation.

3.1.3 Roughness effects on the depletion interaction

It has been shown that the presence of surface roughness can significantly reduce the strength of depletion interaction.[17-20] Studies that have exploited the roughness-dependent depletion interaction often use etching methods to selectively vary the surface topography of colloidal cylinders or platelets.[19, 21] One examination of mixtures of rough and smooth colloid particles used depletants of a different length scale and surface chemistry as the particle.[17] To date, no study has experimentally isolated the role of surface roughness for the depletion interaction using depletants with the same surface chemistry and length scale as the surface roughness features.

3.1.4 Total internal reflection microscopy: considerations for a depletant system

As mentioned in §2.1.5, total internal reflection microscopy determines the particle elevation based on the amount of light scattered by the particle. For a depletant dispersion, the depletants could scatter light and result in misinterpretation of the scattering data. The amount of light scattered by a particle in an evanescent wave with a decay length ξ^{-1} is dependent on the particle size and refractive index relative to the medium it is suspended in.[22, 23] In this study, the depletants used were 60 nm E-S100 polymer particles. The refractive index of E-S100 is 1.39, which is quite similar to the refractive index of water (n = 1.33), and the depletant radii are very small. The combination of the two factors indicates that the amount of light scattered by the depletants can be considered negligible compared to the light scattered by the probe particle.[5, 24]

3.2 Methods

The depletion interaction is dependent on many experimental parameters such as the surface roughness of the colloidal particles, the size and concentration of the depletants, and the ionic strength and pH of the solvent.

We measured depletion interactions for E-S100 coated amine-functionalized polystyrene particles with tunable surface roughness (§2.2.1) in dispersions of E-S100. The depletion interaction parameters were determined for three particles: a particle treated with 70% acetone (smooth surface), one treated with 50% acetone (sinusoidal roughness), and one treated with 30% acetone (discrete, spherical surface asperities).

The E-S100 depletants were 60 nm in diameter with a coefficient of variance of 30.8% (§2.2.1.1). At high depletant concentrations where oscillations are usually

observed, it is possible that the polydispersity of depletants will "smear out" the oscillatory force and subsequent effect of surface roughness on the oscillatory interaction.[25-27] We slightly modified the TIRM technique (§2.2.2) to measure the particle-plate interaction energy in two depletant concentrations. Measurements were taken in a buffered solution at a constant ionic strength in an attempt control the pH of the aqueous solutions. Data analysis to calculate the depletion parameters was done with Matlab R2015 (§2.2.3).

3.2.1 Aqueous solutions for TIRM measurements

We examined the role of surface roughness on the depletion interaction for two depletant concentrations: 0.3% v/v and 0.57% v/v. All measurements were done using particles suspended in 0.5 mM sodium phosphate buffer. The ionic strength was chosen so van der Waals and electrostatic interactions were non-negligible and could be accounted for once depletants were introduced to the system. The final pH of the depletant solutions was 6.14, and the pH of the depletant-free system was 6.84.

E-S100 is a relatively acidic polymer (pKa = 4.9) with a narrow pH stability window: E-S100 particles aggregate in low pH and dissolve in high pH solutions.[28, 29] Since E-S100 is a polyacid, therefore different concentrations of E-S100 in solution will be at different pH. Without the addition of buffer, the pH of the 0.3% v/v dispersion was close to pH 6, while the pH of an unbuffered 0.57% v/v E-S100 dispersion was close to pH 5. Since the particle surface charge is very sensitive to pH in the range close to the pKa, E-S100 dispersions were buffered in order to avoid pH differences from changing the particle surface potentials and influencing the electrostatic repulsive interactions. Sodium phosphate buffer, a mixture of monobasic sodium phosphate (NaH_2PO_4, Sigma

Aldrich) and dibasic sodium phosphate (Na_2HPO_4, Sigma Aldrich) was chosen because its buffer range is 5.8-8. The buffer pH can be tuned by altering the ratio at which the two salts are combined. However, the buffer concentrations used in this study will be much lower than the ideal concentrations (*e.g.* 100 mM) due to limits of the TIRM method. A colloidal particle in 100 mM solution would irreversibly attach to the bottom of the measurement cell.

A 0.5 mM sodium phosphate buffer was used to decrease the shift in solution pH upon addition of E-S100 depletants. The concentration was chosen because based on monoelectrolyte data, it should be possible to observe both van der Waals and electrostatic interactions at that solution concentration, and both contributions could be accounted for upon addition of depletants. pH-controlled depletant dispersions used in this study were made by adding 100 mM sodium phosphate buffer at varying pH to the dispersion to reach a final concentration of 0.5 mM sodium phosphate buffer.

Due to the different concentrations of E-S100, buffers with different pH were needed to reach a final depletant dispersion pH of 6.14. As such, the Debye screening length, and decay length of electrostatic repulsion, was solution-dependent. The theoretical Debye screening length in solution was calculated via:

$$\kappa^{-1} = \sqrt{\frac{\varepsilon_r \varepsilon_0 k_B T}{e^2 N_A \sum c_i {z_i}^2}} \qquad 3.6$$

where e is the elementary charge, c_i is the concentration of the species i, z_i is the charge of species i, N_A is Avagadro's constant, ε_r is the dielectric constant, ε_0 is the vacuum permittivity, k_B is the Boltzmann constant, and T is the temperature. The screening length of solution decreased as the ratio of Na_2HPO_4 to NaH_2PO_4 increased (**Table 3.1**).

Table 3.1. Debye screening length for solutions used to measure roughness effects on the depletion interaction. All solutions were 0.5 mM sodium phosphate buffer.

% E-S100 (v/v)	pH	Debye length (nm^{-1})
0	6.9	11.1
0.3	6.1	11.1
0.57	6.1	10.7

3.2.2 TIRM measurements

All TIRM measurements were taken in 0.5 mM sodium phosphate buffered solution. In the beginning of each measurement, a single colloidal particle was isolated from a dispersion of E-S100 coated amine-functionalized particles using an optical trap. The unused particles were then flushed from the cell and particle elevations in pH 6.85, 0.5 mM buffer solutions were measured. The potential energy curve determined from the particle elevations provided the baseline measurement to calculate the DLVO interactions. Depletant-mediated particle-plate interactions were then measured in 0.3% v/v and 0.57% v/v E-S100 dispersions. In between each measurement, 14 mL solution (14 x the TIRM cell volume) was used to flush the cell. A minimum of 10x cell volume of solution is necessary to the previous solution was completely replaced with the new depletant solution.[30] At the end of every measurement, the colloidal particle was salted out of solution, *i.e.* irreversibly attached to the bottom of the measurement cell, using 100 mM NaCl.

3.2.3 Calculation of DLVO parameters

In 0.5 mM buffer solution, the electrostatic repulsion and van der Waals attraction contribute to the total DLVO interaction. When determining DLVO parameters, the Debye length was allowed to vary within 10% of the calculated value (**Table 3.1**). The electrostatic repulsion was determined via **Equation 2.6:**

$$\Phi_{edl}(h) = \frac{B}{2}\mathrm{erfc}\left(\frac{h}{\sigma_m\sqrt{2}}\right) + \frac{B}{2}e^{-h/\kappa^{-1}}e^{{\sigma_m}^2/2(\kappa^{-1})^2}\left[1 + \mathrm{erf}\left(\frac{h - {\sigma_m}^2/\kappa^{-1}}{\sigma_m\sqrt{2}}\right)\right] \quad 2.6$$

where h is the measured particle-plate separation distance.[31] The electrostatic coupling constant, B, is dependent on the particle radius and the surface potentials, Ψ_i, of the particle and glass, and σ_m, the average Rms roughness is defined as:

$$\sigma_m = \sqrt{{\sigma_{glass}}^2 + {\sigma_{particle}}^2} \quad 2.7$$

where σ_{glass} and $\sigma_{particle}$ are the Rms roughness of the glass slide and colloidal particle, respectively. The Rms roughness of glass was assumed to be negligible compared to the Rms roughness of the particle (σ_{glass} < 1 nm).[32] The electrostatic coupling constant, B, was again constrained by imposing that calculated surface potentials were between -0.5 mV and -100 mV, and $\Psi_{particle} = 1.6\Psi_{glass}$. The Debye length, κ^{-1} was constrained to be within 10% of its theoretical value. The apparent Rms roughness of the interacting surfaces, σ_m, was allowed to vary freely.

The van der Waals interaction was fit to the empirical equation:

$$\Phi_{vdw}(h) = -A^*\exp\left(\frac{-h}{W}\right) \quad 2.22$$

where A^* was allowed to vary between $0.1kT$ and $3kT$, and W was allowed to vary freely. Following the literature and results obtained in Chapter 2, we assumed the van der Waals interaction was independent of depletant and ion concentration in solution.[33-35]

3.3 Results

The gravitational interaction must first be determined in order to obtain the DLVO and depletion interaction energy curves. The gravitational energy was calculated based on the potential energy of the particle at large elevations using **Equation 2.2**:

$$\Phi_{grav}(h) = mgh = \frac{4}{3}\pi R^3(\rho_p - \rho_f)gh \qquad 2.2$$

where m is the particle mass, R is the particle radius, g is the gravitational acceleration, and ρ_p and ρ_f are the density of the particle and solvent, respectively. The particle volume and radius were calculated assuming a particle density of 1050 kg/m^3 for the polystyrene particles and density of 1000 kg/m^3 for the aqueous solutions. A comparison of the particle sizes used in this study is shown in **Table 3.2**.

Table 3.2 Calculated gravitational force and diameter of particles treated with varying concentrations of acetone

% acetone treatment	Gravitational force (fN)	Calculated particle diameter, D(μm) (with 95% confidence interval)
30 (rough)	53.6 ± 5.6	5.9 (5.7, 6.1)
50	48.9 ± 6.8	5.8 (5.5, 6)
70 (smooth)	47.4 ± 9	5.7 (5.3 6)

The calculated particle sizes are consistent with the average particle size (6 μm) cited by the manufacturer. In this study, the apparent correlation of the particle size with surface smoothing was coincidental. The small variation of particle size did not have a significant effect on the particle-plate interaction energy. As seen in **Figure 3.3**, the typical particle elevation increased and the van der Waals attraction became progressively weaker as the particle surface become more rough, which qualitatively agrees with results from §2.3.

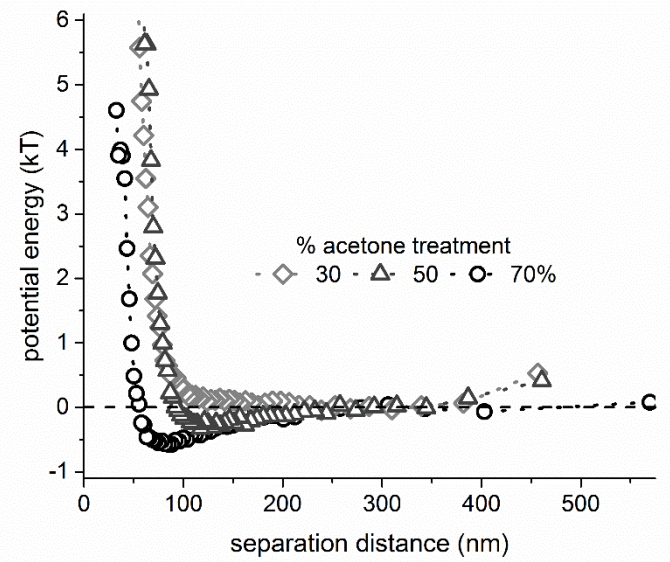

Figure 3.3. In a 0.5 mM sodium phosphate buffer at pH 6.85, the presence of surface roughness increases the particle-plate separation distance and weakens the van der Waals attraction. The smoothest particle (○) is the closet to the glass plate and has the deepest attractive well. While the roughest particle (◇), whose surface roughness is characterized by discrete spherical asperities samples similar particle elevations as the particle characterized by sinusoidal asperities (Δ), the attractive well (due to van der Waals interaction) is deeper for the smoother of the two particles.

3.3.1 Calculation of DLVO parameters: depletant free system

The electrostatic coupling factor, *B*, and the particle surface potentials, Ψ_i, decreased monotonically with surface roughness decreased, and while the fitted Debye length was systematically smaller than the expected Debye length (κ^{-1} = 12.64 nm), it did not depend systematically on surface roughness (**Table 3.3**).

Table 3.3 Fitted Debye length, surface potentials for the colloidal particle and glass slide in the depletant-free system (pH 6.85, 0.5 mM sodium phosphate buffer)

% acetone treatment	Fitted Debye length κ^{-1} (nm)	Ψ_{glass} (mV)	$\Psi_{particle}$ (mV)
30 (rough)	11.1	-8.7	-13.9
50%	11.1	-8.0	-12.7
70 (smooth)	10.7	-4.0	-6.5

Similar to trends for particles in a 1:1 electrolyte, the van der Waals coupling constant decreased and the exponential decay length increased with increasing surface

roughness (**Table 3.4**). Despite the fact that the van der Waals decay length fit parameter *W* was unconstrained, the decay length for the particles in the depletant system was the same order of magnitude as the equivalent parameter for particles in the 1:1 electrolyte system. The van der Waals parameters used to fit the depletant-free system were assumed to be independent of depletant concentration.[33-35]

Table 3.4 Fitted coupling constant A^* and characteristic decay length, *W* for the van der Waals interaction between the colloidal probe particle and glass slide in the depletant-free system (pH 6.85, 0.5 mM sodium phosphate buffer)

% acetone treatment	A^*	*W*
30 (rough)	0.1	71.7
50	1.7	71.7
70 (smooth)	3	58.7

3.3.1.1 Calculation of DLVO parameters: depletant system

As discussed in Chapter 2, the assumptions made regarding the shape of the particle features, used to determine the electrostatic interaction are not correct, so the apparent Rms roughness can appear to depend on the factors other than surface topography. In the depletant systems, it is possible that the non-monovalent electrolyte will also affect the apparent Rms roughness. Despite these concerns, the fitted Rms roughness for particles treated with 30% (◇) and 50% (△) acetone solutions was higher than the Rms roughness fitted to particles treated with 70% (○) acetone solutions, which can be expected based on the actual particle surface topography (**Figure 3.4**).

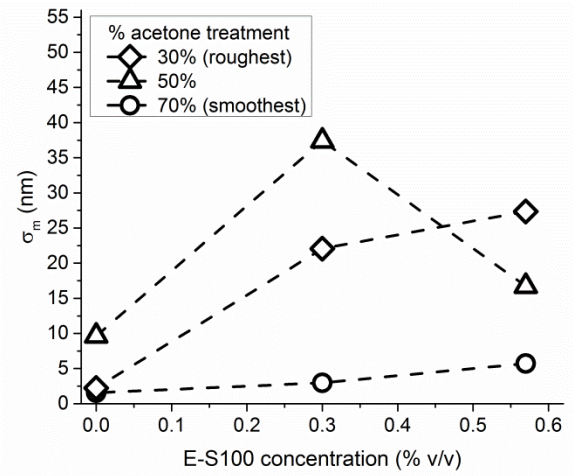

Figure 3.4. The fitted Rms roughness for particles treated with 30% (◇), 50% (△), and 70% (○) acetone in a 0.5 mM sodium phosphate buffer system without any depletants, 0.3% v/v E-S100, and 0.57% v/v E-S100. The Rms roughness for rough particles was larger than that for the smooth particle.

The fitted particle surface potentials were the same order of magnitude as the values found for the 1:1 electrolyte solutions (**Table 3.5**). In general, the rougher particles appeared more negatively charged than the smoothest one, with the exception of the particle treated with 50% acetone in 0.57% v/v E-S100 solution. It is possible that the experimental conditions, which will be discussed further in §3.3.2.1, contributed to the comparatively low surface potential.

Table 3.5 Fitted surface potentials for the colloidal particle and glass slide in solutions with various E-S100 depletant concentrations.

% acetone treatment	$\Psi_{particle}$ (mV)		
	0% v/v E-S100	0.3% v/v E-S100	0.57% v/v E-S100
30 (rough)	-13.4	-18.5	-12.7
50	-12.7	-12.3	-6.3
70 (smooth)	-6.5	-8.3	-12.4

3.3.2 Roughness effects on the depletion interaction

For a smooth system, the attractive component of the interaction clearly increases with the depletant concentration (**Figure 3.5**). The depth of the attractive well in the depletant free system (black circles) is -1.43*kT*, and increases to -1.56*kT* in the 0.3% v/v

E-S100 system (green circles), and to -3.28*kT* in the 0.57% v/v E-S100 system (red circles). The particle-plate separation distance decreases slightly with increasing depletant concentration, the behavior is consistent with the assumption that the Debye screening length decrease (and the electrostatic repulsion is screened) with increasing depletant concentration.

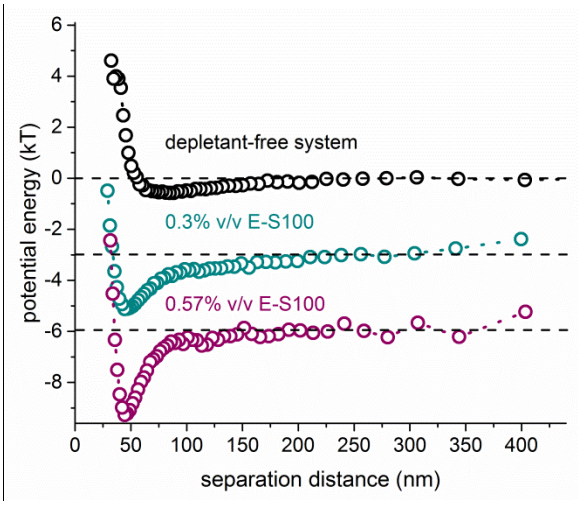

Figure 3.5. Depletant-mediated interaction for a smooth particle (70% acetone) in 0.5 mM phosphate buffer when the depletant concentration is 0% v/v (black symbols), 0.3% v/v (green symbols), and 0.57% v/v (red symbols). The depth of the attractive well increases noticeably as the depletant concentration increases.

The deepening of the attractive well is also seen for rough particles treated with 30% acetone (**Figure 3.6A**) and 50% acetone (**Figure 3.6B**). The reason for the shift in the interaction energy curves for a particle treated with 50% acetone (**Figure 3.6B**) when depletants are initially added to the system is not immediately apparent. However, silica surfaces are prone to charge heterogeneity; it is possible that a part of the glass was less negative and depletant particles adsorbed to the bottom of the TIRM cell and artificially increased surface roughness, suppressing the van der Waals interaction.[36] However, the depth of the attractive well for in the depletant systems is very similar for the two

particles, especially when compared to the attractive interaction for a smooth particle (**Figure 3.5**) in the same conditions (**Table 3.6**).

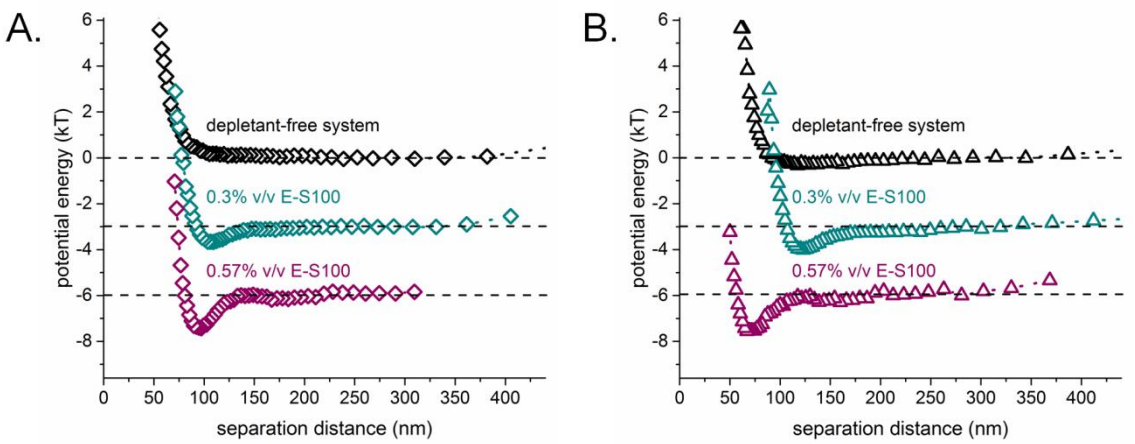

Figure 3.6. Depletant-mediated interaction for a particle treated (A) with 30% acetone, and (B) with 50% acetone when the depletant concentration is 0% v/v (black symbols), 0.3% v/v (green symbols), and 0.57% v/v (red symbols). Both measurements were taken in 0.5 mM phosphate buffer solution.

Table 3.6 Minimum potential energy for the colloidal particles in each of the depletant systems (pH 6.85, 0.5 mM sodium phosphate buffer)

% acetone treatment	Φ_{min} (kT)		
	0% v/v E-S100	0.3% v/v E-S100	0.57% v/v E-S100
30 (rough)	0	-0.7	-1.4
50	-0.3	-1.0	-1.6
70 (smooth)	-0.6	-2.1	-3.3

The relatively small change in the depletion-dependent minimum between particles treated with 30% and 50% acetone is not too surprising: surface roughness significantly decreases the depletion interaction if the Rms roughness is larger than the depletant size (and overlap volume).[19] Based on AFM measurements (**Table 2.2**) and SEM scans of the E-S100 coated particles (**Figure 2.5**), the approximate difference in Rms roughness between particles treated with 30% and those treated with 50% acetone is less than 1 nm, which is much smaller than the depletant size, resulting in a relatively small difference in the depletion interaction.[37] The difference between particles treated

with 50% and 70%, however, is much larger, which would result in a much larger difference in depletion interaction and an increase in the depth of the attractive well.

The total interaction is the sum of the electrostatic, van der Waals, and depletion interactions. The typical particle elevations of the smoothest particle (**Figure 3.5**) are much lower than those of the particles treated with 50% acetone (**Figure 3.6A**), indicating that the van der Waals attraction contributes more to the overall interaction. Furthermore, the particle-plate overlap volume for a particle with sinusoidally shaped surface roughness (50% acetone treatment) is much smaller than the overlap volume for a smooth particle (70% acetone treatment). The combination of the two factors most likely results in the observed qualitative difference between the potential energy curves. A more detailed analysis of the depletion interaction beyond comparing the depth of the attractive well is necessary.

3.3.2.1 Calculation of depletion interaction parameters

Equations 3.2-3.5 were used to fit the depletion interaction energy:

$$\Phi_{dep} = \begin{cases} -\Delta\Pi\left[\frac{4}{3}\alpha^{*3} + 4\alpha^{*2}R - 4\alpha^{*}Rh + Rh^2 - \alpha^{*}h^2\right] & h < 2\alpha^{*} \\ 0 & h > 2\alpha^{*} \end{cases} \qquad \begin{matrix} 3.7 \\ \text{(Eqs. 3.2-3.5)} \end{matrix}$$

where the apparent depletant radius, α^{*}, is dependent on the depletant radius and the solution Debye length, $\Delta\Pi$ is the osmotic pressure, and R is the particle radius. The apparent depletant radius, α^{*}, was bound between $[\alpha + 3\kappa^{-1}]$ and $[\alpha + 6\kappa^{-1}]$ based on literature values for the apparent depletant length for highly charged depletants.[4-6] The particle radius was bound by the 95% confidence limits set by the gravitational fits and the osmotic pressure, $\Delta\Pi$ had to be the same order of magnitude as the theoretical osmotic pressure, nkT. For a 0.3% and 0.57% v/v E-S100 solution, the expected values for $\Delta\Pi$ are $3 \times 10^{-8}\, kT/nm^3$ and 5.8

$\times$ 10^{-8} kT/nm^3, respectively. The fits of depletion interactions using those parameter limits are shown in **Figure 3.7**.

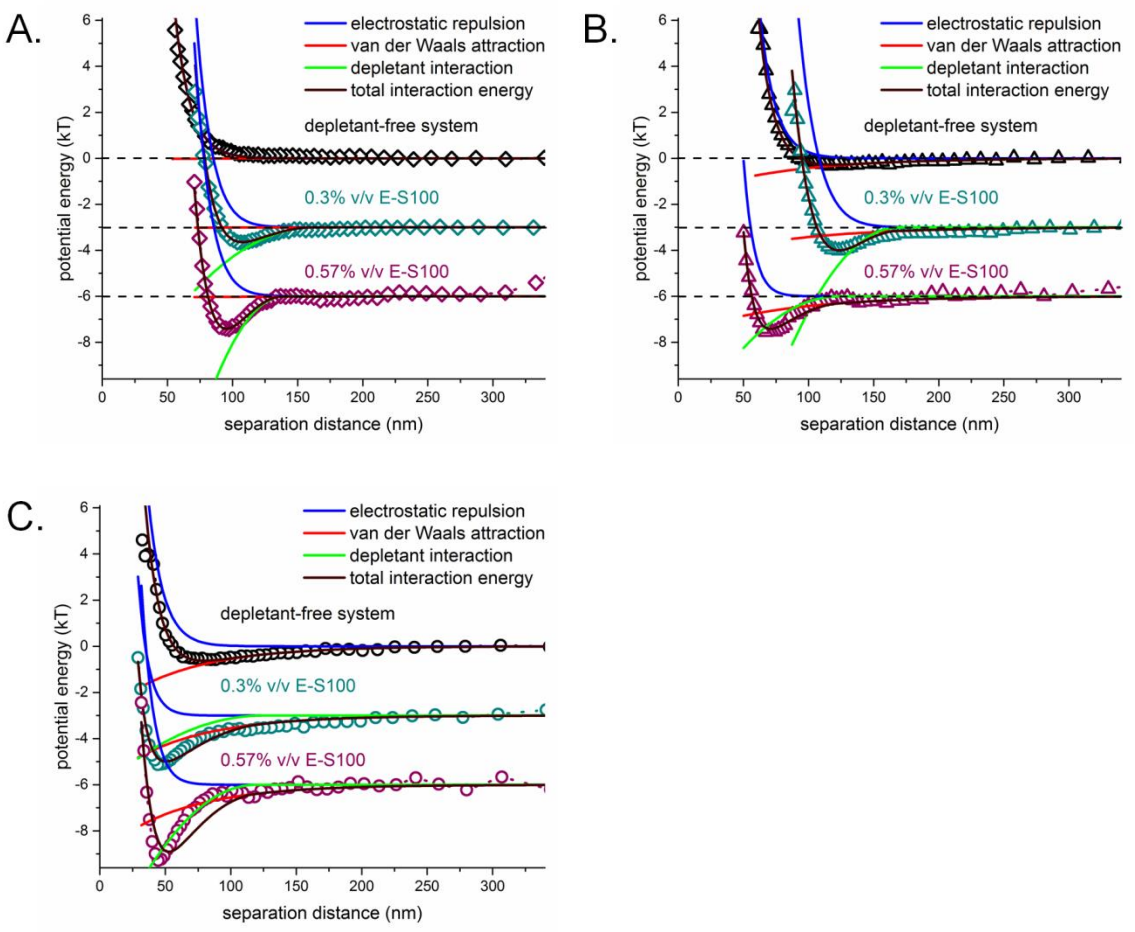

Figure 3.7. Depletant-mediated interactions and fitted interaction energy curves for a particle treated (A) 30% acetone, (B) 50% acetone, and (C) 70% acetone when the depletant concentration in 0% v/v (black symbols), 0.3% v/v (green symbols), and 0.57% v/v (red symbols). All measurements were taken in 0.5 mM phosphate buffer solution.

The fit for the particle-plate interaction energy in 0.57% v/v E-S100 solution was unable to capture the depth of the attractive well and overpredicted the range of the depletion interaction (**Figure 3.7C**). The overprediction of the interaction range could due to an overapproximation of the effective depletant size, α^*. Indeed, once the effective depletant radius is allowed to vary between the actual depletant size, α, and $[\alpha + 6\kappa^{-1}]$,

the fit for the smoothest particle is much better (**Figure 3.8**). The fits for the rougher particles remain unchanged.

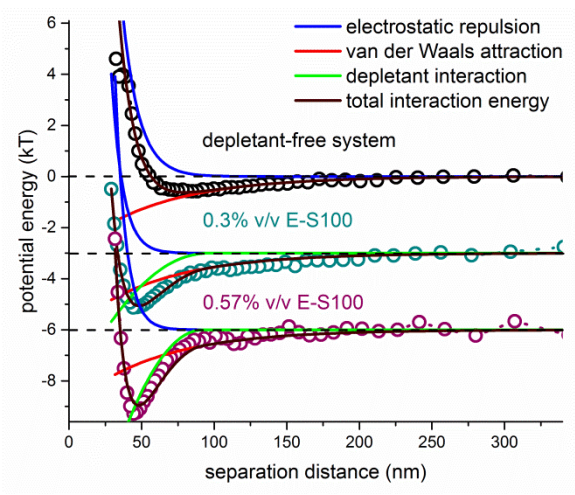

Figure 3.8. Relaxing the constraints for the apparent depletant size resulted in better fitted interaction energy curves to experimental data for a particle treated 70% acetone when the depletant concentration in 0% v/v (black symbols), 0.3% v/v (green symbols), and 0.57% v/v (red symbols). All measurements were taken in 0.5 mM phosphate buffer solution.

The improved fit, particularly for the high (0.57% v/v) depletant system suggests that the depletants in the smooth particle system are less charged than depletants in the rougher particle systems. Given that the depletants were all from the same stock solution, it is unlikely that the depletants are inherently less charged. However, the typical particle-plate separation distance is 50 nm. Given that the colloidal particle, the glass slide, and the depletants are all negatively charged, it seems possible that the close proximity of the substrate surface, the probe particle surface, and of of depletants in the gap region causes the depletant surfaces to undergo charge regulation, *i.e.* to lose some of their charge as a result of the interaction with a nearby charged surface.

The superposition approximation to the Poisson Boltzmann equation used to describe electrostatic interactions between two charged surfaces assumes that the surface potential (or surface charge) of one surface is unaffected by the surface potential of the

other, and vice versa, an assumption that is only valid if the two surfaces are far apart.[38, 39] The approximation is no longer valid when the surfaces get close enough that the electrostatic double layer of two interacting surfaces strongly overlap. Then, the electrostatic interaction is best described using the charge regulation model.[40] Rather than assume that either the surface charge or the surface potential of the interacting surfaces is constant, the chemical potential of the charge-determining ion. H^+ in our case, is constant.[29] As similarly charged surfaces are brought closer together, the electrostatic potential in the gap leads to a strong increase in the local concentration of the counterions, which promotes their recombination with the charged surface groups. In the present case, the deprotonation of the acidic surface groups responsible for the surface charge would be partially reversed at close surface approach, resulting in an apparent weakening of the electrostatic repulsive force as the electrostatic double layers of interacting surfaces overlap.[41]

In the case of the smooth particle-depletant system, as the concentration of depletants in the gap region increases, these depletants will become less charged and appear to be smaller than those in the rough particle systems where particle-plate separations are larger on average (**Figure 3.9**). Regardless of the roughness of the colloidal particle, the apparent depletant size has some dependence on the Debye length and decreases with increasing E-S100 concentration.

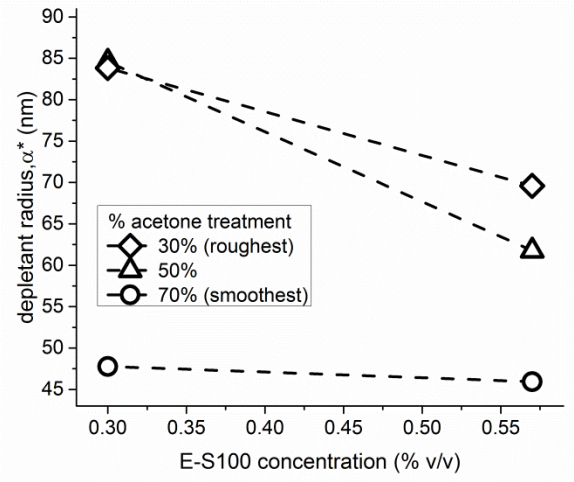

Figure 3.9. The apparent depletant size, α^*, decreases with increasing E-S100 concentration and at a given depletant concentration, increases as surface roughness increases.

The other parameter used to characterize the depletion interaction is the osmotic pressure, ΔΠ. In the simplest approximation, it is only determined by the number density of particles in the bulk and the solution temperature. For a 0.3% v/v and 0.57% v/v solution of E-S100 particles, ΔΠ should be $3.18 \times 10^{-8}\ kT/nm^3$ and $6 \times 10^{-8}\ kT/nm^3$, respectively.

Overall, the osmotic pressure increases with increasing particle concentration, which is expected. However, there calculated osmotic pressure is often larger than is expected and does not continuously increase with E-S100 concentration in the 50% acetone-treated particle system (**Figure 3.10**).

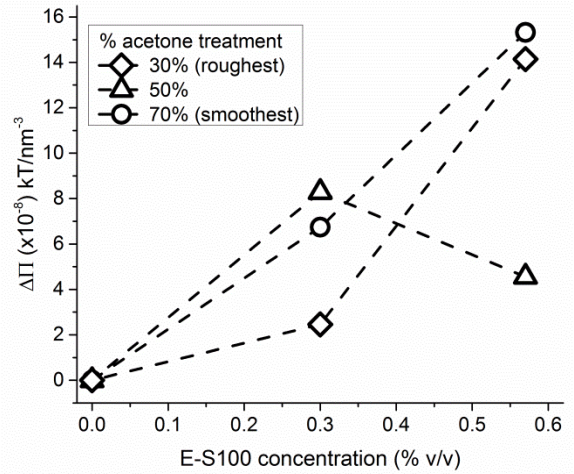

Figure 3.10. In general, the osmotic pressure increases with E-S100 concentration but is much larger than expected and has a maximum at 0.3% v/v E-S100 for the particle treated with 50% acetone (Δ).

Given that no depletant interactions, other than excluded volume effects, are accounted for in the AO potential, it is not too surprising that the osmotic pressure fit does not entirely match the predicted pressure. A better approximation would result if additional interactions, *e.g.* the depletant-depletant, depletant-probe particle, and depletant-substrate interactions were accounted for. Determining the best approximation, however, remains an unresolved challenge and goes beyond the scope of this work.

The effect of surface roughness on the depletion interaction is not systematic for the two depletant solutions. Besides shortcomings in the AO potential, which does not explicitly account for roughness, factors such as probe particle or silica surface charge heterogeneity or the adsorption of depletant particles onto the particle, could all contribute to the fitted osmotic pressure.[18-20, 36]

3.3.3 The oscillatory interaction

At high depletant concentrations, the ordering of depletants in the particle-plate gap is analogous to the ordering of solvent molecules between two molecularly smooth sheets of mica that promotes the oscillatory force. The oscillatory force is suppressed

with increasing surface roughness because rough surfaces do not promote solvent molecule ordering.[14] We would expect to see the same suppression of the oscillatory force as the roughness of colloidal particles increases.

For the measurements done in this study, only a small hint of force oscillations is seen, and only at the highest depletion concentration of 0.57% v/v. The relatively large polydispersity of the depletants used in this study (CV = 30.8%) could explain the very small oscillation seen here: polydispersity in depletant size has been shown to decrease the depth of the attractive well and the amplitude of any oscillations in the interaction energy.[25, 27] For the three particles shown here, the oscillatory force did not become suppressed with increasing surface roughness. As a side note, the experimental data indicate the particle-plate separation distance increased with increasing surface roughness, which fits the theoretical expectation that surface roughness suppresses the attractive (van der Waals and depletion) interactions. A small oscillation with an amplitude of 0.2*kT* was visible for the rough particles (treated with 30% and 50%) but is in fact less clear for the smooth particle (treated with 70% acetone) (**Figure 3.11**).

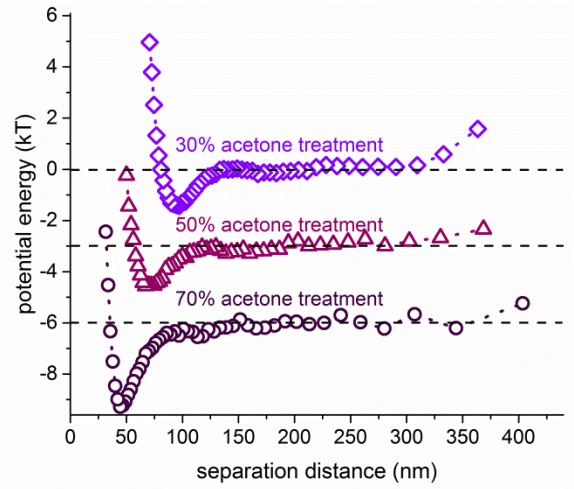

Figure 3.11. Depletant-mediated interactions for particles treated with 30% (◇), 50% (△), and 70% (○) acetone in 0.57% v/v E-S100. A small oscillation is visible for rough particles but is not as clear for the smooth particle.

The oscillations should have a periodicity that is only dependent on the characteristic wavelength of the depletant; since all three measurements were taken in the same depletant and solution conditions, the oscillation should be equidistant from the secondary minimum, regardless of surface roughness. For particle depletants, the characteristic length scale is defined via:

$$\alpha^* = \alpha + s\kappa^{-1} \qquad 3.5$$

where s is dependent on the type of depletant. For E-S100 nanoparticle depletants, the characteristic length scale is between 75.94 nm to 134.92 nm, depending on the degree of surface charging.[4, 7, 15] As shown in **Figure 3.12**, the interaction energy has an oscillation that is roughly 80 nm from the deepest attractive well measured with TIRM. The oscillations do indeed collapse, indicating that the oscillation is independent of surface roughness. All curves have been normalized to the separation distance corresponding to the lowest potential energy, h_m.

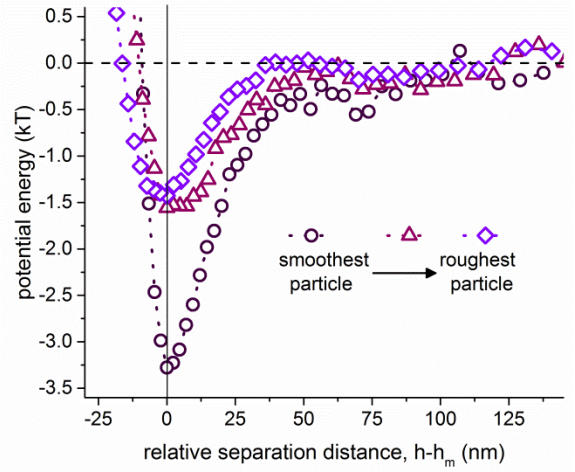

Figure 3.12. The depletant-mediated interaction energy curve for particles treated with 30% (◇), 50% (△), and 70% (○) acetone measured in 0.57% v/v E-S100 solution in 0.5 mM sodium phosphate buffer. The curves have all been normalized by the relative separation distance, h-h_m and indicate a collapse of the oscillation.

3.3.4 Particle variability

Measurements of roughness-dependent depletion interactions highlighted the individual particle variability and need for large sampling statistics. As shown in **Figure 3.13**, depletant-mediated interactions for two smooth particles show markedly different behavior upon addition of depletants to the system. The depletant-mediated potential energy curve in **Figure 3.13A** is similar to what has been previously reported: the addition of depletants increases the particle-plate attraction but does not affect the particle-plate separation distance.[6] The behavior seen in **Figure 3.13B** indicates the particle jumps toward the plate upon addition of depletants, which is not usually attributed to the depletion interaction. It is possible that the particle contained patches with lower charge or the pH of the depletant solution was lower than expected, suppressing the electrostatic interaction and causing the particle to jump toward the surface.

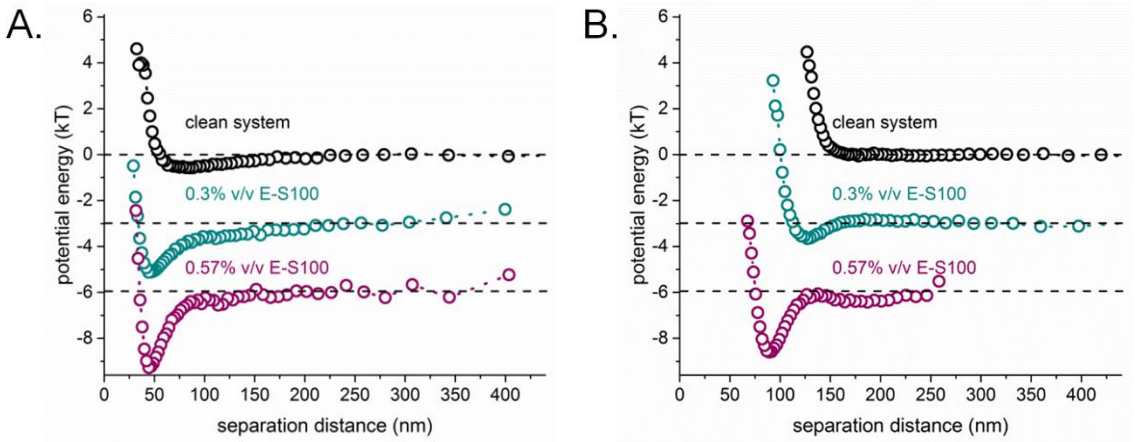

Figure 3.13. Depletant-mediated interaction curves for two particles treated with 70% acetone. For (A) one particular particle, depletants increased the particle-plate attraction but did not influence the electrostatic repulsion, whereas for (B) another particle, the addition of depletants appeared to simultaneously suppress the electrostatic repulsion and increase the particle-plate interaction energy.

3.4 Concluding Remarks

The role of surface roughness in depletion interactions was examined using colloidal probes with varying degrees of surface roughness in a nanoparticle depletant system. Depletants were designed to have the same surface chemistry and size as the roughness features. Measurements were first taken in depletant free sodium phosphate buffered solutions before measuring the interaction energy for particle-plate interactions in two different E-S100 concentrations.

Fits to the data were done using the method that resulted in the best fits for the 1:1 electrolyte systems. The potential energy profiles for depletant-free systems and influence of surface roughness on the interaction energy qualitatively matched results found for 1:1 electrolyte solutions. Fitted parameters were the same order of magnitude and followed similar roughness-dependent trends.

The depletion interaction was described using the Asakura-Oosawa potential energy with an enlarged effective depletant size accounting for the "softening" of the excluded volume interaction due to the depletant charge. While the fit and corresponding assumptions described the total interaction energy for rougher particles, the initial assumption of high nanoparticle charge led to an under-prediction of the attraction well depth and an over-prediction of the range of the attractive interaction for the smoothest probe particle, which samples the shortest separations from the substrate. It was hypothesized that the superposition approximation commonly used to describe the electrostatic interaction for large separation distances is no longer valid under these conditions and that a more appropriate way to describe the electrostatic interaction use

the charge regulation model to account for the apparent weakening of the electrostatic repulsion.

The Asakura Oosawa potential describes the depletion interaction via the osmotic pressure which is assumed to depend only on the depletant concentration. The fitted osmotic pressure was consistently larger than the expected osmotic pressure for all the particles measured, indicating that the simple van't Hoff model is insufficient and suggesting the need to account for the non-idealities expected to arise from depletant-depletant, depletant-probe particle and depletant-substrate interactions. Doing so remains an unresolved challenge however, that goes well beyond the scope of this thesis.

A small oscillation in the interaction energy was observed at the highest depletant concentration examined in this study. Analogous experiments studying solvent structural forces indicated that the oscillatory interaction would be suppressed as surface roughness increased. For this particular set of data, the small oscillations in the interaction appeared insensitive to surface roughness. The periodicity of the oscillation appeared to be independent of the probe particle topography and depended only on the characteristic length scale of the depletant, which was expected. Ultimately, more data will be needed to draw definitive conclusions regarding the role of surface roughness for the onset of depletant ordering.

3.5 References

1. S. Asakura and F. Oosawa, On interaction between two bodies immersed in a solution of macromolecules. *J. Chem. Phys.*, 1954, **22**, 1255-1256.

2. A. Vrij, Polymers at interfaces and the interactions in colloidal dispersions. *Pure Appl. Chem.*, 1976, **48**, 471-483.

3. A. Sharma and J. Y. Walz, Direct measurement of the depletion interaction in a charged colloidal dispersion. *J. Chem. Soc. Faraday Trans.*, 1996, **92**, 4997-5004.

4. T. D. Edwards and M. A. Bevan, Depletion-Mediated Potentials and Phase Behavior for Micelles, Macromolecules, Nanoparticles, and Hydrogel Particles. *Langmuir*, 2012, **28**, 13816-13823.

5. X.-J. Gong, X.-C. Xing, X.-L. Wei and T. Ngai, Direct measurement of weak depletion force between two surfaces. *Chin. J. Polym. Sci.*, 2011, **29**, 1-11.

6. D. Rudhardt, C. Bechinger and P. Leiderer, Direct measurement of depletion potentials in mixtures of colloids and nonionic polymers. *Phys Rev Lett*, 1998, **81**, 1330.

7. S. Biggs, R. R. Dagastine and D. C. Prieve, Oscillatory packing and depletion of polyelectrolyte molecules at an oxide-water interface. *J. Phys. Chem. B*, 2002, **106**, 11557-11564.

8. M. Piech and J. Y. Walz, The Structuring of Nonadsorbed Nanoparticles and Polyelectrolyte Chains in the Gap between a Colloidal Particle and Plate. *J. Phys. Chem. B*, 2004, **108**, 9177-9188.

9. S. Ji and J. Y. Walz, Depletion Flocculation Induced by Synergistic Effects of Nanoparticles and Polymers. *J. Phys. Chem. B*, 2013, **117**, 16602-16609.

10. C. Bechinger, D. Rudhardt, P. Leiderer, R. Roth and S. Dietrich, Understanding depletion forces beyond entropy. *Phys. Rev. Lett.*, 1999, **83**, 3960.

11. J. N. Israelachvili and P. M. McGuiggan, Forces between surfaces in liquids. *Science*, 1988, **241**, 795-800.

12. S. Ji and J. Y. Walz, Depletion forces and flocculation with surfactants, polymers and particles — Synergistic effects. *Curr. Opin. Colloid Interface Sci.*, 2015, **20**, 39-45.

13. J. N. Israelachvili and G. E. Adams, Measurement of forces between two mica surfaces in aqueous electrolyte solutions in the range 0–100 nm. *J. Chem. Soc., Faraday Trans. 1*, 1978, **74**, 975-1001.

14. J. N. Israelachvili, *Intermolecular and surface forces: revised third edition*, Academic press, 2011.

15. M. Piech and J. Y. Walz, Depletion interactions produced by nonadsorbing charged and uncharged spheroids. *J. Colloid Interface Sci.*, 2000, **232**, 86-101.

16. P. C. Odiachi and D. C. Prieve, Effect of added salt on the depletion attraction caused by non-adsorbing clay particles. *Colloids Surf., A*, 1999, **146**, 315-328.

17. M. Kamp, M. Hermes, C. M. van Kats, D. J. Kraft, W. K. Kegel, M. Dijkstra and A. van Blaaderen, Selective Depletion Interactions in Mixtures of Rough and Smooth Silica Spheres. *Langmuir*, 2016, **32**, 1233-1240.

18. K. Zhao and T. G. Mason, Suppressing and enhancing depletion attractions between surfaces roughened by asperities. *Phys. Rev. Lett.*, 2008, **101**, 148301.

19. S. Badaire, C. Cottin-Bizonne and A. D. Stroock, Experimental investigation of selective colloidal interactions controlled by shape, surface roughness, and steric layers. *Langmuir*, 2008, **24**, 11451-11463.

20. D. J. Kraft, R. Ni, F. Smallenburg, M. Hermes, K. Yoon, D. A. Weitz, A. van Blaaderen, J. Groenewold, M. Dijkstra and W. K. Kegel, Surface roughness directed self-assembly of patchy particles into colloidal micelles. *PNAS*, 2012, **109**, 10787-10792.

21. K. Zhao and T. G. Mason, Directing colloidal self-assembly through roughness-controlled depletion attractions. *Phys. Rev. Lett.*, 2007, **99**, 268301.

22. H. Chew, D.-S. Wang and M. Kerker, Elastic scattering of evanescent electromagnetic waves. *Appl. Opt.*, 1979, **18**, 2679-2687.

23. D. C. Prieve and N. A. Frej, Total internal reflection microscopy: a quantitative tool for the measurement of colloidal forces. *Langmuir*, 1990, **6**, 396-403.

24. P. C. Odiachi Jr and D. C. Prieve, Effect of added salt on the depletion attraction caused by non-adsorbing clay particles. *Colloids Surf., A*, 1999, **146**, 315-328.

25. M. Piech and J. Y. Walz, Effect of Polydispersity and Charge Heterogeneity on the Depletion Interaction in Colloidal Systems. *J. Colloid Interface Sci.*, 2000, **225**, 134-146.

26. J. Y. Walz, Effect of Polydispersity on the Depletion Interaction between Colloidal Particles. *J. Colloid Interface Sci.*, 1996, **178**, 505-513.

27. M. Piech and J. Y. Walz, Direct Measurement of Depletion and Structural Forces in Polydisperse, Charged Systems. *J. Colloid Interface Sci.*, 2002, **253**, 117-129.

28. A. San Miguel, J. Scrimgeour, J. E. Curtis and S. H. Behrens, Smart colloidosomes with a dissolution trigger. *Soft Matter*, 2010, **6**, 3163-3166.

29. S. H. Behrens and M. Borkovec, Electrostatic interaction of colloidal surfaces with variable charge. *J. Phys. Chem. B*, 1999, **103**, 2918-2928.

30. X. Xing, G. Sun, Z. Li and T. Ngai, Stabilization of Colloidal Suspensions: Competing Effects of Nanoparticle Halos and Depletion Mechanism. *Langmuir*, 2012, **28**, 16022-16028.

31. D. F. Parsons, R. B. Walsh and V. S. Craig, Surface forces: Surface roughness in theory and experiment. *J. Chem. Phys.*, 2014, **140**, 164701.

32. P. K. Gupta, D. Inniss, C. R. Kurkjian and Q. Zhong, Nanoscale roughness of oxide glass surfaces. *J. Non-Cryst. Solids*, 2000, **262**, 200-206.

33. T. D. Edwards and M. A. Bevan, Polymer Mediated Depletion Attraction and Interfacial Colloidal Phase Behavior. *Macromolecules*, 2012, **45**, 585-594.

34. H.-J. Wu, W. N. Everett, S. G. Anekal and M. A. Bevan, Mapping Patterned Potential Energy Landscapes with Diffusing Colloidal Probes. *Langmuir*, 2006, **22**, 6826-6836.

35. M. A. Bevan and D. C. Prieve, Direct measurement of retarded van der Waals attraction. *Langmuir*, 1999, **15**, 7925-7936.

36. P. Taboada-Serrano, V. Vithayaveroj, S. Yiacoumi and C. Tsouris, Surface Charge Heterogeneities Measured by Atomic Force Microscopy. *Environ. Sci. Technol.*, 2005, **39**, 6352-6360.

37. J. W. Tsao, Master's Thesis, Georgia Institute of Technology, 2014.

38. D. F. Evans and H. Wennerström, *The Colloidal Domain: Where Physics, Chemistry, Biology, and Technology Meet, 2nd Edition*, Wiley-VCH, New York, NY, 1999.

39. W. B. Russel, D. A. Saville and W. R. Schowalter, *Colloidal dispersions*, Cambridge university press, 1989.

40. G. Trefalt, S. H. Behrens and M. Borkovec, Charge Regulation in the Electrical Double Layer: Ion Adsorption and Surface Interactions. *Langmuir*, 2016, **32**, 380-400.

41. T. H. Anderson, S. H. Donaldson, H. Zeng and J. N. Israelachvili, Direct Measurement of Double-Layer, van der Waals, and Polymer Depletion Attraction Forces between Supported Cationic Bilayers. *Langmuir*, 2010, **26**, 14458-14465.

CHAPTER 4

CONCLUSIONS AND OUTLOOK

Colloidal interactions are important for many applications. Preventing particle aggregation of homogenous mixtures can, for example, extend the shelf life of protein formulations produced by the pharmaceutical industry or polymer dispersions used for paints and coatings, etc. Controlling colloidal stability in heterogeneous systems is important for many applications, such as flocculation-based separation techniques or the self-assembly of colloidal macrostructures. In both homogenous and heterogeneous dispersions, the role of surface roughness plays an important role in determining the success of dispersion stability. This study was first to experimentally isolate surface roughness effects on different types of interactions that typically govern colloidal stability.

Surface roughness effects were experimentally measured using colloidal particles with variable surface topography but similar surface chemistry. Rough particles were generated via the adsorption of negatively charged, chemically homogenous, nanoparticles onto positively charged core particles. Surface roughness was tuned using a technique that combines polymer erosion with molecular re-deposition and film plasticization. Particle surface properties were characterized to determine if the process was successful. Scanning electron microscopy (SEM) qualitatively confirmed that technique used to change surface topography did result in particles with variable roughness. Measurements of the Rms roughness of macroscopic surfaces, coated and smoothed with the same nanoparticles and technique as the colloidal particles, were used

as a quantitative characterization of surface topography. Results quantitatively confirmed the change of surface roughness using the particle deposition and smoothing technique. Surface chemistry was characterized by measuring the electrokinetic potential of dispersions of particles with different surface topographies. While the electrokinetic potential is dependent on many different system parameters, the pH at which the electrokinetic potential is 0, called the isoelectric potential (IEP), is only dependent on the surface chemistry. The isoelectric points for dispersions of particles with varying surface topography did not vary systematically with surface roughness and were all similar to the IEP of a dispersion of the coating particles; this confirmed the surface chemistry remained constant throughout the smoothing process. The particles with tunable surface roughness used in this study were generated by modifying a previous method and represent the first study to generate rough particles and vary the surface topography for 6 μm microparticles on a nanometer length scale.

Colloidal interactions were measured using total internal reflection microscopy (TIRM), a force measurement technique with resolution of about ten femtonewton (10^{-11} N), in a monovalent electrolyte. Standard colloidal forces were described using the Derjaguin-Laudau-Verwey-Overbeek (DLVO) theory, which considers the interplay of (mean-field) electrostatics and van der Waals interaction.

Experimental results qualitatively showed the suppression of the van der Waals attraction with increasing surface roughness. The best fit to the data was achieved using an empirical expression to describe the van der Waals attraction and assuming a normal distribution of surface-to-surface separations due to surface roughness to calculate the electrostatic repulsion. The partial success of assuming a normal distribution of

separation distances indicates that surface roughness amplifies the electrostatic repulsive interaction in addition to suppressing the van der Waals interaction.

The van der Waals interaction was described using an empirical equation for an exponentially decaying interaction. The characteristic decay length and the prefactor to the exponential, a constant that can be interpreted as a form of the Hamaker constant, were used as adjustable fit parameters to describe the van der Waals interaction. Both varied systematically with surface roughness. The decay length increased with increasing surface roughness, while the prefactor to the exponential decreased systematically with increasing surface roughness. The prefactor remained in the same order of magnitude as would be expected for the Hamaker constant. Ultimately, it would be desirable to replace the empirical equation for the van der Waals interaction with a description based on first principles that can adequately describe experimental data.

The electrostatic repulsion between interaction surfaces was calculated assuming a normal distribution of surface-to-surface separation distances with a standard deviation that accounted for the Rms roughness of both surfaces. Independently of salt concentration, the fitted standard deviation increased systematically as the surface roughness of the prepared particles increased, as expected. The model provided excellent fits to the data but yielded unrealistically large particle Rms roughness values that decreased with increasing salt concentration, as well as improbably low surface potentials. More realistic assumptions regarding the distribution of surface-to-surface separation distances may provide a remedy for the shortcomings for the present model. If, for example, the surface topography was modeled as a sine wave, the surface-to-surface separation distances would follow the probability distribution of a sine function. The

local separation distances would no longer be normally distributed around an average separation distance, but would most heavily depend on the largest and the smallest local surface-to-surface separations.

Surface roughness effects on the depletion interaction were measured using probe particles with varying surface topography in dispersions of nanoparticles similar to those employed in generating the probe particle roughness. Due to the acidity of the nanoparticle depletant, the pH of solutions had to be buffered. Colloidal interactions were described as a combination of DLVO and depletion interactions. Models for the DLVO interactions that best captured the effects of surface roughness in depletant-free systems with monovalent electrolytes were also used to describe the DLVO interactions in the more complex, buffered systems with depletants. The parameters describing the van der Waals attraction were the same order of magnitude and indicated the same roughness dependence as in the depletant-free system. Moreover, in both systems the fitted magnitude of the surface potentials for the electrostatic model showed a similar (increasing) trend with increasing roughness of the probe particles.

The depletion interactions were described using the Asakura-Oosawa expression for the potential energy with an enlarged effective depletant size expected to accurately reflect the electrostatic interaction range of highly charged nanoparticle depletants. While fits to the data worked well in the case of rough probe particles, which on average retain larger separations from the substrate, the fitted potential for smooth particles, which tend to approach the substrate more closely, under-predicted the strength of the depletion attraction while over-predicting the range of this interaction. A plausible, albeit speculative explanation would be that depletant particles in the narrow gap region

between the probe particle and the substrate undergo charge regulation and lose some of their charge due to their interaction with the nearby surfaces of similar charge. As a result, their effective size (interaction range) would shrink and the local concentration increase, thus providing a rationale for the observed changes in range and strength of the depletion interaction.

In the Asakura-Oosawa model, the osmotic pressure describes the bulk nanoparticle concentration. As expected, the fitted osmotic pressure increased as the depletant concentration in solution increased. However, the fitted osmotic pressure was often larger than expected for a given depletant concentration. The discrepancy between the predicted and experimental osmotic pressure is mostly likely due to limitations of the van't Hoff law used to calculate the osmotic pressure. The depletant osmotic pressure is assumed to follow the idea gas law (non-interacting particles), which is an inappropriate assumption because the depletants are not non-interacting. Determining the best correction to account for the depletant-depletant, depletant-probe particle, and depletant-plate interactions that contribute to the depletion interaction, however, is beyond the scope of this work.

Regardless of surface roughness, a small oscillation in the interaction energy was observed at the highest depletant concentration used in this study. As expected, the periodicity of the oscillation was dependent only on depletant size. Oscillatory forces arise due to ordering of depletants in the particle-plate gap. Analogous experiments studying solvent molecule ordering in the gap between molecularly smooth mica sheets showed the suppression of the oscillatory interaction as the surface roughness increased. The oscillation was very small (>0.5kT), so differences in the oscillation amplitude are

miniscule. More experimental studies at higher depletant concentrations may give more definitive effects of surface roughness on depletant oscillatory forces.

The experimental results highlighted the particle-to-particle variation inherent in colloidal systems. While some general roughness-dependent trends were seen, ultimately, more data are needed to calculate quantitative effects of surface roughness for the depletion interaction.

Despite examples of particle-to-particle variation present in the measured interactions here, this study provided robust experimental evidence for several roughness-dependent interactions. For example, for systems without depletion interaction, the work done here was the first to experimentally verify that increasing the surface roughness without changing surface chemistry, results in a suppression of the van der Waals attraction. The results here also confirmed that regardless of surface roughness, increasing the ionic strength of solution suppressed the electrostatic repulsive interaction. This study also demonstrates the suppression of depletion attraction with increasing surface roughness, a phenomenon that is expected theoretically and has been used to direct particle assembly before but has never been shown experimentally in studies where roughness alone was varied systematically.

The current study varied surface roughness in batch reactions, resulting in an additional size dependence on the interaction energies felt by the particle. Results from this work also demonstrated that even two particles from the same batch could experience drastically different interaction energies, whether due to differences in core particle charge density, or differences in local solvent concentration during the surface tuning steps. Future work could seek to circumvent this problem beginning each TIRM

measurement with a single, rough, particle, and change the surface roughness *in situ* and prevent results affected by size and surface charge variations in a given particle sample.

This work can be used as the starting point for a series of experimental studies on the roughness effects for a variety of colloidal phenomena, such as the influence of surface roughness on lateral capillary interactions at a liquid/liquid interface. Substrates with tunable roughness can be used in conjunction with particles of tunable roughness in measurements of particle-plate interactions relevant for particle-membrane applications. The method of generating chemically homogenous nanoparticles can be used to make particles of various sizes, and allow us to determine roughness effects for depletion interactions for various ratios of depletant size and surface roughness features.